DISCLAIMER

This report was prepared as an account of work sponsored by an agency of the United States Government. Neither the United States Government nor any agency thereof, nor any of their employees, makes any warranty, express or implied, or assumes any legal liability or responsibility for the accuracy, completeness, or usefulness of any information, apparatus, product, or process disclosed, or represents that its use would not infringe privately owned rights. Reference herein to any specific commercial product, process, or service by trade name, trademark, manufacturer, or otherwise does not necessarily constitute or imply its endorsement, recommendation, or favoring by the United States Government or any agency thereof. The views and opinions of authors expressed herein do not necessarily state or reflect those of the United States Government or any agency thereof. Reference herein to any social initiative (including but not limited to Diversity, Equity, and Inclusion (DEI); Community Benefits Plans (CBP); Justice 40; etc.) is made by the Author independent of any current requirement by the United States Government and does not constitute or imply endorsement, recommendation, or support by the United States Government or any agency thereof.

Final Technical Report (FTR)

Cover Page

a. *Federal Agency*	Department of Energy	
b. *Award Number*	DE-EE0008514	
c. *Project Title*	Integrating an Industrial Source and Commercial Algae Farm with Innovative CO_2 Transfer Membrane and Improved Strain Technologies	
d. *Recipient Organization*	Colorado State University	
e. *Project Period*	*Start:* January 1, 2019	*End:* June 30, 2024
f. *Principal Investigator (PI)*	Kenneth F. Reardon Professor Kenneth.Reardon@colostate.edu 970-491-6505	
g. *Business Contact (BC)*	Tiffany Roller Senior Research Administrator Tiffany.Roller@colostate.edu 970.491.5294	
h. *Teaming Partners*	National Renewable Energy Laboratory, Qualitas Health, Inc.	

1. **Acknowledgement:** "This material is based upon work supported by the U.S. Department of Energy's Office of Energy Efficiency and Renewable Energy (EERE) Bioenergy Technologies Office (BETO) under the Efficient Carbon Utilization in Algal Systems Award Number DE-EE0008514."

2. **Disclaimer**: “This report was prepared as an account of work sponsored by an agency of the United States Government. Neither the United States Government nor any agency thereof, nor any of their employees, makes any warranty, express or implied, or assumes any legal liability or responsibility for the accuracy, completeness, or usefulness of any information, apparatus, product, or process disclosed, or represents that its use would not infringe privately owned rights. Reference herein to any specific commercial product, process, or service by trade name, trademark, manufacturer, or otherwise does not necessarily constitute or imply its endorsement, recommendation, or favoring by the United States Government or any agency thereof. The views and opinions of authors expressed herein do not necessarily state or reflect those of the United States Government or any agency thereof.”

3. **Executive Summary:** The motivation and goal for this project were to increase the carbon utilization efficiency (CUE) and areal productivity for algal cultivations, thereby reducing CO_2 costs to cultivation operations and improving economics. This was achieved through a combination of enhanced delivery of inorganic carbon and improved strains of *Nannochloropsis oceanica* capable of higher rates of bicarbonate uptake and metabolism. The project succeeded in these goals. First, a bubble-free, membrane-based technology was developed for delivering CO_2 to cultivations, which increased the CUE from the 15-20% that is standard in the industry to more than 65%. In addition, *N. oceanica* was modified to express a bicarbonate transporter protein, BicA, which enabled the cells to grow more quickly. In addition, advances were made in the protein engineering of carbonic anhydrase (CA) for enhanced stability and catalytic performance, the computational fluid dynamics modeling of algal cultivation systems, and in the life-cycle assessment and technoeconomic analysis of algal production. Together, these outcomes contribute to advancing algal cultivation as an economically viable platform for production of fuels, materials, and other chemical products. The project results aid in addressing the dual challenges of reducing atmospheric CO_2 levels and achieving green energy solutions.

   The project significantly contributed to this field in several ways. First, the evaluation of carbonic anhydrases advanced the science of biocatalysis and immobilized enzyme technology for gas capture. By exploring different CA variants and their performance in thin films, the project expanded the understanding of how enzyme structure and immobilization affect catalytic efficiency in carbon capture applications. Second, the BicA-expressing strain of *N. oceanica* demonstrated a novel approach toward improving algal growth rates under carbon-limited conditions. Third, the computational fluid dynamics modeling revealed the extent and locations of light limitations in typical open raceway pond systems and indicated where improvements could be made. And

finally, the membrane-based approach for CO_2 transfer to algae cultivations resulted in a 90% improvement in CUE compared to standard gas sparging.

The project contributed to the technical effectiveness and economic feasibility of algal cultivations primarily through development of the membrane system for CO_2 delivery with much improved CUE. The reduction of CO_2 costs with no impact on algae growth means improved economics, as demonstrated by the technoeconomic analysis performed in the project.

This project benefitted the public by offering a scalable technology to improve algal cultivations, a nascent industry that with the potential to provide fuels, materials, and other chemicals with greater environmental sustainability than fossil fuel-based approaches. The successful implementation of algal systems has the potential to enhance green energy production, reduce carbon footprints, and stimulate economic growth through the creation of new industries centered around sustainable practices.

4. Table of Contents:

5. Background:

Overview

Increasing the rate at which inorganic carbon can be delivered to cultivations and the rate at which algae can consume inorganic carbon are critical strategies for meeting the DOE 2022 productivity goal. This project addressed those strategies through an integrated plan of novel technology development, engineering modeling, and strain engineering and adaptation. The project focused on *Nannochloropsis oceanica* CCAP84910, closely related to the production strain used by project partner Qualitas Health at their Imperial, TX facility.

In this project, we developed and used membrane modules containing immobilized carbonic anhydrase to transform gas-phase CO_2 into aqueous-phase inorganic carbon. Dissolved inorganic carbon (DIC) addition has been shown to increase the growth rates and lipid productivity of a range of algal species, including *Chlorella vulgaris* (Mokashi et al. 2016) and *Scenedesmus* sp. CCNM 1077 (Pancha et al. 2015). The effluent from this module contained high levels of DIC that were delivered to the ORP at locations guided by a detailed mathematical model of mixing, chemical speciation, and algal consumption. With this controlled CO_2 delivery scheme, the rate of carbon delivery could be matched to the rate of consumption and carbon wasting to the air was substantially reduced.

Since algal strains did not evolve in environments with high DIC levels, we used complementary approaches to develop *N. oceanica* strains capable of increased rates of bicarbonate uptake and metabolism. This new strain was characterized so the strategy can be developed further and transferred.

Carbonic anhydrase protein engineering and application for CO_2 transfer

Carbonic anhydrases (CAs) are pivotal in CO_2 transfer technologies due to their ability to catalyze the rapid conversion of carbon dioxide to bicarbonate and protons, a reaction fundamental to many industrial and environmental processes. These enzymes enhance the solubility and transport of CO_2, making them ideal candidates for carbon capture and sequestration (CCS) systems. In CCS, CAs facilitate the efficient capture of CO_2 from industrial emissions, with potential for integration into power plants and other sectors with high carbon footprints. Research in this area has grown rapidly in the past five years, with efforts focusing on optimizing CA variants for enhanced stability and activity under industrial conditions, where factors like temperature, pH, and pressure pose significant challenges (Talekar et al. 2022, Shao et al. 2024, de Oliveira et al. 2022).

A key subtask of this project was focused on engineering CA variants capable of functioning at pH values lower than the typical value around 8 and at salinity levels approaching that of seawater. In conjunction, another subtask focused on determining an immobilization method and membrane material that will result in a hybrid material with high inorganic carbon flux rates and long lifetime. Such an enzymatic membrane can achieve high dissolved inorganic carbon delivery fluxes into the aqueous phase, which can then be delivered to the pond.

Recent developments have highlighted the potential of genetically engineered and

naturally occurring CA variants that exhibit robust performance in extreme environments. For instance, variants from extremophilic organisms demonstrate remarkable stability and activity at high temperatures and pressures, making them suitable for direct application in flue gas conditions. Protein engineering has emerged as a powerful tool in enhancing the functionality of CA. By employing techniques such as site-directed mutagenesis, directed evolution, and computational design, researchers modified the active sites and surrounding environments of CA enzymes to improve their catalytic efficiency, stability, and substrate specificity. One of the primary goals of engineering CA variants is to increase their activity in extreme industrial conditions, such as high temperatures and non-neutral pH environments, where natural enzymes typically denature. Studies have shown that targeted amino acid substitutions can enhance the thermostability of CA variants, while retaining their catalytic efficiency, thus making them viable candidates for incorporation into industrial processes like CCS (Karmali and Ferreira 2003). Directed evolution has produced more stable variants (Alvizo et al. 2014).

Furthermore, the exploration of immobilization techniques for CAs on various support materials enhances enzyme reusability and operational lifetime, thereby reducing costs and improving feasibility of large-scale implementation. Surface modifications and encapsulation methods also protect enzymes from harsh chemical environments, preserving their catalytic function in CO_2 transfer operations. (Molina-Fernández and Luis 2021, Zhang et al., 2022).

The integration of CAs into CO_2 transfer technologies offers a biotechnological approach that complements chemical and physical absorption methods. Enzymes can be integrated into membrane systems for efficient gas separation and conversion processes (Zhang et al., 2022). However, there has not yet been a report of using a CA-based membrane for carbon delivery into algal cultivations. Using a CA membrane overcomes important limitations of membranes that only transfer CO_2 from the gas phase to a liquid phase. If that liquid phase is water, fluxes are limited by the driving force since CO_2 is present on both sides of the membrane.

Transformation of algae to increase carbon uptake

Algae have evolved Carbon Concentrating Mechanisms (CCMs) to increase the rate of delivery of CO_2 to the first steps of carbon fixation (Giordano et al. 2005). CCMs are induced in ambient CO_2 conditions and knocking out particular components leads to low rates of photosynthesis or even death unless cells are grown in high (up to 5%) CO_2 (Takashi and Hideya, 2009). Thus far, the only genetically proven component of *N. oceanica's* CCM are carbonic anhydrases which interchange CO_2 and HCO_3^-. Both *Nannochloropsis salina* and *N. gaditana* appear to have a bicarbonate pump for CO_2 whereby bicarbonate is actively transported across the plasma membrane and then presumably converted to CO_2 by intracellular carbonic anhydrases (Hanson et al., 2014). There have not been any reports of expression of cyanobacterial bicarbonate transporters into a (eukoryotic) alga.

CO_2 transfer technologies for algal cultivations

Transferring CO_2 efficiently into algae cultivations is a critical process for optimizing

algal growth and maximizing biomass production, especially for biofuel applications. The standard method involves direct bubbling (sparging) of CO_2 or a CO_2-enriched air or waste gas mixture directly into algal culture systems. This approach can be easily implemented in both open pond systems and closed photobioreactors, using spargers that distribute gas bubbles evenly through the liquid medium. The key to this process is optimizing the bubble size and residence time within the medium, as these factors significantly influence the dissolution rate of CO_2 and its uptake by the algae. Recent studies suggest that microbubbles, due to their high surface area to volume ratio, can enhance CO_2 transfer efficiency, providing a more effective and economically viable solution compared to larger bubbles (Yang et al., 2018).

An alternative approach involves the use of membrane contactors, which facilitate CO_2 transfer across a semi-permeable membrane into the algal cultivation system. This method allows for precise control over CO_2 delivery rates and prevents gas losses to the atmosphere, making it particularly advantageous in closed systems. By maintaining a stable carbon supply, membrane contactors can significantly improve algal growth rates and biomass productivity. Recent advancements in membrane technology have focused on improving the durability and permeability of these contactors to withstand prolonged operational periods, potentially reducing operational costs and increasing the sustainability of large-scale algae cultivation (Bilad et al. 2014).

6. Project Objectives:

6A. Project Impact:

Successful achievement of the project milestones will accelerate technical progress toward the 2022 areal productivity goals and will help drive down the cost of algal biofuel production.

The project contributed to the technical effectiveness and economic feasibility of algal cultivations primarily through development of the membrane system for CO_2 delivery with much improved CUE. The reduction of CO_2 costs with no impact on algae growth means improved economics, as demonstrated by the technoeconomic analysis performed in the project. The cost savings derived from progress made in this project, if successful, will be captured in yearly state of technology assessments of the integrated system performance at small scale deployment and contribute to BETO's multi-year program plan (MYPP) outyear targets and mapped onto a path towards $3/GGE by FY2022.

This project benefitted the public by offering a scalable technology to improve algal cultivations, a nascent industry that with the potential to provide fuels, materials, and other chemicals with greater environmental sustainability than fossil fuel-based approaches. The successful implementation of algal systems has the potential to enhance green energy production, reduce carbon footprints, and stimulate economic growth through the creation of new industries centered around sustainable practices.

A bubble-free, membrane-based technology was developed for delivering CO_2 to cultivations, which increased the CUE from the 15-20% that is standard in the industry to more than 50%. The combined strategies were expected to result in an areal productivity increase of at least 20% along with a cost savings resulting from increased CUE.

6B. Project Goals:

The overall goal of this project was to demonstrate increased CUE and areal productivity through enhanced delivery of inorganic carbon and improved strains of *N. oceanica* capable of higher rates of bicarbonate update and metabolism. The intent was to increase CUE through use of enzymatic membrane technology to transfer CO_2 from a gas to water as bicarbonate and designing the delivery locations in an ORP with a detailed mathematical model. Together, the aim was to achieve the FOA goal of increasing CUE by 25% over the QH baseline level of 55% to a target of 69%, demonstrated in small ORPs located at the QH facility at Imperial, TX.

At the same time, the development of variants of *N. oceanica* with higher bicarbonate uptake rates was intended to enable us to demonstrate a 20% increase in areal productivity in small ORPs. The improved productivity and biomass yields derived from both strain improvement and carbon delivery system development were to be conceptually integrated in a fuel production process based on the NREL developed combined algal processing pathway. The cost savings derived from progress made in this project, if successful, were to be captured in yearly state of technology assessments of the integrated system performance at small scale deployment and contribute to BETO's multi-year program plan (MYPP) outyear targets and mapped onto a path towards $3/GGE by FY2022.

The CO_2 source to be used in this is fermentation off-gas from NBB, a large craft brewing company, located in Ft. Collins, CO. This is a very high purity (> 99.99%) CO_2 stream and was chosen because the purity will allow for smaller membrane units than would be needed with other sources and contains no chemicals that would inhibit algal growth, as is often the case with other industrial CO_2 sources. The use of high purity CO_2 sources also incurs less transportation costs for the gas. In addition to fermentation off-gas, the CO_2 stream from Haber-Bosch ammonia production has very high purity and could also be used in the same system.

The end-of-project goal is to demonstrate the use of model-directed, optically controlled, dissolved inorganic carbon delivery that achieves a 25% increase over baseline inorganic carbon utilization efficiency in the integrated system measured over a 6-week semi-continuous cultivation demonstration run at the QH test site (mini-ponds plus membrane module plus CO_2 monitoring) enhanced carbon delivery strategy, combined with targeted and/or adapted modification of *N. oceanica*, will result in a 20% growth rate increase.

6C. Summary of the tasks within the Statement of Project Objectives

Task 1: Develop membrane system for transfer of CO_2 to water as bicarbonate.
Work on the enzymatic membrane system was directed to the design, construction, and laboratory testing of a module capable of transferring gas-phase CO_2 to aqueous-phase bicarbonate.

Subtasks:
Subtask 1.1: Protein engineering of carbonic anhydrase to improve pH tolerance
Subtask 1.2: Preparation and characterization of carbonic anhydrase membranes
Subtask 1.3: Construction, process modeling, and testing of CO_2 transfer module

Task 2: Engineering of *Nannochloropsis oceanica* for enhanced carbon uptake.
This objective focused on enhancement of *N. oceanica* for improved growth and productivity in the high-bicarbonate environments that will result from implementation of the enzymatic membrane module. This work included both targeted engineering (constitutive overexpression of a bicarbonate transporter) and strain adaptation to high bicarbonate environments.
Subtasks:
Subtask 2.1: CCM engineering in *N. oceanica*
Subtask 2.2: Strain adaptation to high bicarbonate levels and lower pH
Subtask 2.3: Characterize novel strains

Task 3: System integration, deployment, and validation.
This objective focuses on the integration of the bicarbonate delivery module with the cultivation system, process modeling, validation of the system performance, and cost and sustainability assessment. The work included development of a mixing model for the open raceway pond cultivation system and of a CO_2 monitoring system, then testing of the bicarbonate delivery module and use of the resulting data to improve and validate the engineering process model.

Subtasks:
Subtask 3.1: Determine optimal carbon introduction location to raceway pond
Subtask 3.2: Develop and test system for gas-phase CO_2 monitoring and control
Subtask 3.3: Evaluate performance of C delivery and strain uptake
Subtask 3.4: Engineering process modeling
Subtask 3.5: Concurrent TEA and LCA

7. Project Results and Discussion:

7A. Project Outcomes

This project produced several important outcomes: development of carbonic anhydrase variants with enhanced ability to be active at lower pH and higher salinity; genetic modification of N. oceanica to express a cyanobacterial bicarbonate

transporter; development of a membrane-based carbonation system for improved CUE; a detailed computational fluid dynamics model with biochemical terms to provide improved predictions of mixing and growth in algal open raceway ponds; and robust life cycle assessments and technoeconomic modeling to provide insights into the potential benefits of the experimental research.

7B. Task Results

Task 1: Develop membrane system for transfer of CO_2 to water as bicarbonate.

Subtask 1.1: Protein engineering of carbonic anhydrase to improve pH tolerance

Milestone 1.1.1: Select four native carbonic anhydrase enzymes for computational supercharge design, by computationally evaluating native carbonic anhydrase enzymes to predict the total surface charge, pH optima and thermal stability. Generate five variants for each of the four selected native enzymes by Rosetta supercharged enzyme design. These supercharged variants will have net surface charges ranging from -24 to +16 to represent the physiological range.

The goal of this milestone was to generate variants of native CA enzymes based on computational protein design algorithms. The aim was to create CA variants that functioned effectively at lower pH levels than native variants and maintained extended stability once incorporated into a membrane system.

Protein engineering has been used to alter the pH optimum of enzymes (Ma et al. 2016) particularly through altering surface charge (Qiu and Lai 2013, Li et al. 2015). Based on these results, we hypothesized that native CA variants displaying significant positive or negative surface charge may exhibit a range of pH optima. To evaluate effects of a range of surface charges we selected the native CA with the most negative and most positive surface charge from each of the three families. These native variants were expressed, and the pH activity optimum and pH activity range evaluated. We used these six variants as starting points for computational design. Using two separate Rosetta supercharge algorithms, each variant was designed to have a more negative and more positive surface charge.

CAs catalyze the hydration of CO_2 to bicarbonate, and are found in genetically distinct classes including α-, β-, γ-, δ- and ζ. We hypothesized that different CA classes may exhibit natural variation in pH optima and/or may be more amenable to altered pH optima through protein engineering efforts. The result of this design effort was therefore computationally designed variants for each starting structure, encompassing computationally designed variants for each CA family represented in this study (α, β and γ).

Experimentally determined structures for α-, β-, and γ CA enzymes were obtained from the Protein Data Bank (PDB). These representative structures were then submitted to the Dali protein structure comparison server (http://ekhidna2.biocenter.helsinki.fi/dali/) to identify a larger pool of experimentally determined structures for three select CA families, α, β and γ (Holm and Laakso 2016). The Dali server compares protein structures in 3D to identify biologically interesting similarities that may not be detected by comparing sequences alone.

A set of CAs from the α, β, and γ families with diverse surface charges representing three distinct structural classes was identified to evaluate variations in pH optima and range. These CA variants were further computationally designed to have a broader range of surface charges relative to the native variants.

Milestone 1.1.2: Demonstrate a carbonic anhydrase variant with an active half-life of 10 hours at pH 6.

Milestone 1.1.2 was achieved by demonstrating a carbonic anhydrase (CA) variant with an active half-life of 10 hours at pH 6. The task involved testing the retention of activity in the CA variants under specific conditions. The process included trials to measure how effectively the CA variant remained active over time and under varying pH levels.

CA hydration assays were performed with 10 nM of protein titrated with 20 mM CO_2 in a solution with different salinity levels (0, 10 and 35 ppt), and with an MES buffer that regulated the start pH at 6.3. The drop of the pH upon addition of CO_2 was very rapid and the initial speed of the reaction was calculated considering three consecutive pH readings in the buffering range of MES (>5.5). All tests were done in sextuplicates and average k_{cat} values were calculated for each of the above conditions after subtracting the non-enzymatic reaction rates for every given experimental condition. Enzymes were expressed and purified at over 98% purity.

The A3 variant from *Methanosarcina thermophila* TM-1 was found to have the highest k_{cat} values at pH 6.3 in 0, 10, and 35 ppm salinity level. Thus, A3 was chosen for activity retention testing. As shown in Figure 1-1, variant A3 maintains 51% and 49% of the initial CO_2 hydration activity after incubation for 10 and 20 h, respectively, in a 10 ppt solution at pH 6.3. In the 35 ppt salinity solution, A3 maintains its activity by 54% and 40% at the same time points.

The A3 variant is a natural CA variant from *Methanosarcina thermophila* TM-1, an anaerobic methanogenic archaeon isolated from a thermophilic sludge in California. This well-known enzyme (Cam) belongs to the γ-class of carbonic anhydrases that are ubiquitously found in Bacteria and Archaea and are less frequently found in Eukaryotes (so far only in photosynthetic organisms). The functional protein is a homotrimer with well described divalent metal-coordinating active sites formed in the interfaces of the monomers. Cam has the properties of a secreted protein and on top of its ability to hydrate/dehydrate carbon dioxide/bicarbonate it plays a role in capturing acetate from the extracellular environment and facilitating the growth of *Methanosarcina* in acetate. At low pH values, the catalytic activity of the enzyme is expected to drop. However, our results demonstrated that activity is at a detectable level at lower pH and furthermore, it remains over time under those same experimental conditions of high salinity/low pH.

Subsequently, additional CA variants were expressed, purified, and tested. A total of 12 variants, (6 natural and 6 computationally designed) were tested at three different salinity levels (0, 10 and 35 ppt) and three different pH set points. Several of the variants tested stand out as the having to promise to perform well for the hydration

of carbon dioxide at high salinity/low pH environment (Figure 1-2). A3, E1, F1 and E3 were selected as the most promising variants to scale up for testing in the hydrogel membranes.

In addition, a database-mining approach was used to identify potential CA variants in bacteria from acidic environments. This led to the identification of CAs from *Sulfobacillus thermosulfidooxidans* (stCA) and *Leptospirillum ferriphilum* (lfCA). These were cloned into pET15b in *E. coli* BL21(DE3). Furthermore, *Human carbonic anhydrase 9* (hCA9), reported to be functional at low pH, was cloned and expressed in the same way. A plate reader assay was developed to measure CA activity with bomothymol blue or methyl red. The activity of the three variants was compared to bovine CA (Sigma). All three overproduced CAs showed good activity at pH 6.11 with methyl red (Figure 1-3), while bovine CA had almost no activity. Of the three novel CAs tested, hCA9 was most active at pH 6.11 and 8.31; however, this might be a function of the expression level.

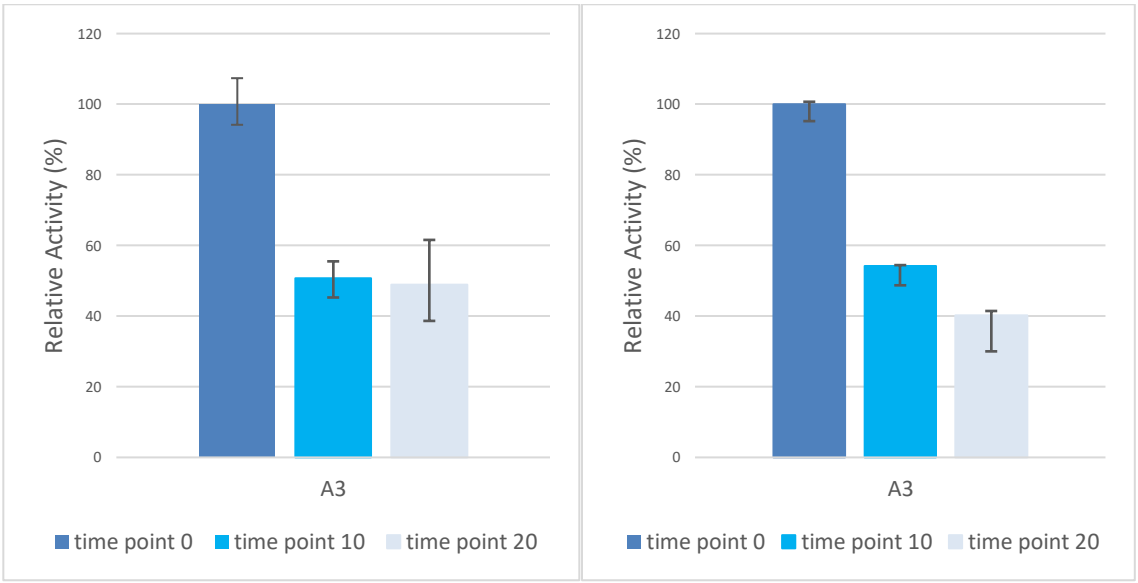

(A) (B)

Figure 1-1: Relative activities for A3 (Cam) variant at pH 6.3 and at (A) 10 ppt and (B) 35 ppt salinity showing retention of activity by 50% or more after 10 h incubation.

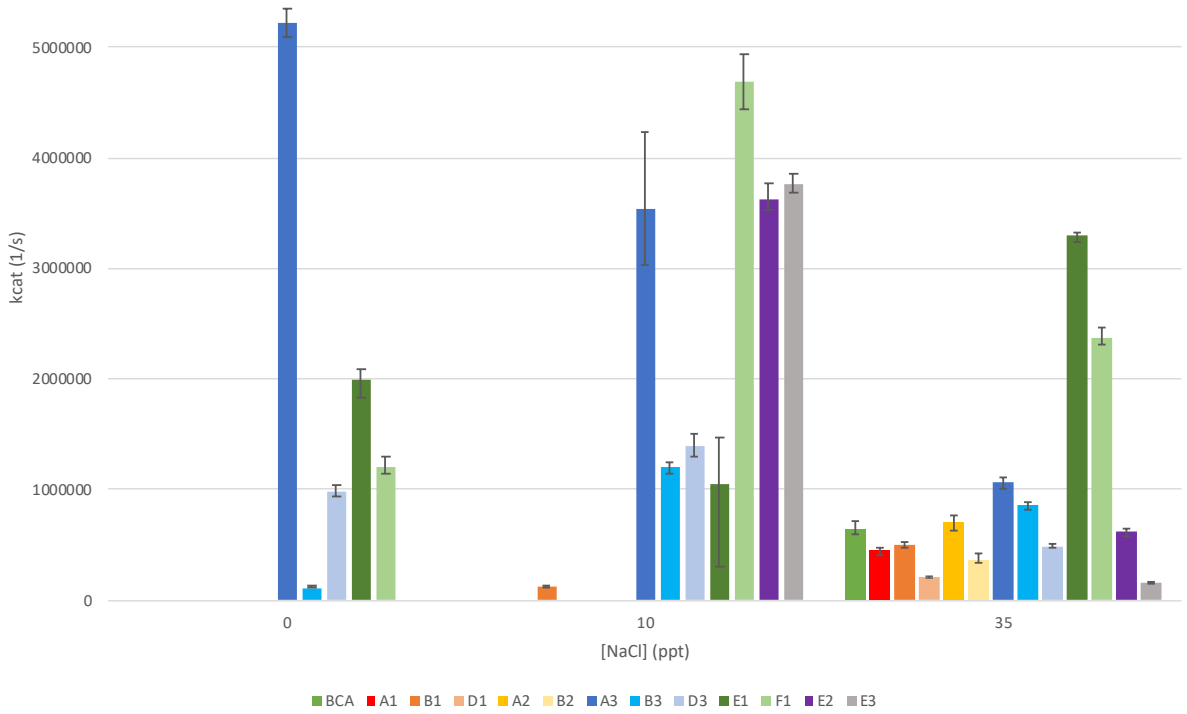

Figure 1-2: k_{cat} values calculated for 12 different CA variants plus the commercially available BCA used as a control at a solution of pH 6.3. The experimental conditions are like those expected in the hydrogel membrane representing a local low pH environment in the pond environment.

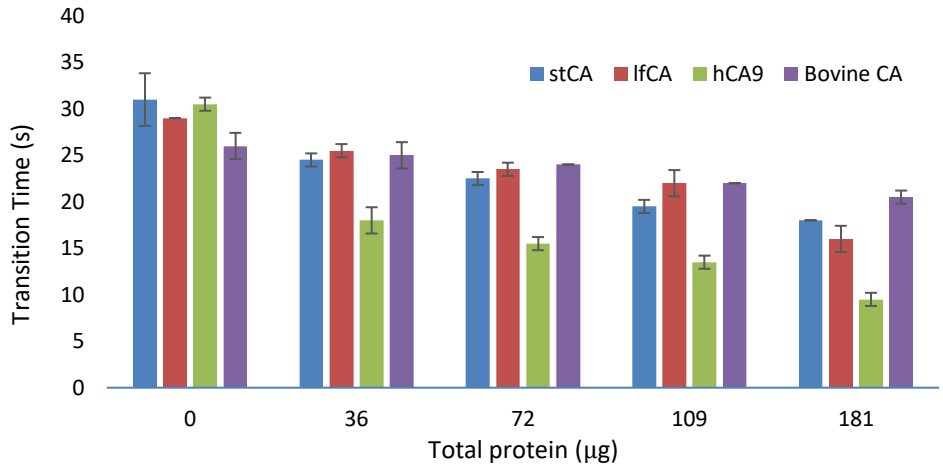

Figure 1-3. Transition time (for a specific pH change) of stCA, lfCA, hCA9 and bovine CA at pH 6.11 with methyl red. Shorter bars correspond to higher activity.

Subtask 1.2: Preparation and characterization of carbonic anhydrase membranes

Milestone 1.2.1: Demonstration of bicarbonate transfer into an aqueous phase from gaseous CO_2 using small-scale (< 10 cm^2) CA membrane.

CA has been integrated into a variety of polymeric membranes and materials for the purpose of carbon sequestration. There has not yet been a report of using a CA-based membrane for carbon delivery into algal cultivations. Using a CA membrane overcomes important limitations of membranes that only transfer CO_2 from the gas phase to a liquid phase. If that liquid phase is water, fluxes are limited by the driving force since CO_2 is present on both sides of the membrane.

The material initially applied for CA immobilization was a hydrated membrane structure based on a thermoplastic elastomer hydrogel that remains highly elastic and mechanically resistant to fatigue even at hydration levels exceeding 90 wt%. This hydrogel design allows direct application of a precursor solution as a thin coating or film to any solid support, prior to rapid crosslinking by low intensity UV-A light exposure. Since the crosslinking is achieved without any chemical additives, there is no residual chemical to inhibit enzyme activity. The solvated poly(ethylene oxide) matrix within the hydrogel intrinsically enhances localized CO_2 solubility and provides a stabilizing environment ideal for maximizing active enzyme lifetimes. However, it was unknown whether the brief UV-A exposure would damage the entrapped CA. Thus, work on this task began with development of methods to entrap the enzyme in the hydrogel followed by evaluation of the effect of UV-A exposure on the CA activity.

Bovine CA was used for the tests to achieve this milestone. The synthesis of ω-anthracenylpolystyrene-b-poly(ethylene oxide) diblock copolymer (polystyrene-b-poly(ethylene oxide)-anthracene, SO-An) was done by a method that allows for exact control over block molecular weights, overall composition, chain-end functionality, and melt morphology. Two methods were used to crosslink the hydrogel: (1) A method using a low intensity, highly efficient LED source (365 nm ± 5 nm) (described in the Q1 report); and (2) A method using a broad spectrum Omnicure S200 Mercury Vapor Lamp. Method 1 has been used to crosslink both 5 wt% and 10 wt% block copolymer micelle solutions into elastic solids of fixed shape, exhibiting excellent long-term stability (retention of shape and mechanical elasticity) over 1-month soak times in aqueous solutions. Method 2 was used for these milestone tests during the time between use of a demonstration LED source and our purchase of a larger version of that source. The CA assay selected was adapted from: http://www.worthington-biochem.com/CA/assay.html, although the immobilization of the enzyme in the membrane limits comparisons with guaranteed activities of free CA in solution to which commercial certificates of analysis refer upon purchase. The procedure used to determine membrane-immobilized CA activity relative to non-CA containing "blank" solutions was to first measure a reference (blank) rate of pH change. Enzyme activity in the gel was calculated as:

$$\text{enzyme activity}\left(\frac{\text{units}}{\text{mg}}\right) = \frac{2 \times (t_0 - t_a)}{t_a \times m}$$

where m = the mass of enzyme in the gel. This mass was calculated from the known mass of the hydrogel membrane added to the buffer solution, and the concentration of CA enzyme in the precursor solution used to form the membrane. As an additional control, this procedure was then repeated in the presence of CA enzyme-loaded hydrogel precursor gels that had not been exposed to UV irradiation.

The results of the CA activity assay are presented in Table 1-1. CA activity was determined for both hydrogel membranes that had been exposed to UV light (cured) and those that had not (uncured). Four replicates were run in each case. CA was loaded into the membranes at 0.005 mg/ml in both cases, with the membrane masses examined distributed between 61 and 135 mg total. Note that the calculated activities are normalized by the mass of CA present.

The data demonstrate that the immobilized CA within the hydrogel membrane can successfully transfer bicarbonate into an aqueous phase from dissolved gaseous CO_2 using small-scale (< 10 cm^2) CA membrane.

Table 1-1. Carbonic anhydrase (CA) activity measured in both UV cured and uncured hydrogel membranes.

Sample	[CA] in membrane (mg/ml)	Mean activity (units/mg CA)
UV-cured (n=4)	0.005	182 ± 41
Uncured (n=4)	0.005	181 ± 61

Milestone 1.2.2: Demonstration of bicarbonate transfer into an aqueous phase from gaseous CO_2 using small-scale (< 10 cm^2) CA membrane with flux greater than 10^{-5} mol/s·m^2 maintained for at least 1 day.

The overall goal of Subtask 1.2 was to develop membranes that convert gaseous CO_2 to aqueous bicarbonate solution. This was accomplished using CA embedded in the membrane. Such an enzymatic membrane can achieve high bicarbonate delivery fluxes into the aqueous phase, which can then be delivered to an algal growth pond. CA-containing membranes were produced with different concentrations of CA and different hydrogel formulations. The membranes were tested in a module consisting of a modified dead-end filtration unit in which the feed-side gas is separated from the receiving aqueous phase by a sealed CA membrane.

To immobilize the CA, a photoreactive block copolymer hydrogel network was used. The hydrogel material is comprised of a spherical micelle-forming block copolymer species: photoreactive ω-anthracenylpolystyrene-*b*-poly(ethylene oxide) diblock copolymer (SO-An). Carbonic anhydrase (Worthington Biochemical Corporation, activity of 4,030 U/mg dry weight) was used at a concentration of 0.5 mg CA/mL DI water for the carbonic anhydrase swelling solution. The water-only membranes were made as a control to compare the rates of inorganic carbon production of a membrane with and without carbonic anhydrase.

The hydrogel membrane stability and bicarbonate flux were improved by sandwiching the hydrogel between a hydrophobic filter membrane layer and a metal mesh screen layer (Figure 1-4). Previously, the hydrogel was molded and cross-linked in a thin layer on top of a porous hydrophilic filter membrane. However, it was determined that CO_2 would first have to dissolve into the water-filled pores of the hydrophilic membrane and then diffuse through the pores before it would reach the hydrogel, which significantly slowed gas diffusion and reaction. Therefore, by incorporating a hydrophobic PVDF membrane (0.45 µm pores, 75% porosity), water would be excluded from the filter membrane pores and the hydrogel would be in direct contact with the gas-filled pores. Additionally, the addition of a mesh screen layer (~1 mm x1 mm pores, ~75% porosity) on the solution side of the membrane allowed for higher gas pressures to be applied to the membrane.

The inlet on the lower chamber of the membrane holder was connected to a regulated CO_2 line. The exposed DI water was collected into vials and held at room temperature with minimal headspace to avoid CO_2 degassing from solution. Dissolved inorganic carbon (DIC) measurements were taken of the sample water at the end of each timepoint using a Shimadzu TOC-L Laboratory Total Organic Carbon Analyzer.

Testing of the updated prototype design and hydrogel membrane manufacturing resulted in improved transfer of bicarbonate that met Milestone 1.2.2 by producing inorganic carbon fluxes greater than 10^{-5} mol/s·m^2 for at least 1 day. Figure 1-5 and Table 1-2 show that bicarbonate flux indicated via pH and determined from samples for DIC content was steady over 24 hours for two different membrane modules, one with CA and one without. Incorporating CA significantly improved bicarbonate flux. Furthermore, a test in which the CO_2 pressure was increased from 3 psi to 7 psi resulted in a 213% increase in carbon flux.

In subsequent tests, we determined that the SO-An hydrogel presented significant mass transfer limitations because it could not be cast thin enough. As an alternative, we used a thin-film of covalently attached BCA hydrogel with bovine serum albumin (BSA) as the matrix and crosslinking via glutaraldehyde. The BSA-based hydrogel covalently binds both the BSA and BCA together via several functional groups found in proteins, which could provide a more stable concentration of BCA within the membrane over time. Additionally, the use of an aqueous-based casting solution is less detrimental to enzyme activity and is easily cast into a thin layer on the surface of the carrier membrane. Tests demonstrated that BCA in the BSA hydrogel membrane provided an increase in carbon flux of approximately 25% more than the flux through BSA-only hydrogel membrane (Table 1-3). The BSA-based CA membranes retained at least 25% of their enzyme activity after two months when stored at 4 °C, indicating good long-term stability.

Table 1-2. Two trials measuring dissolved inorganic carbon (DIC) flux through two membrane modules, one with hydrogel only and one with CA-encapsulated hydrogel run continuously over 25 hours at 3 psi.

	Membrane	Time (h)	DIC (mg/L)		Δ DIC (mg/mL)	Flux (mol/m²·s)
			Inlet	Outlet		
Trial 1	Hydrogel only	1	1.226	7.473	6.247	2.83E-06
		15	1.665	8.270	6.605	2.99E-06
		25	2.055	7.848	5.793	2.62E-06
	CA Hydrogel	1	0.5233	25.45	24.93	1.13E-05
		15	0.7165	27.23	26.51	1.20E-05
		25	1.008	27.64	26.63	1.21E-05
Trial 2	Hydrogel only	1	1.013	44.14	43.13	1.95E-05
		15	0.6754	44.62	43.94	1.99E-05
		25	1.756	45.34	43.58	1.97E-05
	CA Hydrogel	1	1.525	123.4	121.9	5.57E-05
		15	0.9246	52.50	51.58	2.31E-05
		25	1.100	49.84	48.74	2.22E-05

Table 1-3. Estimated carbon flux across different fabricated hydrogel membranes cast on hydrophobic PVDF (0.45 µm pore diameter) carrier membrane. *Based on previously determined relationship between measured pH and inorganic carbon (IC) concentration with added CO_2 in 50 mM phosphate buffer. The membrane area was 375 mm^2 in 35 ppt NaCl, pH 7.85 and 50 mM phosphate buffer at 0.6 mL/min.

Membrane	CO_2 Gas Pressure (psi)	Estimated* ΔFlux (mol/m²·s)
UV-Hydrogel	3	1.6E-04
Toluene cast hydrogel	0.5	2.8E-04
BSA Hydrogel	0.5	2.4E-04
BSA+BCA Hydrogel	0.5	3.0E-04

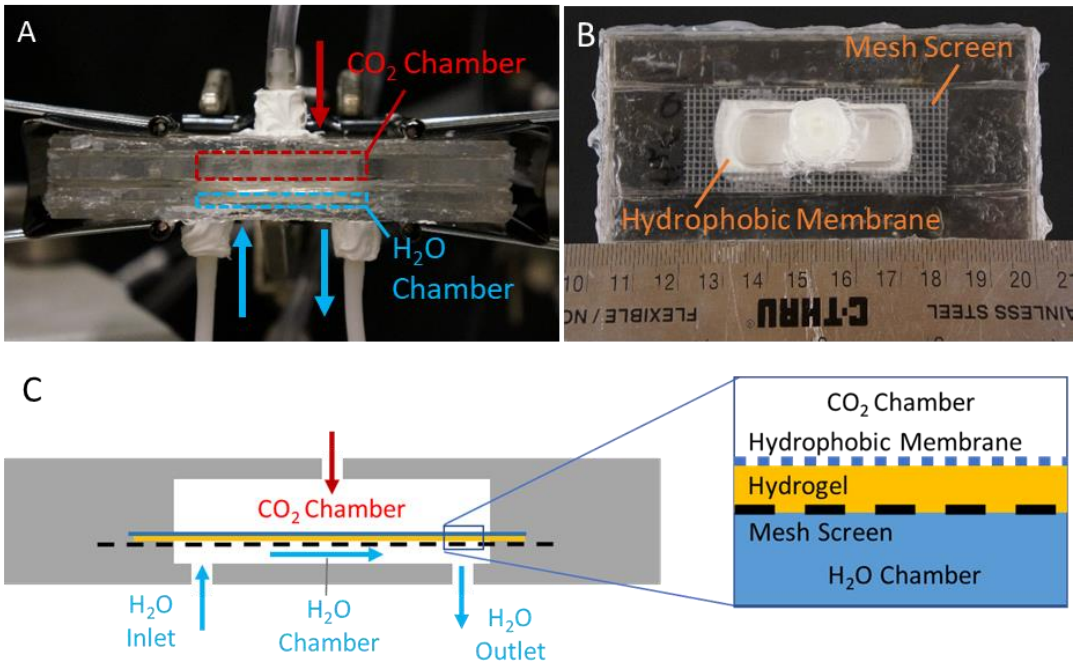

Figure 1-4. Photos of the miniature membrane module used for flux testing with the (A) side view labeled for gas and fluid chambers and the (B) top view labeled with membrane components and (C) side view schematic of gas and solution chambers with flow and membrane components.

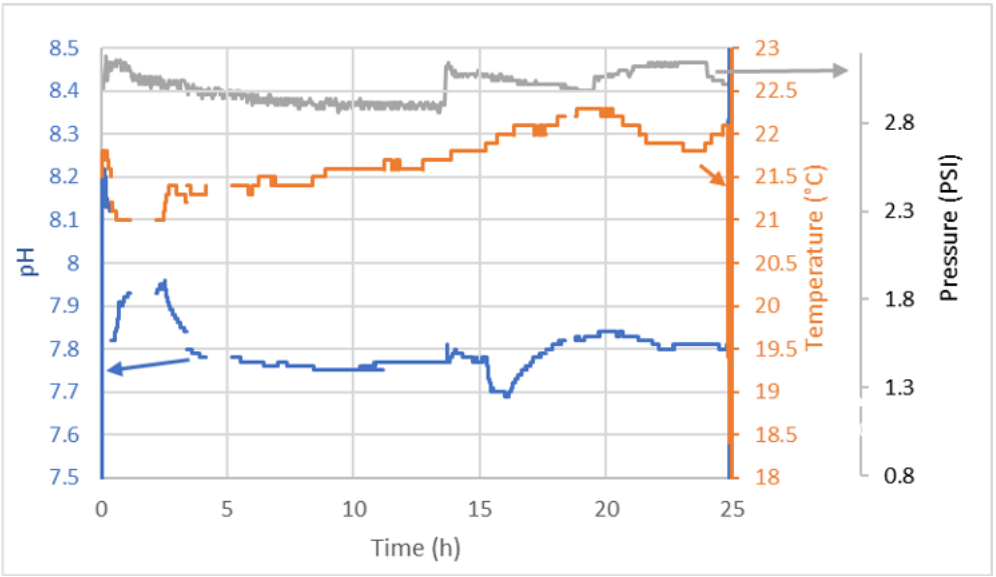

Figure 1-5. Plot of continuously measured CO_2 gas pressure applied to a CA-hydrogel membrane module and the measured resulting pH and temperature of 20 mM phosphate buffer (starting pH 8.2) flowing out of the module.

Subtask 1.3: Construction, process modeling, and testing of CO_2 transfer module

Milestone 1.3.1: Demonstration of initial prototype module function for delivery of inorganic carbon into an aqueous phase.

The overall goal of this task is to develop and test a prototype membrane module capable of converting gaseous CO_2 to aqueous bicarbonate solution. The purpose of this module was to improve the efficiency in which carbon dioxide can be converted to bicarbonate. This was accomplished using CA embedded in the membrane. Such an enzymatic membrane can achieve high bicarbonate delivery fluxes into the aqueous phase, which can then be delivered to an algal growth pond. The initially developed prototype module consisted of a modified dead-end filtration unit in which the feed side gas is separated from the receiving aqueous phase by a sealed CA membrane. Initial testing was conducted without aqueous phase stirring and low-pressure CO_2 on the gas side of the membrane.

Bovine CA was immobilized in the photoreactive ω-anthracenylpolystyrene-*b*-poly(ethylene oxide) diblock copolymer (SO-An). Enough polymer material was placed on the center of a 47-mm diameter hydrophilic PVDF filter disk (Sterlitech, 0.45-μm diameter pores) to cover a ≥22 mm diameter area. The hydrogel coated filter disk was compressed between two panes of 1/8" thick quartz glass separated by metal washers of 0.5 mm thickness to set the membrane thickness and held in place using binder clips. A vacuum filtration flask with a 47-mm filter cassette (Millipore Sigma) was used to evaluate CO_2 transfer across fabricated membranes. Pressure in the lower chamber was maintained at 1 atm over 1 hour, 6 hours, and 24 hours. Dissolved inorganic carbon (DIC) measurements were taken of the sample water at the end of each timepoint using a Total Organic Carbon Analyzer.

Due to the partial pressure of CO_2 in the atmosphere, equilibrated deionized water contains approximately 0.5 mg/L dissolved CO_2 at standard temperature and pressure. This concentration was corroborated using the TOC analyzer for blank measurements of DI water for DIC content. DIC detection measures inorganic carbon in the forms of carbon dioxide, carbonic acid, bicarbonate anion, and carbonate anion. DIC measurements of DI water samples exposed to 100% CO_2 gas through fabricated membranes contained slightly more DIC than unexposed DI water (Table 1-4). Longer exposure to CO_2 gas resulted in higher DIC content in solution. The developed module successfully delivered inorganic carbon to solution. It was anticipated that fabricating thinner membranes and increasing membrane surface area will improve the solubilization rate of CO_2 into aqueous solution.

In addition, a senior design team from the Department of Chemical and Biological Engineering at CSU developed and applied a mathematical model of the membrane module. The module was represented as a three-compartment system (Figure 1-6). Control volume 1 (CV-1) consists of the portion of the reactor where CO_2 diffuses into the hydrogel membrane. Due to the solubility of CO_2 in water at ambient pressures, this portion is amenable to analysis via Henry's law as the mole fraction of CO_2 in the aqueous membrane will generally be quite small (< 0.03). CV-2 corresponds to the interior of the membrane and is where simultaneous diffusion and reaction of the species of interest occur. This section was described with the

appropriate form of the reaction-diffusion equation in which each species diffuses in the z-direction (through the membrane) while simultaneously reacting. CA is known to demonstrate Michaelis-Menten kinetics, and the modeling work was conducted using literature data for an enzyme with pH optimum of 8.5. CV-3 represents the water sweep stream where convection mass transfer carries the bicarbonate/CO_2 away from the membrane surface. This section can be modeled with the convection-diffusion equation where each species diffuses in the z-direction (into the sweep stream) and advects in the x-direction (along the membrane surface).

Equations representing the reaction and mass transfer phenomena in each region were solved numerically for a system at 25 °C. Figure 1-7 shows the concentration profiles of both CO_2 and bicarbonate within the membrane as a function of the z-coordinate (membrane thickness) for one example CA concentration.

The concentration profile in the aqueous flow passing across the membrane depends on the flux through the membrane and the flow characteristics. Figure 1-8 shows the concentration profiles in the liquid compartment of the membrane for different liquid flow rates. The membrane is located at z=0. Plots are shown for a range of the Peclet number, Pe_L, representing the ratio of convective mass transfer to diffusive mass transfer. PeL is calculated as

$$Pe_L = u_\infty L/D = Re_L Sc$$

where Re_L is the Reynolds number and Sc is the Schmidt number. The latter is not a function of flow characteristics, so flow affects Pe_L and mass transfer via Re_L. Smaller Pe_L predict further penetration of the boundary layer into the free stream (greater boundary layer thickness) while Pe_L =10000 results in a boundary layer that is barely visible. Thus, more turbulence enhances mass transfer rates in this system.

Table 1-4. DIC measurements of DI water exposed to CO_2 in the prototype module.

Sample	**DIC Measurements (mg/L)**	
DI water	0.5 mg/L	
Exposure Time	Control Membrane	CA Membrane
1 h	0.8	0.7
5.5 h	1.8	1.2
19.5 h	2.3 2.2	4.9 2.8

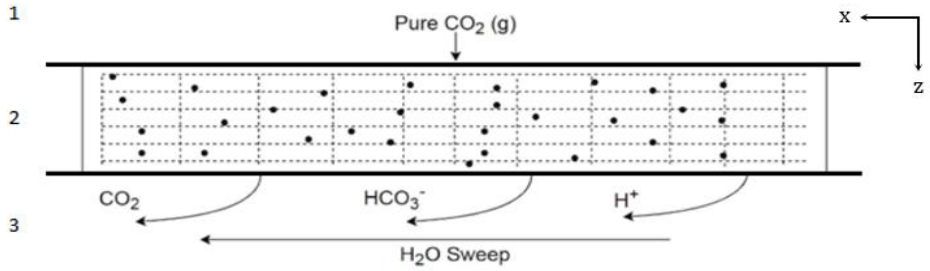

Figure 1-6. Physical model of the enzyme membrane system.

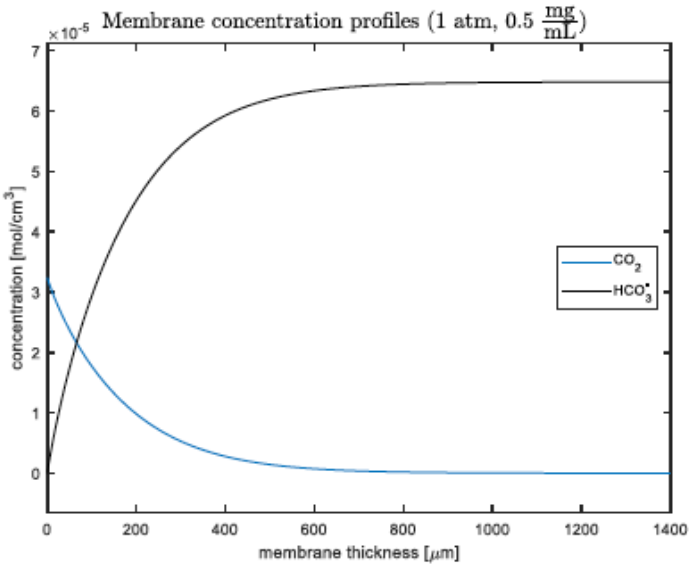

Figure 1-7. Membrane interior concentration profiles for CO_2 and bicarbonate at CO_2 pressure of 1 atm and a uniform membrane CA concentration of 0.5 mg/mL.

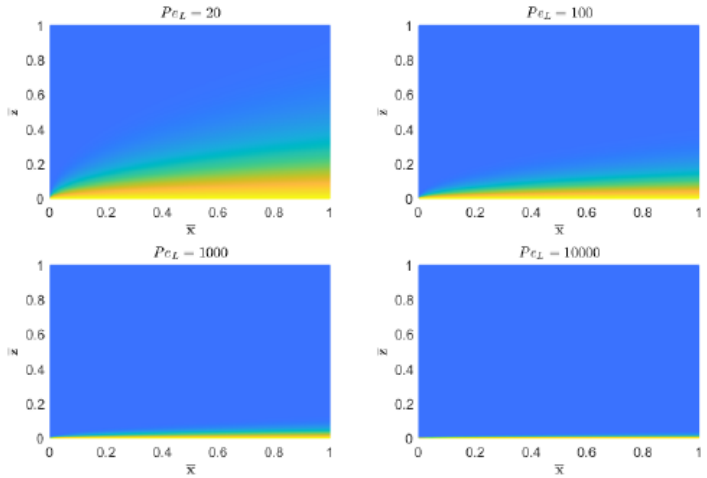

Figure 1-8. Concentration profiles inside sweep, above membrane, for various Peclet numbers.

Task 2: Engineering of *Nannochloropsis oceanica* for enhanced carbon uptake

Subtask 2.1: CCM engineering in N. oceanica

Milestone 2.1.1: Show expression of a reporter protein such as YFP in at least two separate transformation events.

Expression of transgenic bicarbonate transporters is a key goal of our experimental efforts. However, there is no documented transformation event for strain CCAP84910 in the published literature. *Nannochloropsis* is a Eustigmatophyte alga and is classified within the Stramenopile supergroup of eukaryotes. Numerous other strains of *Nannochloropsis* have been transformed successfully. Gene expression in this group has been successful using native promoters. Specifically, other strains of *N. oceanica* have been successfully transformed using a native bidirectional promoter. We adopted the methodology published by Poliner *et al.* (2018a,b), and Poliner *et al.* (2019) for our first round of transformation experiments. Details for this protocol and its successful application are provided below.

All experiments were carried out in f/2 medium and 24-hour light. Light fluxes ranged from 80-250 µmol photons m^{-2} s^{-1}. Strain screening was carried out in 24 well plates or 50 mL flasks, both with continuous agitation. All base plasmids for *Nannochloropsis* were obtained from AddGene. All PCR and cloning experiments were conducted according to methods standard in the field.

The transformation of *N. oceanica* CCAP 849/10 was performed by slightly modifying existing electroporation protocols used for other strains of *Nannochloropsis* (Vieler et al. 2012). Total RNA was isolated using TRIZOL according to the manufacturer's protocol. RNA (0.4 mg) was used to make cDNA using the Invitrogen Superscript III First Strains Synthesis Kit. RT-PCR was performed using the Promega GoTaq Kit. Amplicons were visualized using standard electrophoresis protocols. GFP fluorescence and cell counts were measured using a BD Accuri C6 flow cytometer equipped with a blue excitation laser. One-week old *N. oceanica* cells were used for protein extraction.

Several different transformation vectors were created while developing transformation protocols. Most were based around the bidirectional promoter originally described by the Farre group (Poliner et al. 2018a,b), which allows for the transcription of both the antibiotic selection cassette as well as the target gene. A full list of promoter/gene expression cassettes is given in Table 2-1.

The Neomycin resistance gene (NeoR) in our expression plasmid confers resistance to G418. After selection on 500 µg/ml G418 f/2 agar plates, two to three weeks old resistant colonies were subcultured in liquid f/2 media in the presence and absence of 500µg/ml G418 to confirm antibiotic resistance. Three wild type and 15 independent transgenic lines were cultured in 24-well plates. WT cells grew only in the absence of antibiotics, whereas transgenic lines grew in both conditions, suggesting the presence of the transgene in the selected resistant colonies. We also showed the integration of the expression cassettes into the *N. oceanica* genome in randomly selected GFP_BicA transgenic lines using PCR with primers directed specifically at the BicA gene.

We used endpoint RT-PCR to observe the production of both GFP and BicA-GFP transcripts (Figure 2-1). We demonstrated the production of transcripts encoding actin, GFP, and the BicA protein in several independent lines. Note that we did not get successful amplification of actin in all strains. All TKK strains should contain the BicA-GFP construct, while NOC_GFP strains should only contain the GFP transcript. We observed GFP transcripts in 75% of all tested strains and BicA in 75% in the TKK transformants. Each strain represents an independent transformation event.

We verified the expression of GFP using two independent techniques. The first used flow cytometry to identify transformants with GFP expression. Figure 2-2 shows the characterization of 24 independent transformants, all with GFP fluorescence above the WT (A). These strains were created with the TKK063 vector, which drives GFP and antibiotic selection using a bidirectional promoter. Figure 7B shows a fluorescence histogram comparing a WT and single transformant culture. This illustrates that every cell within the transformant population maintains a high fluorescence relative to WT.

The second technique to verify the expression of GFP involved using a GFP-specific antibody to detect GFP in protein extracts of CCAP84910 using standard immunoblotting techniques. We looked at two independent expression systems, one containing a BicA-GFP fusion protein and the other a GFP-Aqueorin fusion protein. This revealed high molecular weight bands associated with both expression systems and low molecular weight bands of approximately 25kDa that represent the GFP protein alone. We presume this was due to degradation of the fusion protein *in vivo*.

Table 2-1. List of vectors, their promoter system, and number of independent transgenic lines showing GFP/eYFP fluorescence. BicA is the bicarbonate transporter from cyanobacteria. TKK012 and TKK013 are N-terminal and C-terminal GFP fused BicA constructs, respectively. TKK063 is the GFP-expressing control plasmid. pNOC_Stacked_GFP_aequorin plasmid is a GFP-tagged aequorin expressing control plasmid. pRIBI is a bidirectional promoter used to express both GFP or GFP tagged genes and NeoR/KanR are antibiotic genes used for selection. pNR is the nitrate reductase promoter from *Phaeodactylum tricornutum*. pCIP1 is diatom infecting viral promoter. p35S is the cauliflower mosaic virus promoter. pH4 is the Histone 4 promoter from *Phaeodactylum tricornutum*. pEF2 is elongation factor 2 promoter from *Phaeodactylum tricornutum.*

Vector Name	Expression promoter	Gene	Positive transformant Identified
TKK012	pRIBI	GFP_BICA	78
TKK013	pRIBI	BICA_GFP	80
TKK063	pRIBI	GFP	24
pNOC_GFP_Aequorin	pRIBI	GFP_Aequorin	81
TKK059	pNR	eYFP	15
TKK060	pCIP1	eYFP	15
TKK061	p35S	eYFP	15
TKK062	pH4	eYFP	24
TKK064	pEF2	eYFP	24

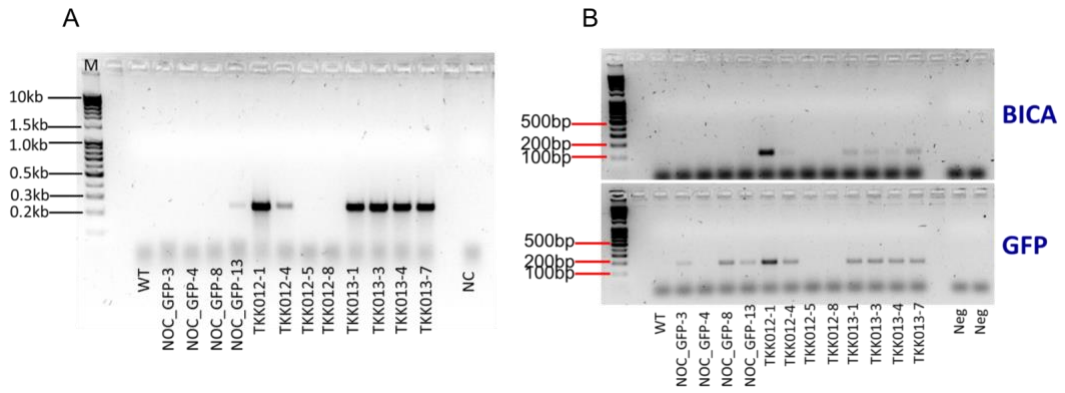

Figure 2-1 – Images of DNA electrophoresis gels showing amplification of DNA products associated with the actin (A), BicA and GFP (B) RT-PCR reactions. NOC_GFP strains do not contain the BicA gene, while all strains, save WT, will contain that GFP gene. NC and Neg indicate negative controls. Absent bands in (A) suggest RNA levels below detection limits.

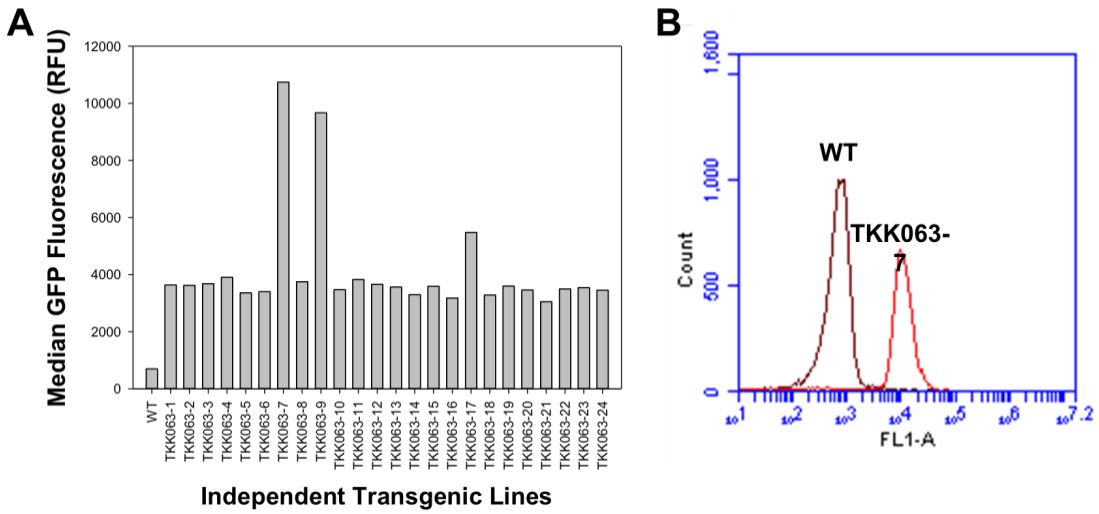

Figure 2-2 – High GFP fluorescence in independent transgenic CCAP84910. (A) Median cell fluorescence at 533/30 nm via flow cytometry. (B) Histogram comparing populations of transgenic, GFP expressing cells (TKK063-7) and WT cells.

Subtask 2.2: Strain adaptation to high bicarbonate levels and lower pH

Milestone 2.2.1: Demonstration of optimized parameters for selection strategy in indoor photobioreactors under continuous cultivation for enrichment of mutagenized population under continuous selection stress in the presence of high bicarbonate concentration.

The goal of this milestone was to demonstrate the environment and parameters needed for developing a selection strategy in indoor photobioreactor systems. To achieve this, we built a capability to vary the inorganic carbon (Ci) concentration (as

bicarbonate concentration) independent of changes in pH in indoor reactors and varied the concentration until a significant growth defect was observed. Under the conditions tested, pH 8 and Ci concentrations between 2 and 150 mM, we demonstrated a 20% growth defect that is solely linked to Ci concentration. This environment was used to test for improvements by mutant strains.

The resistance of *N. oceanica* CCAP84/910 to different oversaturating Ci concentration was assessed in a modified Sea water medium (D-ASM), adapted from the UTEX ASM media by changing the following parameters: The Tricine buffer 25 mM was replaced by Tris Buffer 10 mM to decrease the organic buffering capacity, the NH_4 and NO_3 were replaced by 5 mM urea to ensure that the medium alkalinity remained constant, the B12 vitamin was replaced by a mix bringing the final vitamin concentrations to cyanocobalamin 3.69 $x10^{-10}$ M, biotin 2.05 $x10^{-9}$ M, thiamin 2.96 $x10^{-7}$ M. While the $NaHCO_3$ concentration increased from culture to culture the total Na concentration was kept stable at 300 mM with NaCl, creating a medium salinity comparable to 17.5 ppt sea water. The culture started at 0.010 OD750 and was diluted back to about 0.08 after 3 days and the growth rate was measured over the following 12 h. The pH of the culture was kept stable at 8.0 using a proportional CO_2 injection system controlled and logged using Arduino-based microcontrollers (Figure 2-3). This system avoids overshoots often observed with pH controllers and allows Ci uptake monitoring in real culture conditions. The temperature was kept stable at 27.5 ºC with a water bath and the light was constant at 270 uE. The control of the pH by Arduino was done with an Arduino nano every, an Atlas scientific pH module with customer grade probes, three-point calibrated at 20 ºC before the beginning of the measurements. The pH measurement was not temperature compensated.

We demonstrated that the Arduino-controlled system can keep the culture pH stable (+/-0.01 pH unit) even at very low Ci concentration, without overshooting the CO_2 concentration beyond the 0.1 pH unit. It also suggests that the voltage reading from the mass flow controller can be used as a readout of the real-time Ci consumption at different Ci concentration.

We used the Arduino-controlled system as a mimicked light and temperature system for controlled growth with continuous CO_2 delivery. To demonstrate the environment and parameters needed for developing a selection strategy, we built a capability to vary the inorganic carbon concentration (as bicarbonate concentration) independent of changes in pH in indoor reactors and varied the concentration until a significant growth defect was observed. Under the conditions tested, pH 8 and Ci concentrations 2-150 mM (as $NaHCO_3$), we demonstrated a 20% growth defect that is solely linked with Ci concentration. We observed that the increase of Ci in the media over 6 mM doesn't favor the growth of *N. oceanica* (Figure 2-4). The 2 mM base concentration reflects the concentration of Ci in sea water. Based on these data, we proceeded with selecting for mutant strains that are able to overcome the growth defect seen at IC concentrations over 20 mM (or > 240 ppm).

Figure 2-3. Setup used for the proportional CO_2-controlled injection based on pH as well as CO_2 consumption monitoring. B/Cube function used to correct the pH by sending a voltage to the mass flow controller.

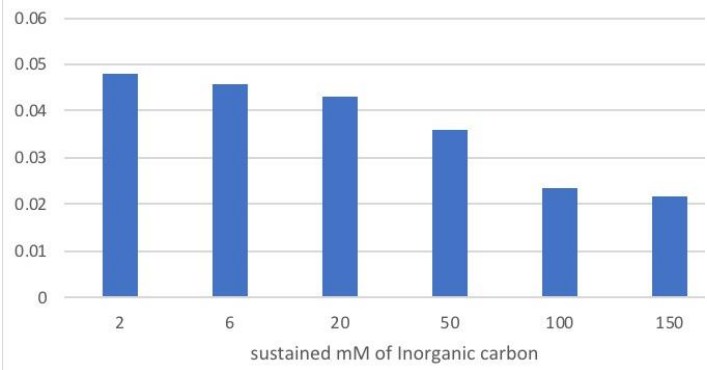

Figure 2-4. (A) Influence of oversaturating Ci concentration on growth rate of *N. oceanica* measured using OD750, (B) Growth rate calculated using the fitting curve of the growth rates.

Subtask 2.3: Characterize novel strains

Milestone 2.3.1: Initial photophysiological and systems biology comparisons of the responses of the bicarbonate transporter engineered N. oceanica strains to high and low bicarbonate levels, demonstrating upregulation of carbon assimilation metabolic cascade in the engineered strain. Nannochloropsis oceanica *CCAP84910 genome sequenced and initial annotation completed.*

Strain modifications, whether targeted or random, can be understood and improved upon with careful characterization. To facilitate this in *N. oceanica*, we sequenced and performed initial annotation. The resulting database was used in proteomics analysis of this strain. Photophysiological characterization was part of Subtask 2.1.

Paired end-read Illumina sequencing was conducted with 3.94M reads for a total of 118kM bases. After filtering, the sequencing was found to have 3144 scaffolds, of which 1546 were longer than 1000 bp. Upon assembly using tools at LANL, the genome was found to be 30.96 Mbp. The corresponding protein database has 11131 entries, significantly more than the only other *N. oceanica* database (IMET1) with 9915 entries. The LANL pipeline led to annotation of 6173 (55.5% of the total) entries. No entries in the previous IMET1 database are annotated.

Proteomics method development (using WT *N. oceanica*) involved comparison of extraction methods (in-solution vs. filter-assisted; urea vs urea + sodium deoxycholate); comparison of scan ranges; comparison of database search algorithms; and evaluation of GRAVY (hydrophobicity) values. The resulting optimized method (extraction with 8M urea + 2% sodium deoxycholate) yielded identification of 1344 proteins and 4249 peptides.

The proteomics methodology was applied to samples from cultivations of WT and WT::BicA strains. Each strain was cultivated in 5% CO_2 or air, in duplicate.

A list of the proteins that were found to be differentially abundant ($p < 0.05$) in the BicA mutant vs. in the WT when both were grown in 5% CO_2 is presented in Table 2-2. The protein identifications were obtained using the genomic sequence and annotation developed in this project. Thirty-four proteins were significantly more abundant in the mutant than in the WT and 23 were less abundant.

Table 2-2. Differentially abundant proteins between the BicA mutant and WT strains of *N. oceanica* grown in duplicate in shake flasks in a 5% CO_2 atmosphere.

Description	Abundance ratio (BicA/WT)	p value	Coverage (%)	#Peptides
Similar to BGLU11: Beta-glucosidase 11 (Oryza sativa subsp. japonica OX=39947)	8.4	0.000	1	1
Similar to CEP1: KDEL-tailed cysteine endopeptidase CEP1 (Arabidopsis thaliana OX=3702)	0.61	0.000	2	1
Similar to iolG: Myo-inositol 2-dehydrogenase (Thermotoga maritima (strain ATCC 43589 / MSB8 / DSM 3109 / JCM 10099) OX=243274)	2.22	0.000	23	7
Similar to argG: Argininosuccinate synthase (Thermotoga neapolitana (strain ATCC 49049 / DSM 4359 / NS-E) OX=309803)	0.52	0.000	18	7
Similar to AF 2205: Uncharacterized protein AF 2205 (Archaeoglobus fulgidus	3.91	0.000	12	6

(strain ATCC 49558 / VC-16 / DSM 4304 / JCM 9628 / NBRC 100126) OX=224325)				
Similar to ydhF: Oxidoreductase YdhF (Escherichia coli (strain K12) OX=83333)	2.64	0.000	2	1
Protein of unknown function	301	0.000	0	1
Similar to Actin (Achlya bisexualis OX=4766)	1.76	0.000	35	12
Protein of unknown function	0.74	0.000	42	2
Protein of unknown function	2.96	0.001	10	1
Similar to UVH3: DNA repair protein UVH3 (Arabidopsis thaliana OX=3702)	0.76	0.001	1	1
Similar to CYP20-1: Peptidyl-prolyl cis-trans isomerase CYP20-1 (Arabidopsis thaliana OX=3702)	1.27	0.001	65	13
Similar to Histone H4 (Mastigamoeba balamuthi OX=108607)	1.90	0.001	39	7
Protein of unknown function	1.87	0.002	7	1
Similar to Fucoxanthin-chlorophyll a-c binding protein chloroplastic (Chattonella marina var. antiqua OX=859642)	1.93	0.002	15	2
Similar to FAO1: Long-chain-alcohol oxidase FAO1 (Lotus japonicus OX=34305)	0.68	0.004	1	1
Similar to Fucoxanthin-chlorophyll a-c binding protein chloroplastic (Chattonella marina var. antiqua OX=859642)	1.69	0.005	16	3
Similar to ACSBG2: Long-chain-fatty-acid--CoA ligase ACSBG2 (Gallus gallus OX=9031)	0.53	0.006	14	7
Similar to SRSF2: Serine/arginine-rich splicing factor 2 (Pan troglodytes OX=9598)	0.79	0.006	5	1
Similar to Cytochrome c (Abutilon theophrasti OX=3631)	0.76	0.007	11	2
Similar to fusA: Elongation factor G (Magnetospirillum magneticum (strain AMB-1 / ATCC 700264) OX=342108)	0.48	0.008	14	9

Similar to 14-3-3-like protein (Fucus vesiculosus OX=49266)	1.67	0.008	61	13
Similar to HERC1: Probable E3 ubiquitin-protein ligase HERC1 (Homo sapiens OX=9606)	0.46	0.008	0	1
Similar to GRXS15: Monothiol glutaredoxin-S15 mitochondrial (Arabidopsis thaliana OX=3702)	3.68	0.009	18	2
Similar to SMU2: Suppressor of mec-8 and unc-52 protein homolog 2 (Arabidopsis thaliana OX=3702)	0.78	0.009	3	1
Similar to ccp1: Cytochrome c peroxidase mitochondrial (Neosartorya fumigata (strain ATCC MYA-4609 / Af293 / CBS 101355 / FGSC A1100) OX=330879)	1.65	0.009	33	9
Similar to PBG1: Proteasome subunit beta type-4 (Arabidopsis thaliana OX=3702)"	1.57	0.010	10	2
Similar to THFS: Formate--tetrahydrofolate ligase (Arabidopsis thaliana OX=3702)	1.83	0.010	11	11
Similar to gcvP: Glycine dehydrogenase (decarboxylating) (Synechococcus sp. (strain RCC307) OX=316278)	1.74	0.010	19	2
Protein of unknown function	0.62	0.011	21	5
Protein of unknown function	1.40	0.011	1	2
Similar to TCTP: Translationally-controlled tumor protein homolog (Triticum aestivum OX=4565)	1.43	0.011	13	3
Similar to Rpl23a: 60S ribosomal protein L23a (Rattus norvegicus OX=10116)	1.63	0.013	46	1
Similar to PSME1: Proteasome activator complex subunit 1 (Homo sapiens OX=9606)	1.61	0.015	35	7
Similar to rpsA: 30S ribosomal protein S1 (Coxiella burnetii	0.86	0.018	34	16

(strain RSA 493 / Nine Mile phase I) OX=227377)				
Similar to CDC48: Cell division cycle protein 48 homolog (Glycine max OX=3847)	1.43	0.019	31	3
Similar to Triosephosphate isomerase cytosolic (Secale cereale OX=4550)	1.26	0.021	30	7
Similar to Histone H3 (Urechis caupo OX=6431)	0.74	0.023	29	6
Similar to Bm1 44725: GTP-binding nuclear protein Ran (Brugia malayi OX=6279)	0.25	0.024	13	2
Similar to NME1: Nucleoside diphosphate kinase A (Pongo abelii OX=9601)	1.75	0.027	30	4
Similar to cbbX: Protein cbbX homolog chloroplastic (Guillardia theta OX=55529)	1.37	0.028	29	12
Similar to MPPalpha1: Probable mitochondrial-processing peptidase subunit alpha-1 mitochondrial (Arabidopsis thaliana OX=3702)	1.43	0.029	24	8
Protein of unknown function	1.34	0.030	47	17
Similar to Rack1: Receptor of activated protein C kinase 1 (Rattus norvegicus OX=10116)	0.86	0.030	46	12
Similar to VHA-D: V-type proton ATPase subunit D (Arabidopsis thaliana OX=3702)	3.01	0.032	5	1
Similar to CDC48: Cell division cycle protein 48 homolog (Glycine max OX=3847)	3.81	0.032	36	4
Similar to SDH1: Succinate dehydrogenase [ubiquinone] flavoprotein subunit mitochondrial (Oryza sativa subsp. japonica OX=39947)	0.68	0.033	10	5
Similar to gsr: Glutathione reductase (Dictyostelium discoideum OX=44689)	1.82	0.034	6	2
Similar to TM 1269: [FeFe] hydrogenase maturase subunit HydE (Thermotoga maritima (strain ATCC 43589 /	0.15	0.034	1	1

MSB8 / DSM 3109 / JCM 10099) OX=243274)				
Similar to TCP17: Protein TCP17 (Trypanosoma cruzi OX=5693)	0.057	0.034	17	3
Similar to SAHH: Adenosylhomocysteinase (Petroselinum crispum OX=4043)	1.46	0.036	6	2
Similar to ADK1: Adenosine kinase 1 (Arabidopsis thaliana OX=3702)	1.96	0.037	3	1
Protein of unknown function	0.13	0.037	28	4
Similar to groL1: 60 kDa chaperonin 1 (Synechococcus sp. (strain JA-3-3Ab) OX=321327)	0.23	0.039	37	18
Protein of unknown function	0.64	0.044	4	1
Similar to Ndufs6: NADH dehydrogenase [ubiquinone] iron-sulfur protein 6 mitochondrial (Rattus norvegicus OX=10116)	0.37	0.049	18	2
Similar to RPS0: 40S ribosomal protein S0 (Coprinopsis cinerea (strain Okayama-7 / 130 / ATCC MYA-4618 / FGSC 9003) OX=240176)	1.66	0.049	17	5

Milestone 2.3.2: Completed photophysiological and systems biology comparisons of the responses of three engineered/adapted N. oceanica *strains to high and low bicarbonate levels compared to the parent strain, demonstrating upregulation of carbon assimilation metabolic cascade in the improved strains and providing data to determine the best strategy for generating strains capable of rapid bicarbonate uptake.*

A new, highly sensitive proteomics mass spectrometer was installed at CSU, and an updated method development was completed for *N. oceanica* label-free, quantitative proteomics. Three biological replicates for each condition, and the analysis was performed in a non-targeted manner. The four conditions compared were wild type (W) vs. BicA transgenic strains (B) under conditions of with (C) and without (O) bicarbonate feeding. In total, 5,747 unique proteins (4295 with a minimum of two peptides) and 41,483 unique peptides were identified. Highlights of three of the pairwise comparisons are presented in Table 2-3.

The B0 vs. W0 comparison clearly shows that the expression of BicA had a large influence on the cells, even without exogenously supplied bicarbonate. Many more proteins were expressed at higher levels in the B0 than in the W0 condition.

The BC vs. B0 comparison also revealed large proteome changes. Interestingly, bicarbonate feeding resulted in a greater number of proteins being *less* abundant rather than more abundant – and this trend was true also for the BicA protein.

Finally, the BC vs. WC comparison revealed a smaller number of proteins with altered abundance, but more proteins were present at higher levels in the BC condition.

A volcano plot of the BC vs. B0 comparison (Figure 2-5) provides more insight into the distribution of protein changes upon providing bicarbonate to the BicA-expressing cells. Many proteins were found with high confidence to have changed in abundance to large extents. Additional database mining is required to link the protein functions (where annotations have been made) to the conditions compared in this analysis.

Table 2.3. Comparison of protein abundances among wild type (W) vs. BicA transgenic strain (B) under conditions of with (C) and without (O) bicarbonate feeding.

Comparison	Criterion	Number of proteins
BicA transgenic + bicarbonate feeding (BC) vs. WT + bicarbonate feeding (WC)	Only in BC	37
	>2x in BC vs. WC	69
	>2x in WC vs. BC	33
	Only in WC	12
BicA transgenic + bicarbonate feeding (BC) vs. BicA transgenic, no bicarbonate feeding (B0)	Only in BC	12
	>2x in BC vs. B0	107
	>2x in B0 vs. BC	562
	Only in B0	81
BicA transgenic, no bicarbonate feeding (B0) vs. WT, no bicarbonate feeding (W0)	Only in B0	24
	>2x in B0 vs. W0	114
	>2x in W0 vs. B0	8
	Only in W0	4

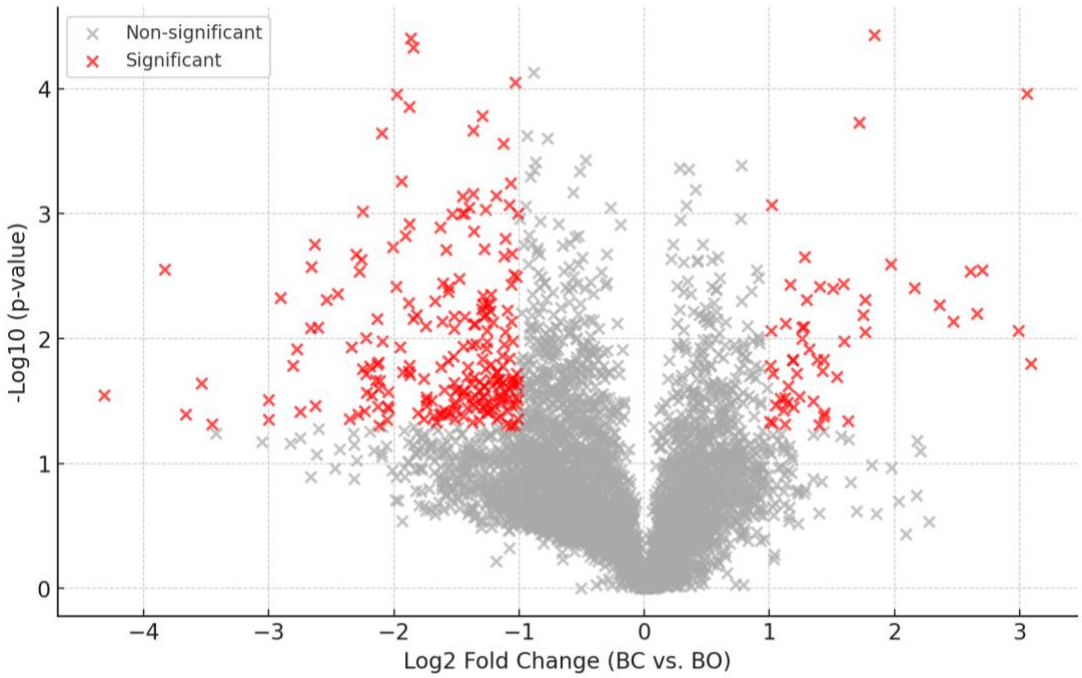

Figure 2-5. Volcano plot of proteins with changed abundance upon bicarbonate addition to *N. oceanica* cells expressing BicA. Red symbols indicate proteins with at least two-fold abundance change and p-value of 0.05 or less.

Task 3: System integration, deployment, and validation

Subtask 3.1: Determine optimal carbon introduction location to raceway pond

Milestone 3.1.1: Demonstrate that the CFD model with time-varying carbon point source can predict distributions of pH and bicarbonate to < 10% of measured values (abiotic).

The goal of Subtask 3.1 is to develop and implement a comprehensive computational fluid dynamics (CFD) model to be used for identification of optimal raceway operation, including injection location(s) of the carbon and makeup nutrient sources, long-time uniformity of cell light histories, and maximal cellular utilization of the preferred carbon source. The ability to accurately simulate turbulent and laminar mixing, chemical kinetics of carbon speciation, and cell trajectories allows us to use CFD as the key design tool to obtain optimal raceway operation and performance.

A three-dimensional transient multiphase simulation of a mini-raceway pond was carried out to fully characterize its hydrodynamic behavior. The simulation was carried out with ANSYS Fluent v16 and visualized via paraView 5.7.0. The mini-raceway pond exhibits very different flow patterns at the two bends as compared to simulations of a 900-L mesoscale raceway pond. At the first 180° bend, the liquid moves faster at the outer part of the bend, while there is a low velocity region at the outer part of the second 180° bend, resulting in a dead zone. Moreover, the dead zones also show different flow patterns at and after the two bends (Figure 3-1). First,

the dead zone is absent at the first bend, indicating the absence of a strong reversed pressure gradient that would slow the fluid.

To better illustrate this flow behavior, low vertical velocity (|u_z |≤0.1 m/s) data are filtered out and the velocity fields in regions showing more significant vertical motion are identified, as shown in Figure 3-2(b). At the first bend of the mini raceway, despite the small pond dimensions, the paddle wheel generates a strong flow field with appreciable kinetic energy that exhibits unstable behavior in the vicinity of the paddle wheel. Moreover, because of the geometry of the mini-pond, the width/depth ratio is approximately W⁄D = 0.965, which is small compared to the W⁄D of an industrial pond, which can easily exceed 10. As the result of the low W⁄D value in the mini-pond and large kinetic energy of the flow upstream of the first bend, as well as the secondary flow effect, the flow at the outer first bend has a strong downward motion where |u_z |can reach 0.2 m/s (Figure 3-2(a)). This downward motion is so strong that it brings the flow at the inner first bend upward and the flow tends to rotate at the first bend. As a result, the flow at the first bend exhibits a significant swirling motion. In contrast, the flow is less vigorous at the second bend due to dissipation of its kinetic energy. The fluid still moves downward at the outer bend wall, but not strong enough to create an upward motion in the inner region.

Using the predicted velocity field, unsteady state particle tracking was performed using the Fluent discrete phase model (DPM) to predict the motion of individual microalgae. Those studies did not include the transport and mixing of individual chemical species such as carbon dioxide and bicarbonate. To ensure that the addition of species transport equations to the Fluent simulations yield accurate, predictable results it is necessary to compare the simulations for molecular transport via diffusion and convection with laboratory studies. The original plan was to measure local pH and bicarbonate concentration. It was found that the addition of a slightly acidic stream to the raceway pond did not yield detectable changes with the available pH meter, and there was no conventional means to measure bicarbonate concentration. Instead, an inert, colored tracer was added to the pond and tracked via video. The color intensity was normalized to the injected stream and compared with the transport of the species predicted by Fluent.

The time dependent distribution of the tracer dye was captured and recorded by a high-speed camera at 240 frames per second and processed using Matlab. The simulation results were rendered by the mass fraction of the dye tracer and the opacity was mapped onto the magnitude of mass fraction so that high concentrations would appear to be darker and less transparent, making the visualization more realistic. The simulation is compared against the frames of the dye tracer recording to validate the ability of the CFD simulation to quantitatively predict species transport.

As shown in Figure 3-3, the results of the tracer dye and the simulations are in close agreement for the four timepoints shown. At 6 s after injection (Fig. 3-3a), the tracer is transported away from the wall by the swirling flow field and has begun to propagate toward the inner bend, as shown by both simulation and observation. Even at this short time the results indicate that the CFD model accurately captures the flow field and molecular diffusion processes. When t = 12 s (Fig. 3-3b), the tracer

reaches the midline of the straight section, and the outer region of that straight channel appears to be darker than the inner region, which is caused by the low velocity magnitude and strong recirculation in the dead zone formed after the divider. This flow behavior is better demonstrated via the use of the pathlines shown in Fig. 3-4. As can be seen, most stream tracers go to the outer region of the channel, while only a very small portion enter the so-called dead zone, which also proves the existence of a strong recirculation in the dead zone predicted by our CFD model.

As time increases to 18 s and then 24 s (Figs. 3-3c,d), the dye begins to span the width of the straight section, although a gradient can clearly be seen. By 24 s, the tracer has reached the paddle wheel and will soon begin a second circuit. As with the earlier times, the distribution and intensity of the dye captured by camera are in good agreement with the prediction.

Since the simulation data and the experimental results are in good agreement, it is likely that this system is highly convection dominated and molecular diffusion effect plays a relatively small role.

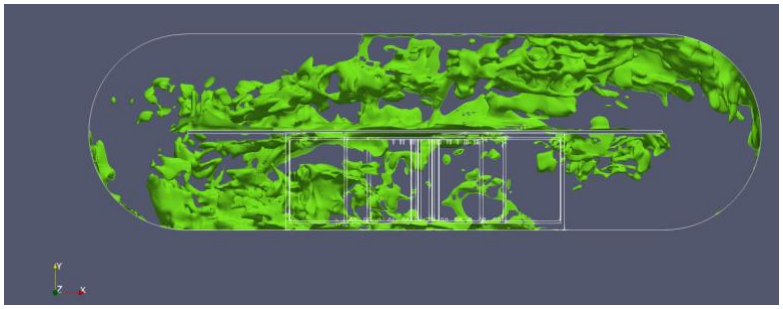

Figure 3-1. Contours highlighting dead zones at t = 127.1 s, where a dead zone is defined as a region where the velocity magnitude is less than 0.1 m/s.

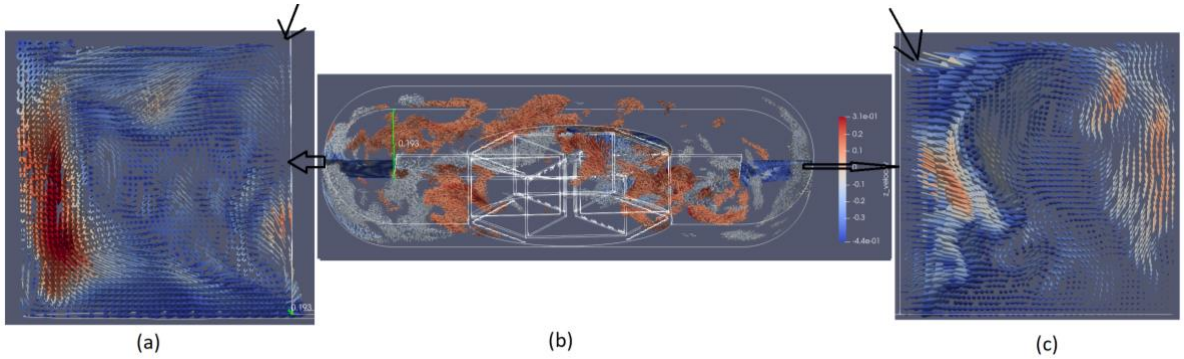

Figure 3-2. (a) The velocity field in a vertical plane at the first bend, where the left edge is the outer wall. The velocity field is colorized using $|u_z|$. Note the liquid at the inner bend flows upward. (b) The velocity field corresponding to high vertical motion regions where $|u_z| > 0.1$ m/s. Again, the velocity field is colorized using $|u_z|$. (c) The velocity field in a vertical plane at the second bend, where the right edge is the outer wall. Again, the velocity field is colorized using $|u_z|$. Note at this bend the liquid at the inner wall flows downward. D = 0.2 m and W/D = 0.965.

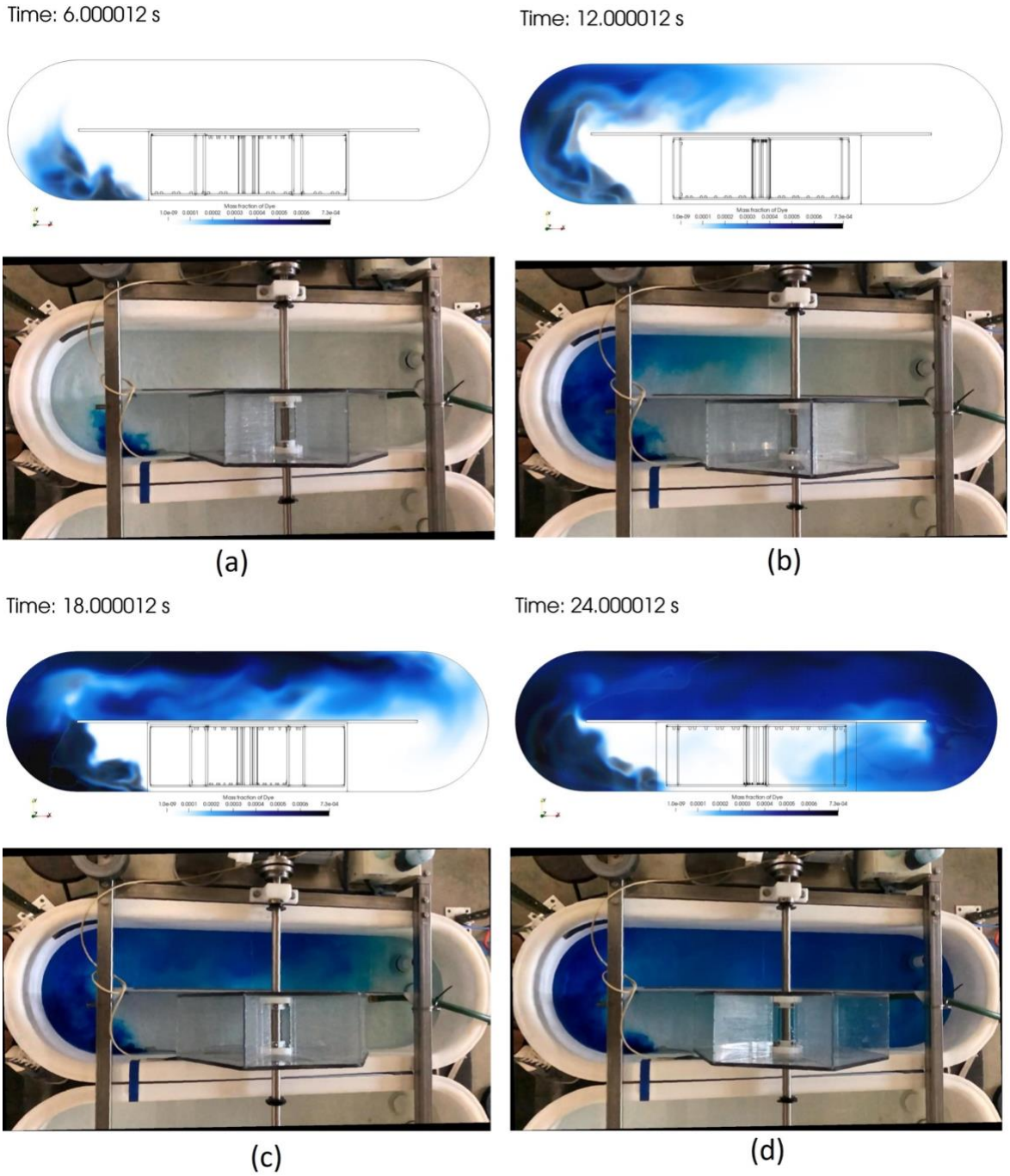

Figure 3-3. The volume rendering results of the CFD simulations (upper row) compared with the results of the tracer dye (bottom row) at (a) t = 6 s (b) t = 12 s (c) t = 18 s, and (d) t = 24 s.

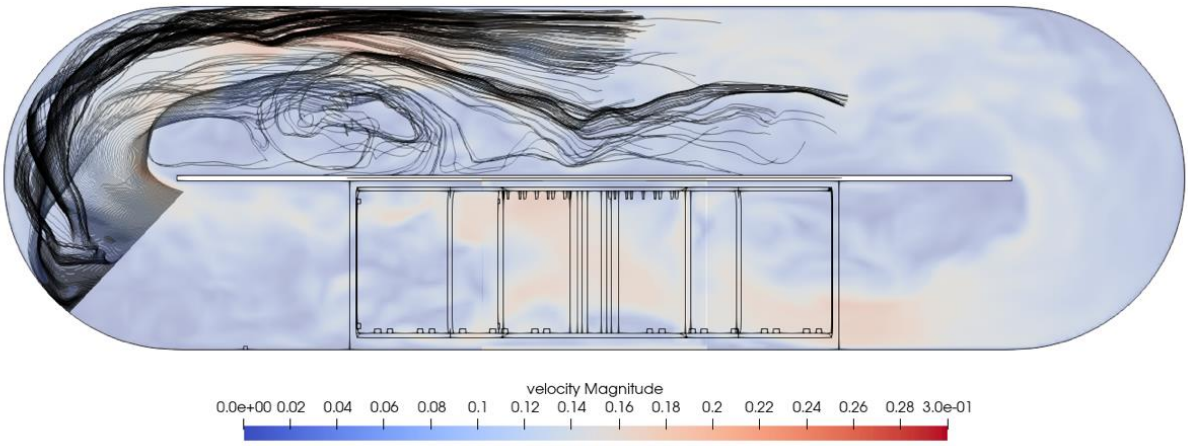

Figure 3-4. Pathline plots illustrating the three-dimensional flow at and downstream of the first 180° bend. The contours are colored by the velocity magnitude located at the cross section measured 4 cm from the bottom.

Milestone 3.1.2: Apply comprehensive CFD model to select at least 3 potential C source injection location(s) in the raceway that lead to the most uniform mixing of carbon throughout the raceway volume. Tracer experiments will be done to identify configuration with <2% non-uniformity.

The open-source library openFoam version 6.0 was used to predict and quantify inorganic carbon and proton species transport, and to model the photosynthetic reactions as well as water self-ionization reactions. This choice was made due to difficulties encountered in accurately modeling the photosynthetic chemistry using ANSYS Fluent. A solver was developed to model two incompressible, isothermal immiscible fluids (gas + liquid) using the volume of fluid (VOF) model with a phase-fraction based interface capturing approach. The arbitrarily coupled mesh interface (ACMI) approach was used to model the rotating motion of the paddle wheel. The multi-dimensional limiter for explicit solution (MULSE) approach was used to accurately model the phase change with a reduced computational cost and effectively ensure the boundedness of the VOF field.

A three-dimensional transient simulation was carried out to model the hydrodynamic characteristics of the mini-raceway pond. To ensure that a specific aqueous species such as bicarbonate is restricted to the liquid phase and not lost to the air, a modified species transport equation is used:

$$\frac{\partial c}{\partial t} + \nabla \cdot (\emptyset U c) - \nabla^2 (\emptyset D_T c) = 0$$

where *c* is a species concentration, $\emptyset$ is the phase fraction in the liquid, and D_T is the binary diffusion coefficient of the species. The velocity field *U* is computed using openFoam.

Due to the motion of the paddle wheel, there exists a hydraulic rise near the paddle such that the water depth is slightly higher downstream of the paddle than upstream. To accurately calculate the light intensity in the liquid phase as a function of depth,

the position of the liquid-gas interface is determined using a searching algorithm and the distance between each liquid mesh cell and its corresponding liquid-gas interface was calculated afterward. An effort was made to ensure the distance and the light intensity can be correctly calculated in parallel computations.

With the use of Dirichlet boundary condition to simulate injection, the model was run for the conditions listed in Table 3-1 and the locations of the pH regulation injector and inorganic carbon injector located shown in Figure 3-5a, and the light intensity function used in the simulation shown in Figure 3-5b.

The results for bicarbonate concentration, pH, accumulated inorganic carbon consumption by photosynthesis, and the concentration of CO_2 are shown in Figure 3-6. The inorganic carbon as well as low pH fluid are injected starting at 100.0 s and are tracked for 50 s. This scenario simulates a case with high enough cell density that the light decays 95% of its maximum intensity at 1.2 cm from the interface. Using that light intensity decay rate, it can be seen in Figure 3-6c that the accumulated inorganic carbon consumption is confined to a thin layer near the interface. The proton injector cells occupy a relatively large volume, representing the case with a high flow rate of low pH fluid. As that injected low pH liquid is transported around the pond and serves to keep the overall pond pH from continuously increasing. The results indicate that the protons injected into the system are absorbed by the water self-ionization reaction and can only impact a limited region, suggesting that multiple pH injectors are required, especially for larger ponds.

In order to determine optimal locations to inject inorganic carbon and low pH liquid, 6 cases were tested whose configurations and the locations of the injectors are listed in Figure 3-7 and Table 3-2. As in the previous simulation, the aqueous inorganic carbon and low pH liquid streams are injected starting at 100 s and tracked for 50 s. The standard deviation is used to describe the amount of variation and dispersion of bicarbonate concentration and indicate the uniformity of bicarbonate and these results are shown in Figure 387. Based on the standard deviation for the 6 test cases, the test case with highest standard deviation is case 4, for which the inorganic carbon injector is located upstream the paddle wheel and low pH liquid is supplied downstream, near the tip of the divider downstream the paddle wheel region. This configuration is reasonable and expected as high velocity of liquid is observed at these two locations and thus, the species are transported more efficiently, and a better uniformity is achieved.

Table 3-1. Inorganic carbon injector and proton injector for 6 test cases.

Case	Inorganic carbon injector #	Proton injector #
1	2	1
2	1	1
3	5	1
4	4	1
5	5	2
6	3	3

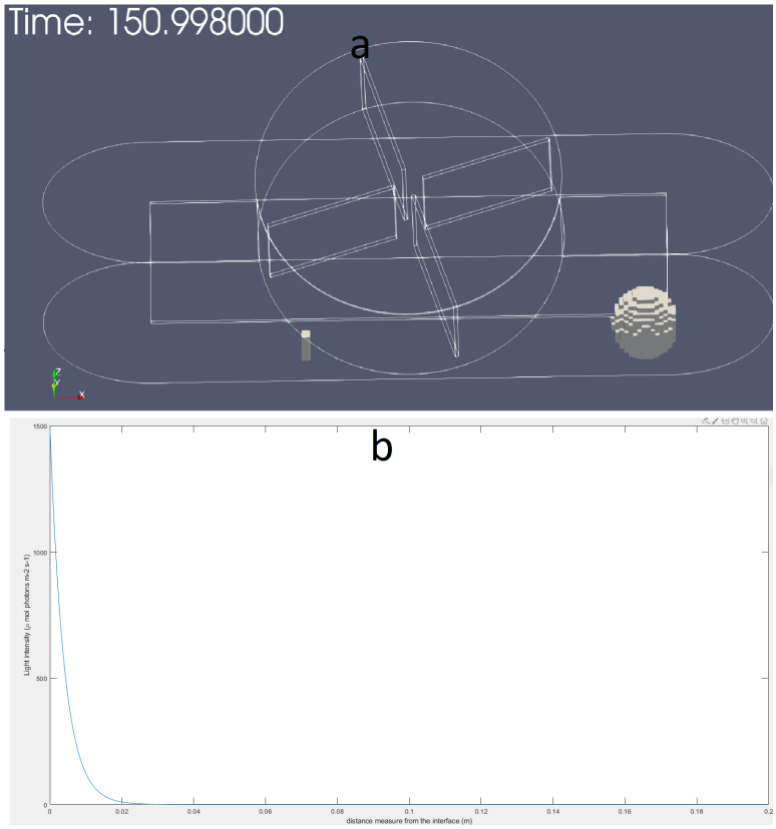

Figure 3-5. a) location of an inorganic carbon injector and an acidic pH injector. b) The light intensity function used for the simulation.

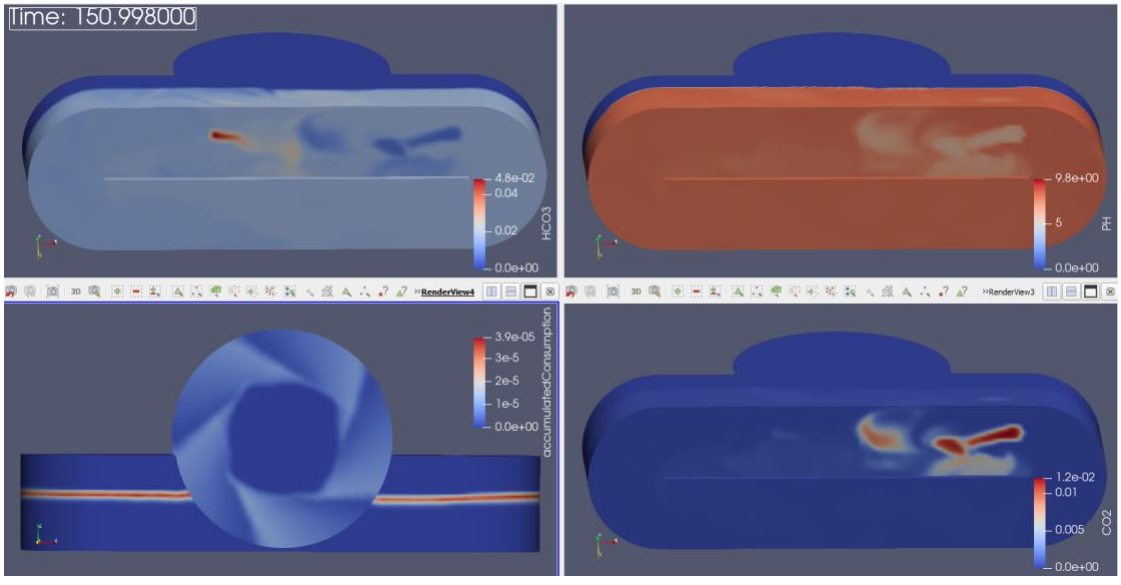

Figure 3-6. Concentration of HCO_3^-, pH, accumulated inorganic consumption, and concentration of CO_2 at flow time 150 s.

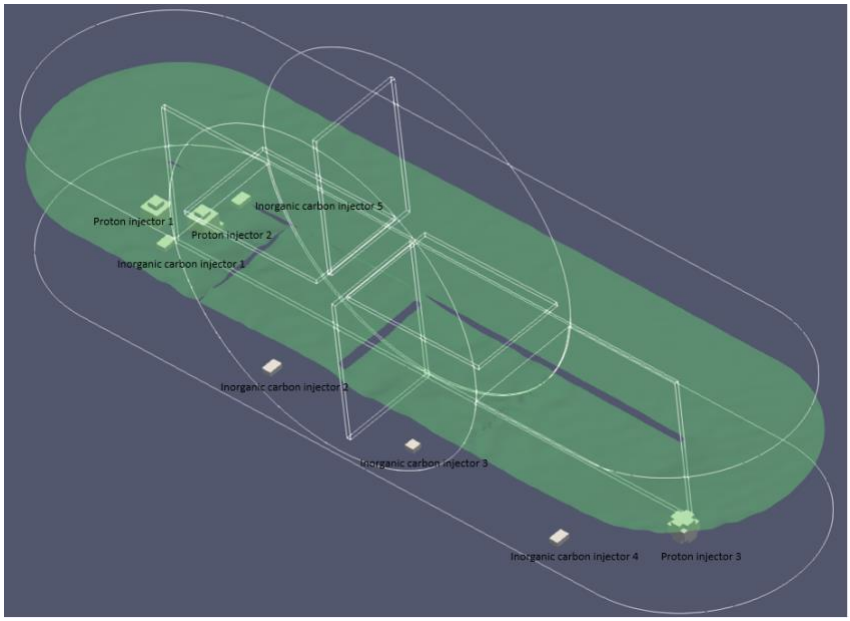

Figure 3-7. Locations of inorganic carbon injector(s) and low pH injector(s) to explore combinations that achieve the composition best uniformity.

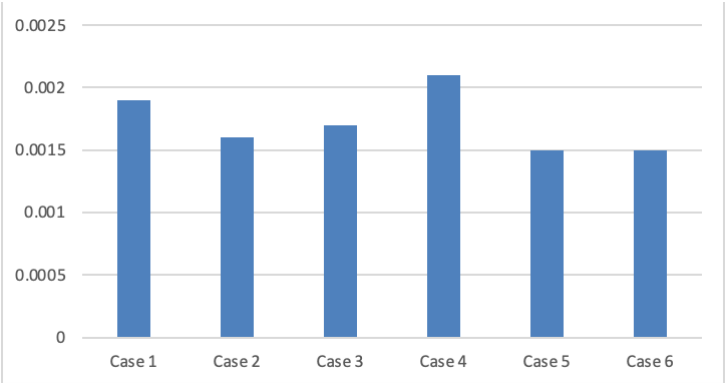

Figure 3-8. Standard deviation of 6 test cases of injector locations (Table 3-1).

Milestone 3.1.3: Carry out long-term simulations of raceway operation mimicking operational conditions anticipated in follow-on multi-week experiments in mini-ponds. Compare simulations against dissolved carbon concentration and cell culture growth rates to demonstrate model prediction capabilities. (M33)

It was determined that the respiration rate must be taken into consideration to accurately model the cellular growth rate at higher biomass concentrations. With that, the multiplicative specific growth model was:

$$\mu = (\mu_{max}\left(\frac{I_{av}}{K_I+I_{av}}\right)\left(\frac{S_{IC}}{K_{IC}+S_{IC}}\right)\eta_{pH} - \mu_{resp}) \cdot B$$

In this model, as the biomass concentration approaches its maximum, the light

intensity decays rapidly with depth and can only penetrate a small distance from the surface. In addition, the illumination the pond receives is limited where the growth rate is close to the respiration rate and the net growth rate is near zero. However, the model requires the determination of the unknown parameters μ_{max} and μ_{resp} by fitting the modeled biomass concentration to the actual biomass concentration.

To reduce the number of trials, the experimental cultivation data without any inorganic carbon injectors was used as the baseline case and the assumption was made that the bicarbonate species concentration and pH were uniform in the pond. Although the assumption would not be strictly correct for the actual scenario where the bicarbonate species and pH were not spatially uniform, particularly near the interface where growth occurs, a good initial guess for μ_{max} and μ_{resp} can still be acquired. A Matlab code was implemented whereby the pond is discretized into finite horizontal layers where the light intensity at each layer is calculated and converted to the net growth rate. The experimental measurements of dissolved inorganic carbon (DIC) and pH were supplied and the ODE solver ode15s was used to integrate the net growth rate and compared with the experimental biomass concentration to determine the value for μ_{max} and μ_{resp}. The Matlab code indicated that the optimal values for μ_{max} and μ_{resp} were 0.002013 s^{-1} and 0.005308 s^{-1}. The values were used as the initial guesses and further fine-tuned using more detailed CFD simulations for which the bicarbonate concentration and pH were no longer assumed to be spatially uniform. The optimal values for μ_{max} and μ_{resp} were refined to be μ_{max} = 0.001969 s^{-1} and μ_{resp} = 0.0005099 s^{-1}.

Figure 3-9 shows the modeled biomass concentration compared to the experimental data. The initial biomass concentration at Day 0 was 0.066 g/L, and without injectors. The simulation was carried out to predict the biomass over 17,000 minutes (11.8 days). The predicted biomass using the listed parameters agrees well with the experimental data, suggesting that the improved multiplicative model can significantly enhance the model prediction capability.

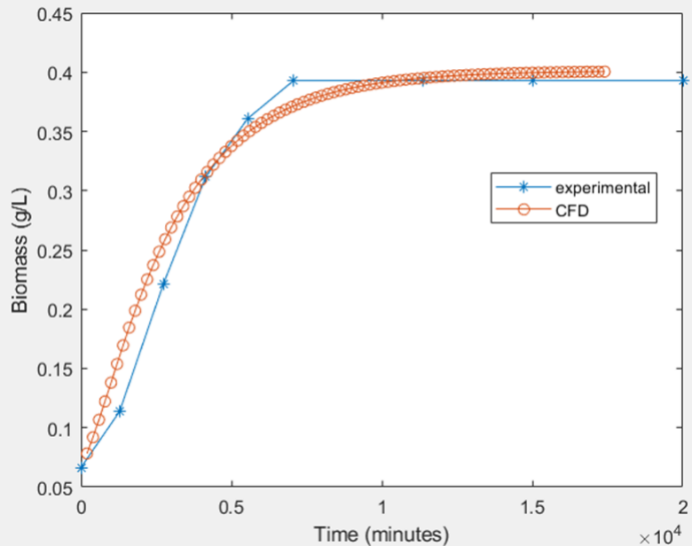

Figure 3-9. Long term modeled and experimental biomass concentration.

Subtask 3.2: Develop and test system for gas-phase CO_2 monitoring and control

Milestone 3.2.1: Demonstration of CO_2 off-gas and dissolved bicarbonate uptake monitoring, continuously demonstrated in a mini-pond, over at least 2 weeks of cultivation of WT N. oceanica *CCAP 84910.*

The goal of this task was to demonstrate continuous carbon uptake measurements and achieve a full carbon mass balance in a small mini-pond system. A 2-week pond experiment growing *N. oceanica* was conducted with a series of data loggers, with in-situ monitoring of the pond physiology and compositional analysis of the harvested biomass. This experiment supported the need to document the efficiency of carbon delivery and capture in algae cultivation, data that are generally absent in the literature for large-scale cultivation.

The precise measure of photosynthetic CO_2 uptake over the course of a culture can be measured using a defined set of sensors. This set is limited to a pH meter, a temperature meter, a conductivity/salinity meter, and dissolved CO_2 probe for the culture medium as well as inlet and outlet gas CO_2 sensors, pressure sensors, humidity sensors, and temperature sensors.

The complexity of the carbon chemistry in water as well as the effect of the growth of algae in reactors or ponds require a substantial number of sensors which, in the current state of technologies, is not available on the market. Therefore, efforts have been put into the designing of a system able to monitor, log, and react to different parameters of algal culture using an open-source ecosystem of microcontrollers, and adaptable sensors. Arduino and derived microcontrollers exist in many performance ranges and are easily programmable on computers using a C++ type language.

Pond biomass sampling was performed twice a day on 8 days over an approximate two-week period, once at 6:30 AM and again at 12:00 PM. At each timepoint, four 50 mL aliquots were taken from each pond. Two 50-mL aliquots were spun down and freeze dried to submit for CHN, one 50 mL aliquot was used for AFDCW, OD, and pH measurements, and the last 50 mL aliquot was used for TOC/IC analysis.

To track both growth and carbon distribution between the media and the cells, we have developed an accurate and high-throughput method for organic and inorganic carbon concentration in solution and with suspended cells through modification of a TC/TOC analyzer method. CHN analysis was performed on the spun down, freeze-dried biomass using an Elementar Vario EL Cube CHN Analyzer. Approximately 5 mg of each sample was weighed into a small tin foil packet and was combusted at 950 °C and analyzed using a thermal conductivity detector.

The cumulative amount of injected CO_2 used to stabilize the pH was monitored using customized mass flow meters from Alicat Scientific, using the process flow installation as described in Figure 3-10. A script to provide daily values of totalized flow was produced in R programming language. The script consists of a user interface to import the selected .CSV file for integration. The script outputs an Excel file with daily values of CO_2 volume input and carbon mass input. The Excel output allows for easy plotting of the values in search of daily trends due to possible environmental factors.

Two 100-L open raceway ponds located in a greenhouse were inoculated with a culture of *N. oceanica* 849/10 using a modified artificial sea water medium and followed the growth. The experiment lasted over 18 days, featuring a sample harvest at the 11th day of half the volume replenished with new medium. The growth curves based on OD750 (Figure 3-11) did not reveal any growth problems and bacteria or predator contamination over the course of this experiment was low enough that it did not seem to affect growth rates. The photosynthetic activity was also measured by tracking the dissolved oxygen in the culture medium.

Among the parameters to be measured to complete the CO_2 mass balance, we focused first on obtaining a reliable measure of the CO_2 intake to the culture, keeping the pH constant. After the first hours, we determined that the CO_2 diffusion stone in the pond 4 was not operating. Correction of the problem brought the pH back to the set point. For the rest of the experiment, the pH stayed stable at 7.8-8.0 demonstrating that the CO_2 supply efficiently compensated the photosynthetic consumption of inorganic carbon. Both ponds had a gradual increase in the CO_2 accumulation rate, and a slope reduction after the day 11 harvest, which is consistent with the reduced cell density (Figure 3-12). The cumulative masses calculated for Ponds 1 and 4 was 93.8 and 75.1 g CO_2.

The measure of the total carbon content of the biomass was done using a TOC/TIC analyzer. Comparing the values at the two maxima and minima, we calculated the total amount of carbon sequestered by the biomass. The biomass sequestration of carbon was 14.35 and 12.90 g total for pond1 and 4, respectively.

The medium organic carbon content depends on 2 major parameters, the medium composition and then the production of soluble molecules by algae or the presence of cell debris non eliminated by centrifugation. Here, the medium's carbon composition is related to the presence of EDTA and vitamins that account for a total of about 1.95 ppm of carbon. The organic carbon detected in the medium at T0 was higher than what is expected from the medium alone (Figure 3-13). It is possible that this detection came from cell debris added with the inoculum or an inherent presence of non-pelleted cells from the supernatant of the centrifugation. Even though the organic carbon content in the medium as background is significant, a general increase trend was observed, corresponding to 1.080 g for pond 1 and 1.112 g for pond 4.

The presence of inorganic carbon in the medium is not expected to fluctuate. The results obtained from our experiment reveal a small increase of inorganic carbon over time (Figure 3-14). It can be calculated that 1.9 g and 2.4 g of inorganic carbon were sequestered through this increase in pond 1 and pond 4 respectively and is likely a result of an increased alkalinity. This increase in inorganic carbon content of the media corresponds to 68 and 201 mmol increase in alkalinity.

Based on the above data, a calculation of the carbon capture efficiency relative to the supplied CO_2 to the culture and the carbon entrained in the biomass is possible (Figure 3-15). About 80% of the injected CO_2 is lost as gas, either at the level of the bubbling line were bubble reach the surface of the medium before being completely dissolved, or by evaporation at the interface between the growth medium and the

ambient air. By Henry's Law, this evaporation is favored by the low concentration in CO_2 in air as the CO_2 concentration in the media is higher than what air saturation levels would have allowed. About 15% of the total CO_2 injected in the culture is being used for biomass production. While this number is relatively low, large improvements can be achieved by managing the CO_2 delivery/dissolution efficiency.

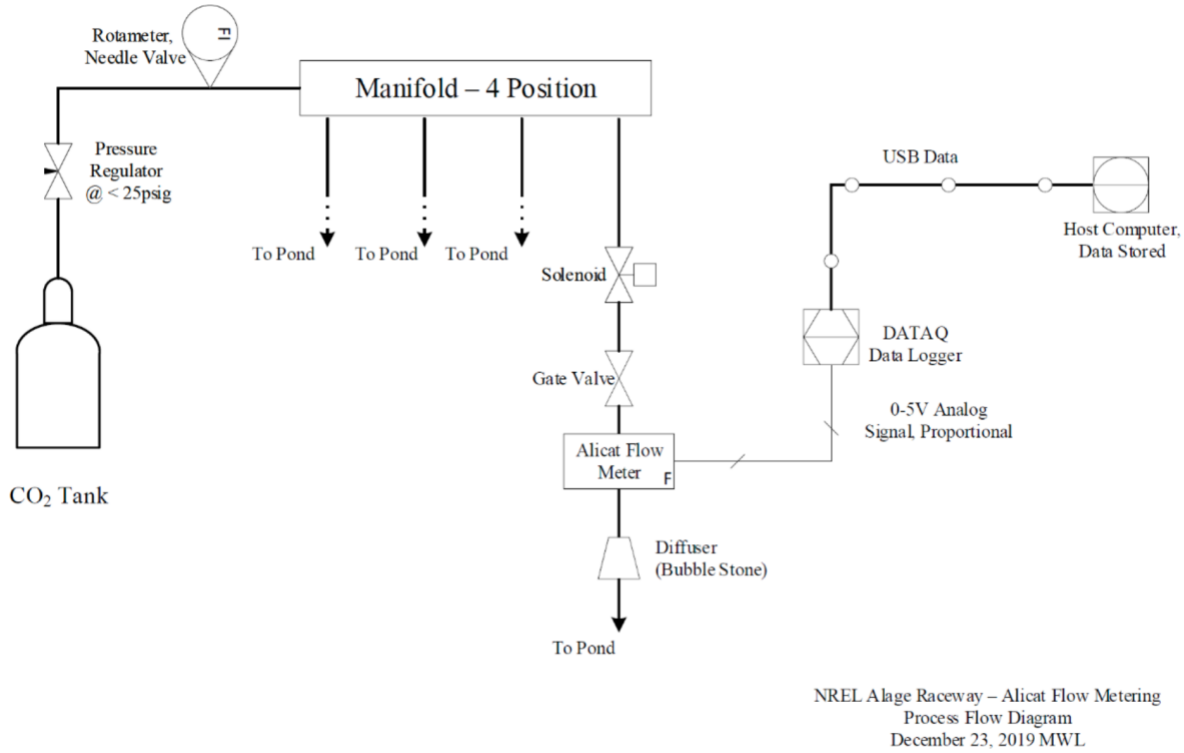

Figure 3-10. Overview of the C monitoring strategy.

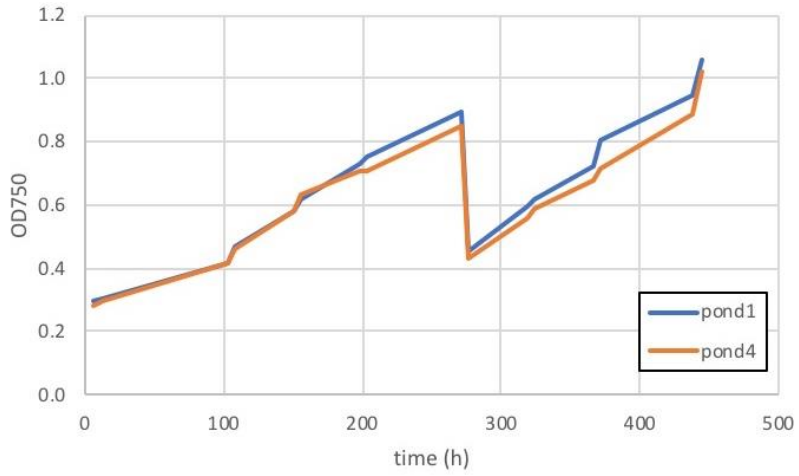

Figure 3-11. Evolution of the optical density at 750 nm during the experiment.

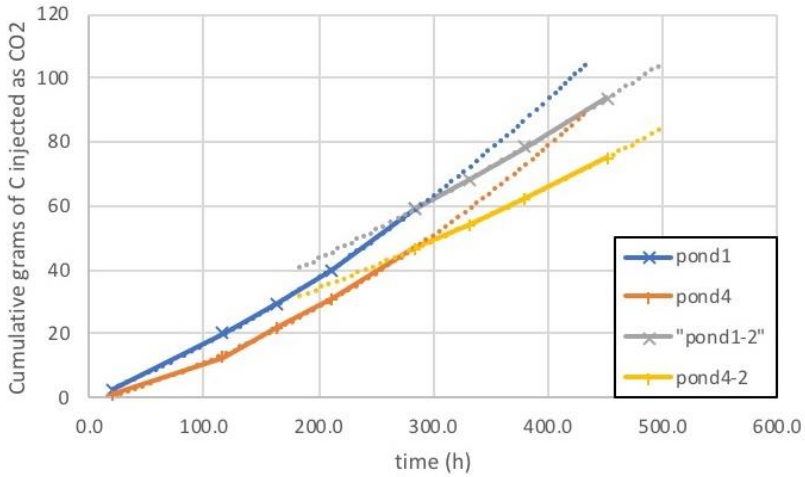

Figure 3-12. Cumulative CO_2 (g) delivered to the ponds.

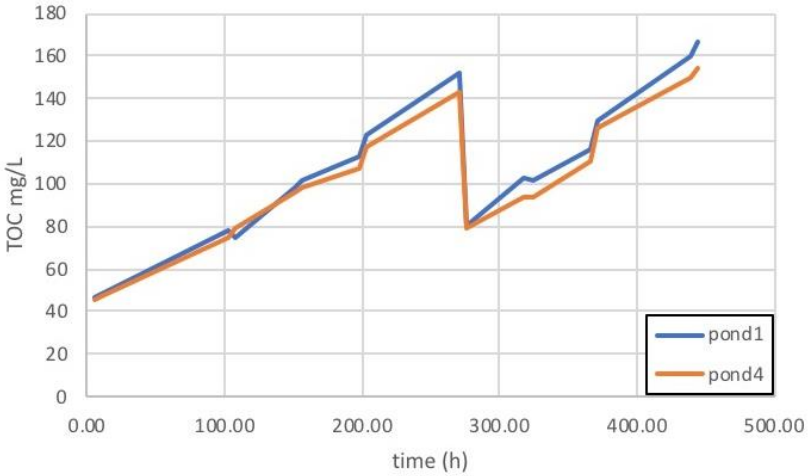

Figure 3-13.Total organic carbon content in the ponds during the experiment.

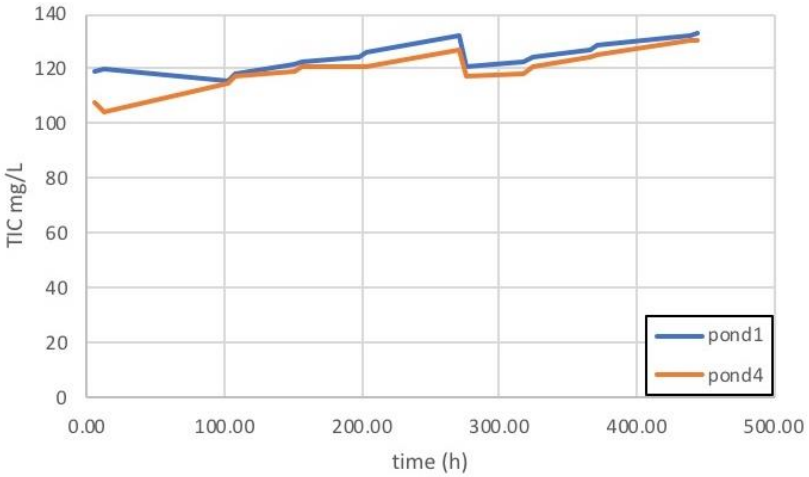

Figure 3-14. Inorganic carbon content in the medium during the experiment.

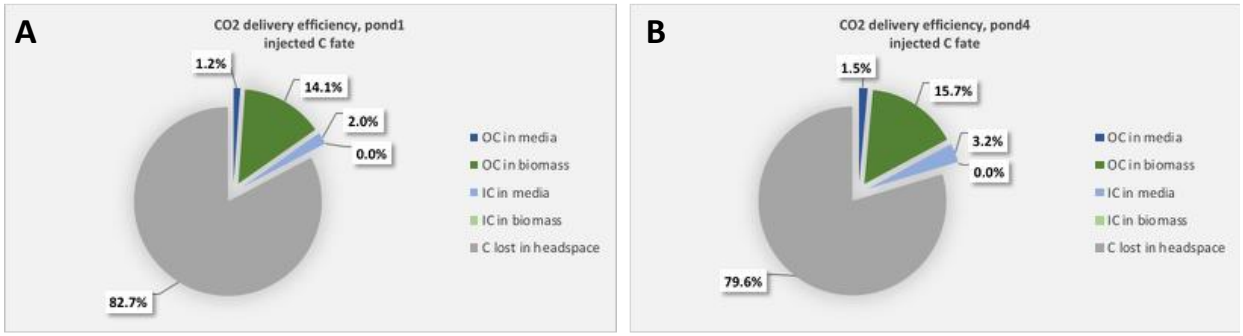

Figure 3-15. Carbon capture efficiency and partitioning between organic and inorganic fractions of the cultures (A and B, pond 1 and 4 respectively). The differences in the IC concentration in the biomass was considered below the limit of detection.

Subtask 3.3: Evaluate performance of C delivery and strain uptake

Milestone 3.3.1: Deployment of membrane module prototype in mini-pond at the NBB site; completion of a cultivation of N. oceanica.

The intent of this milestone was to demonstrate capabilities in cultivating *N. oceanica* in 100-L mini-ponds and to incorporate a bubble-free membrane CO_2 delivery system. The activity was originally set to occur at New Belgium Brewery; however, the COVID-19 pandemic resulted in the NBB site being closed to non-essential personnel. The demonstration was thus conducted in the Powerhouse facility at CSU.

The major outcome was the generation of a complete dataset for WT *N. oceanica* grown in biological triplicates at CSU. In addition, data were collected to inform the modelling aspects of this project. Light attenuation through the cultures was measured to optimize DIC and proton supply in the ponds (Figure 3-16). Data in Figures 3-17 and 3-18 demonstrate the productivity of WT culture ponds at CSU as both OD750 and cell number concentration. This suggests that if cultures are to be maintained in exponential growth phase, 72 h dilutions are the maximum timeframe for harvesting. Data in Figure 3-19 illustrate that the medium composition used in this project, coupled with the light intensities available in the current lighting array, enable cells to maintain maximum quantum photochemical yields for over one week.

A baseline of biomass productivity for *N. oceanica* growth is presented in Figure 3-20. Data in Figure 3-21 report the maximum and global specific growth rates for the ponds, calculated via all major parameters for algal cultivation (OD, cells/mL, chl a/mL, biomass g/L, organic carbon/mL). Finally, the pH, temperature, and dissolved oxygen concentrations in the ponds throughout the course of these experiments are shown in Figures 3-22 to 3-24 These were measured at hourly intervals (as per the best practices of algal cultivation 2015 DOE BETO Algae Platform Review).

In addition, WT *N. oceanica* was cultivated using the fermentation off-gas from New Belgium Brewing in Fort Collins, CO. According to gas analysis results, the fermentation off-gas from New Belgium Brewing contains 79.5-99.8% CO_2, 0-16%

N_2, 0-4% O_2, and a trace amount of other gases such as methane, dimethyl sulfide, ethanol, and isoamyl alcohol. To whether these trace levels of chemicals in the fermentation off-gas are inhibitory to algae growth, we cultured wild-type *N. oceanica* (strain CCAP 849/10) in 500-mL flasks at the brewery. During the cultivation, pH was controlled at 8.2 by sparging either the fermentation off-gas or the pure CO_2. There were two flasks for each treatment. The cell growth was monitored as OD750.

The fermentation off-gas or the pure CO_2 was delivered by a peristaltic pump in the culture flask to supply carbon and control pH. The flasks, with aseptic connectors, were placed on top of an orbital shaker in a growth chamber. The LED light panel was placed above the flasks in the chamber (Figure 3-25). The light intensity was 500 µmol/m^2·s, continuously. The temperature in the chamber was 18-20 °C.

There was no significant difference in the algae biomass concentration during the cultivation between the treatment and the reference (Figures 3-26 and 3-27). These results indicate that the fermentation off-gas is not inhibitory to *N. oceanica* and is equivalent to pure CO_2 to supply the carbon and control pH for the cultivation.

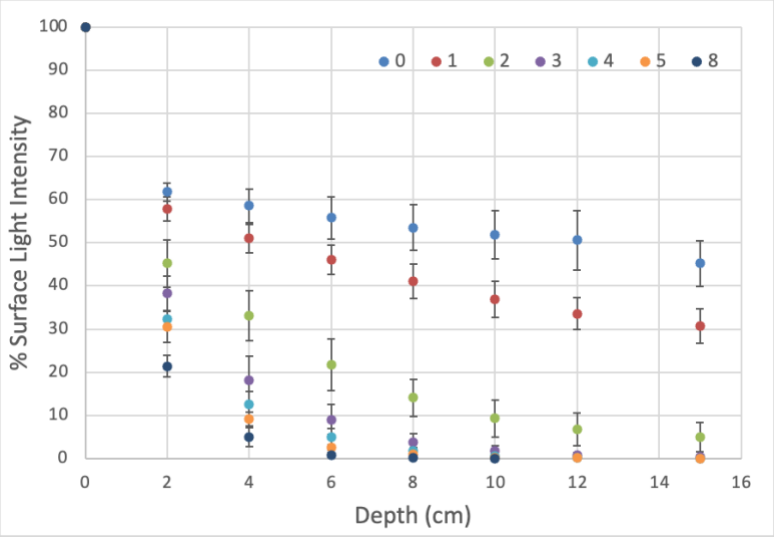

Figure 3-16. Light measured at 2 cm depths over the course of the 8-day pond culture growth. N=3, error bars = stdev.

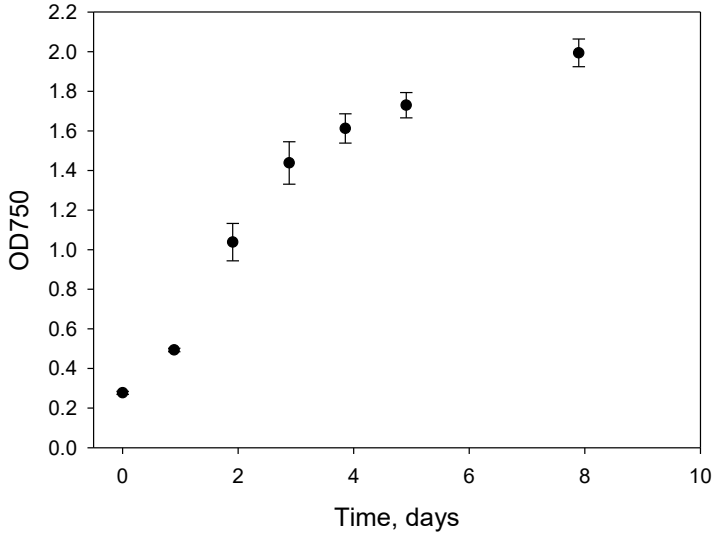

Figure 3-17. OD750 of WT cultures over the course of the 8-day pond culture growth. N=3, error bars = stdev.

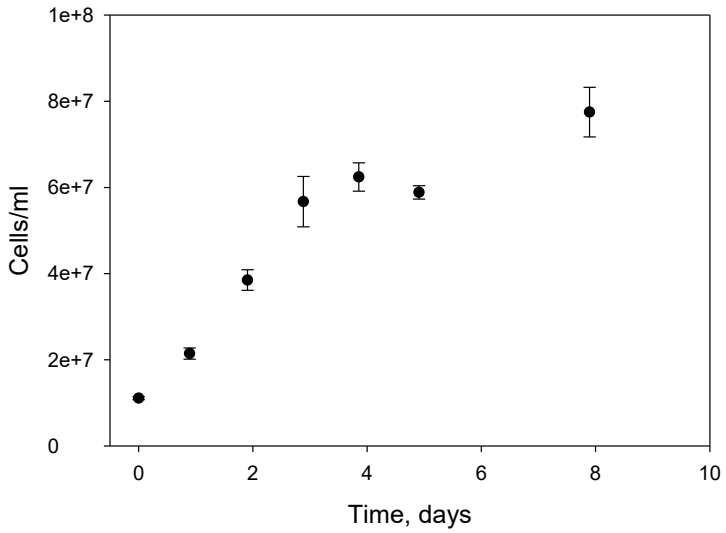

Figure 3-18. Cell number concentration of WT cultures over the course of the 8-day pond culture growth. N=3, error bars = stdev.

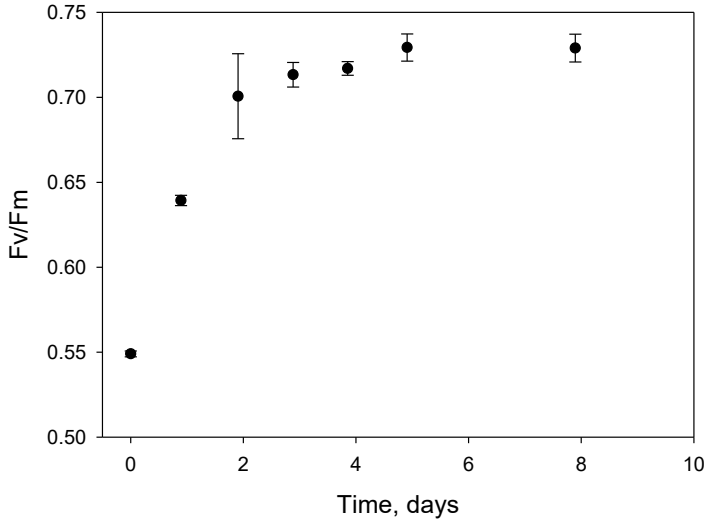

Figure 3-19. Maximum photochemical quantum yields of photosystem II (Fv/Fm) of WT cultures over the course of the 8-day pond culture growth. Cultures were dark adapted for 30 min. N=3, error bars = stdev.

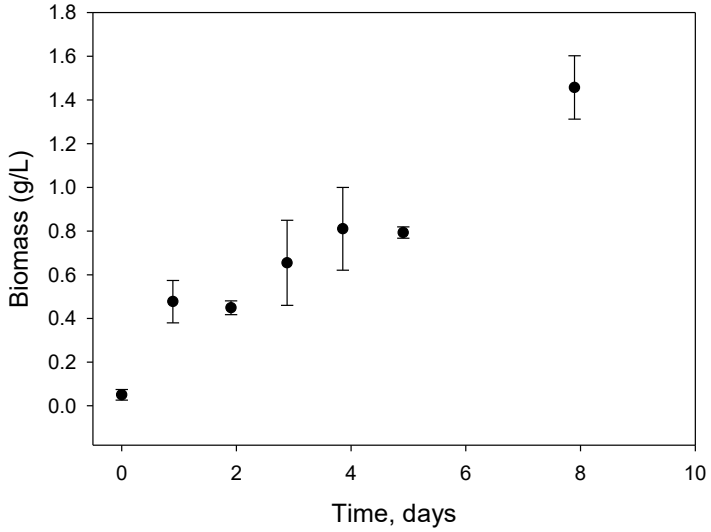

Figure 3-20. Biomass of WT cultures over the course of the 8-day pond culture growth. Biomass was quantified after lyophilization for 48 h. N=3, error bars = stdev.

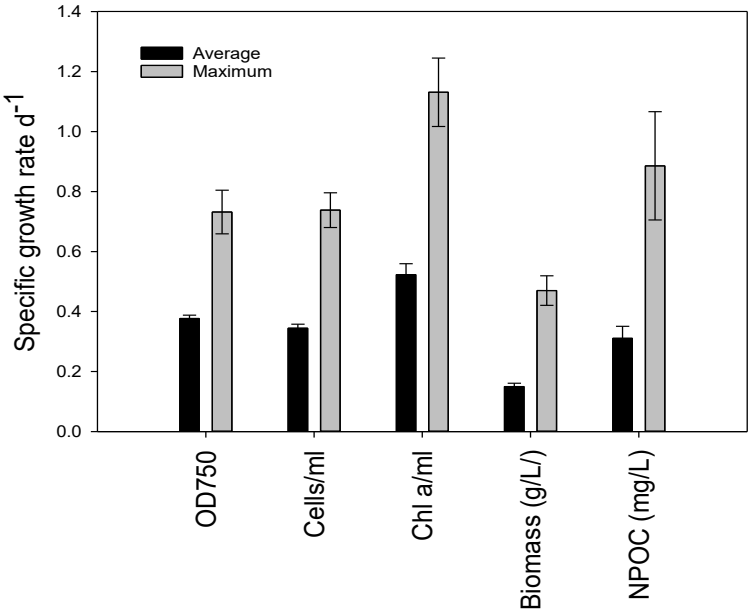

Figure 3-21. Maximum and global specific growth rates WT cultures over the course of the 8-day pond culture growth. Specific growth rates were calculated as ln(y1-y0/x1-x0). N=3, error bars = stdev.

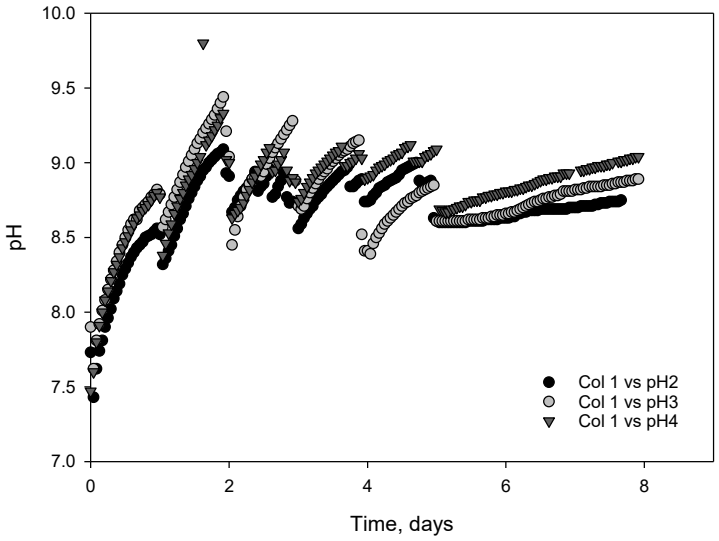

Figure 3-22. pH of WT cultures over the course of the 8-day pond culture growth. 2, 3 and 4 denote separate ponds used for culturing.

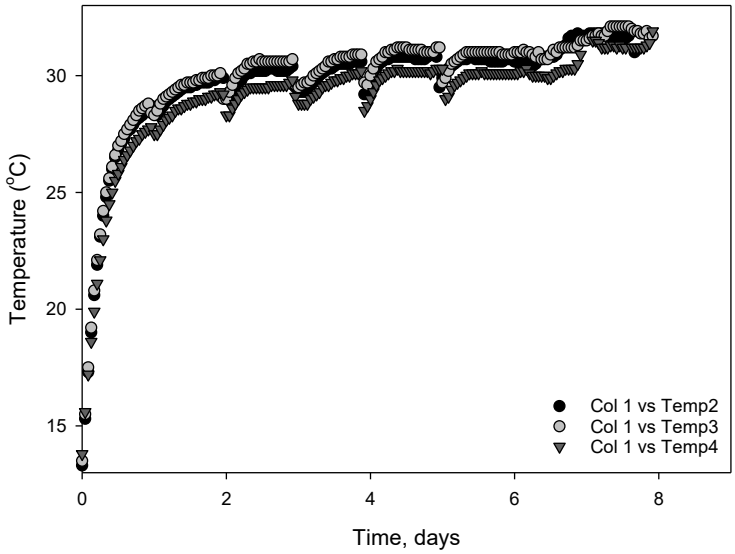

Figure 3-23. Temperature (°C) of WT cultures over the course of the 8-day pond culture growth. 2, 3 and 4 denote separate ponds used for culturing.

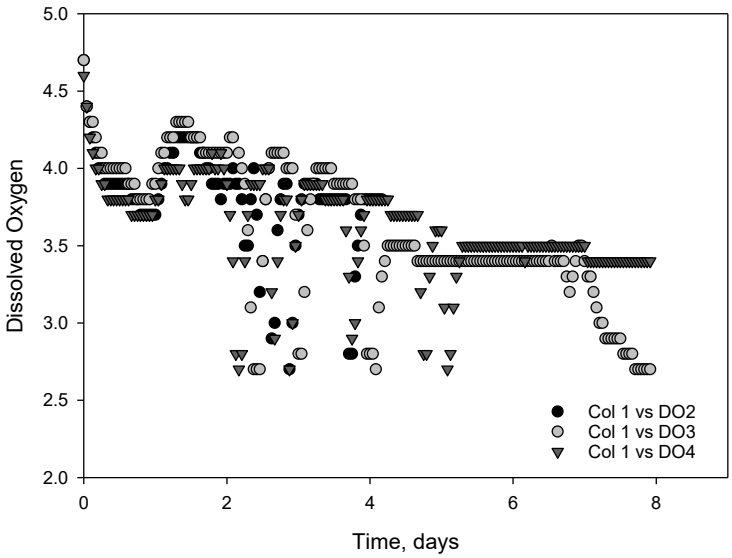

Figure 3-24. Dissolved oxygen of WT cultures over the course of the 8-day pond culture growth. 2, 3 and 4 denote separate ponds used for culturing.

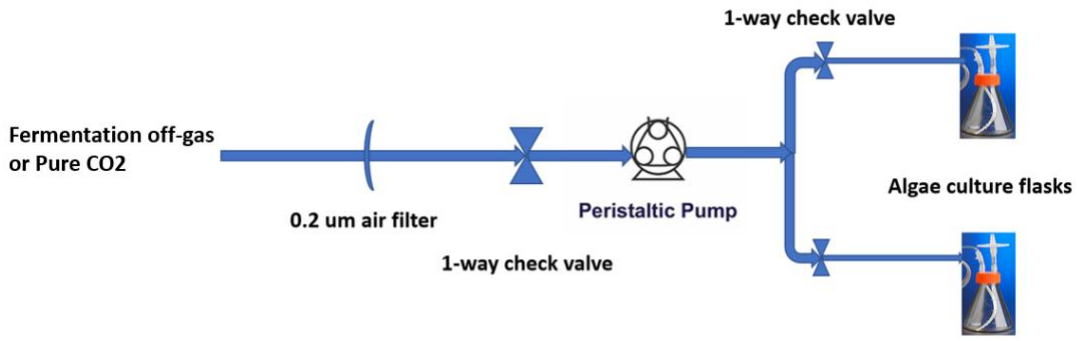

Figure 3-25. Schematic design of the algae cultivation on fermenter off gas.

Figure 3-26. Algae cultivation at New Belgium Brewing. Left: day 0; Right: day 7

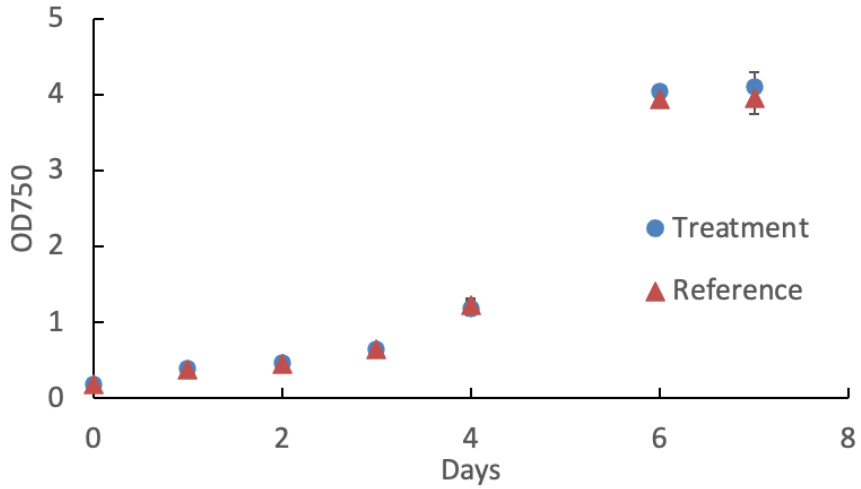

Figure 3-27. The growth of wild-type *N. oceanica (*strain CCAP 849/10) in 500 mL flasks at NBB. Treatment: fermentation off-gas; Reference: Pure CO_2.

Subtask 3.4: Engineering process modeling

Milestone 3.4.1: Set baseline cost and sustainability metrics for system and process performance with respect to energy and mass balance using at least two integrated potential conceptual integrations of CO_2 delivery and biomass productivity improvements.

One of the main previously identified gaps in terms of data for the assessment work was the need for accurate estimates of water circulation in algae farms and associated energy consumption of pumps. This subtask entailed a joint effort to combine the detailed water and medium circulation data from CSU's MATLAB model (on an hourly basis) with the rigorous thermodynamic models from Aspen Plus to estimate the energy consumption for specific operations within an updated algae farm framework.

Previous work at NREL was leveraged to re-design an algae cultivation facility with both water and CO_2 delivery networks. Starting from large scale (5,000 acres) raceway-based facilities (Davis et al. 2016), several changes were carried out in Aspen Plus simulations so they account for the size and cultivation conditions of the ponds employed by Qualitas Health. The main adjustments were:

- Scaling down from 5,000-acre algae farms to a unit comprised of 48 ponds of 1.1 acre each;
- Re-sizing pipelines to account for a lower number of smaller ponds and a lower pump pressure for medium recirculation;
- Adjusting several algae-growth related parameters (pond depth, algae concentration at harvest, CO_2 uptake efficiency, and evaporation rate); and
- Including the operations particular to the operational strategy in the ECUA project (use of a membrane module, with ancillary storage tanks and pumps).

Table 3-2 presents the main streams for which more granularity is required to estimate the effect of coupling bicarbonate delivery to an algae farm with carbonic anhydrase membrane modules. The simulations consider that 80% of the CO_2 needed for algae growth is obtained through the air/pond interface, while the remaining 20% are supplied by the membrane-based system (or by a supplemental bicarbonate source when additional carbon is needed).

Initial technical results pointed to energy consumption with pumping of medium/fresh water in this updated algae growth strategy being largely stable throughout the seasons of the year. In other words, the energy required to circulate individual streams in the algae farm is essentially only a function of the estimated outlet pressure of the pump corresponding to each stream. Table 3-2 also shows the required outlet pump pressures to circulate the different streams through the algae facility (between ponds, tanks, membrane modules, and the dewatering section) and the specific power consumption for each of these components. By employing detailed flowrates determined with CSU's Matlab model, it is possible to estimate the minimum and maximum power requirements associated with the algae facility.

In general, the power demanded by paddlewheels is the major driver in the total energy consumption of the algae farm (and remains essentially constant throughout the day, with or without algae growth, at a value above 56 kW). However, this

energy requirement can be lowered through a reduction in the mixing velocity of the culture medium during the night (Rogers et al. 2014). Other operations have lower impact on total energy consumption. Power demand for medium recirculation from the dewatering facility back to the ponds may present wide variations on an hourly basis. Early estimates for the average power consumption for year-round operation are *ca.* 9 kW (extrapolated from summer simulations), which is much lower than the energy associated with paddlewheels. The circulation of medium through the membranes for CO_2 fixation, on the other hand, is less variable but would account for an average 9 kW throughout a year's worth of operation of the facility. Finally, the energy demand to send the bicarbonate solution from storage tanks to the ponds vary considerably on an hourly basis, with an estimated average power consumption of 7 kW. Power consumption for CO_2 pumping is not considered in the simulations: it is assumed that CO_2 is delivered at relatively high pressure to the facility, and this allows to CO_2 delivery without the requirement of additional pressure changes.

The specific energy consumption values reported in Table 3-2 above for water and pond media pumping were integrated with the dynamic engineering process model to determine facility wide energy consumption on an hourly basis throughout the year. Flowrates within the engineering process model have been fully integrated with the dynamic microalgae growth model detailed in Greene et al. (2021) and this integration allows for the full characterization of mass and energy streams for the algae cultivation facility in any location across the United States with temporal resolution. Furthermore, multiple facility configurations have been explored including multiple pathways for carbon sourcing, carbon delivery to the facility, carbon delivery to open raceway ponds, and other important parameters such as harvesting frequency. Two main scenarios are described below to outline modeling capabilities. The first scenario is the baseline representative of current industry practice in which pure CO_2 is delivered to ponds via gas sparging and is injected into the ponds based on microalgae growth rates coupled with pH changes in the pond. For the baseline scenario, ponds are harvested with an intermittent 5 day harvesting sequence. For a facility like Qualitas with 48 ponds, this translates to ~10 ponds being harvested each day with roughly 30-40% of the pond volume removed from ponds and sent to the dewatering facility. However, harvested volume is entirely dependent on microalgae growth rate and desired biomass concentration post-harvest, values incorporated as inputs into the engineering process model. Figure 3-28 shows the facility wide algae cultivation energy consumption for 48 pond facility with 52 wetted acres of cultivation area located in Southern California generated with the engineering process model.

As seen in Figure 3-28, harvesting flow rates are constant for 5 days at a time, and reflect the staggered harvesting operation in which only a fraction of ponds in the facility are harvested each day. Operating the facility in the fashion assumes that initial pond inoculation is staggered to match the desired harvesting sequence, and by the time the final group of ponds is harvested, the initial group of ponds has had 5 days to grow out and is once again ready for harvest. To determine flowrates, the harvested volume is assumed to be removed from the pond over a 6-h draining period and pumped back to the pond from the dewatering facility over a 6-h fill period. Operating within these time constraints ensures that the ponds can be

drained and filled overnight, avoiding pond downtime during daylight hours and optimizing pond operations for maximum algae growth.

The second scenario is based on using the enzymatic membrane to deliver CO_2 to the ponds, mainly in the form of bicarbonate. To regulate pond pH and meet the continuous carbon demand of the growing microalgae, an hourly harvesting sequence is required for successful operation. An hourly harvesting sequence is a novel concept for microalgae production; however, this approach may offer several unexpected benefits. Operating within a smaller cell concentration range could optimize growth by controlling light attenuation from self-shading and maintain optimal light conditions within the culture. Furthermore, hourly harvesting would allow for a continuous supply of pond medium to pass through the enzymatic membrane and also for pond medium to be supplied to the pond continuously without any concern of exceeding pond volume limitations. One goal of this modeling work was to quantify and understand the additional pumping energy requirements from the added infrastructure required to pump pond media from ponds to dewatering, from dewatering to the membrane, through the membrane module, from the membrane to the storage tank, and finally from the storage tank back to the ponds. Figure 3-29 illustrates the facility wide energy consumption with the added infrastructure for a continuous hourly harvesting sequence.

As seen in Figure 3-29, there are additional pumping requirements when operating the facility with a continual hourly harvesting sequence. While removal and delivery of media from the ponds occur on an hourly basis, the energy associated with pumping media through the membrane module (purple line) and pumping to the storage tank (red line) are constant for 24-h periods. The constant 24-h flow rates are a function of assuming that daily harvested volumes are held in settling tanks and total volume from dewatering to the membrane is split over 24 h to minimize membrane flowrates and allow for 24/7 membrane operation. The bicarbonate storage tank allows for on-demand delivery of bicarbonate to the ponds and the flowrate from the storage tank to ponds (dark orange lines) follows the microalgae growth trends. Figure 3-30 outlines the total facility-wide energy consumption to compare the two scenarios and determine the increase in required process energy.

The energy consumption of the membrane scenario with continual harvesting is on average 45% higher than the baseline scenario (Figure 3-30). What is not reflected is the expected increase in microalgae growth rate and CO_2 utilization efficiency when using the membrane module; this was incorporated in subsequent model improvements, along with determination of whether the added capital expenditure for the bicarbonate storage tank, the membrane module, additional piping and pumps, and the increased operational expenditure from the 45% increase in operational energy is offset by the expected increase in microalgae production from more efficient carbon delivery and optimized growth from minimized self-shading. This economic trade-off will be explored in detail through TEA with the completed engineering process model providing a robust foundation.

In summary, the completed engineering process model is capable of dynamically calculating facility wide media and fresh-water flowrates for both the baseline (gas sparging) scenario as well as the enzymatic membrane scenarios on an hourly basis

throughout the year across the United States. Mass and energy calculations are based on outputs from the high fidelity microalgae growth model from Greene et al., 2021 [3] which predicts microalgae growth rate as a function of ambient conditions, strain-specific characteristics, and pond geometry. The carbon logistics module based on the work of Somers and Quinn (2019) allows for scenario analysis of carbon sourcing including flue gas from coal, natural gas, and pure CO_2 sources with functions to determine CO_2 capture and delivery energy based on pipeline distance, pressures, and source stream characteristics. The dewatering module calculates the daily energy required for algae dewatering based on outputs from the cultivation facility with energy consumption and costing based on the work of Davis et al. (2016). The HTL and fuel upgrading model based on the work of Jones et al. (2014) and Sheehan and Savage (2017) considered outputs from the dewatering facility as well as the microalgae composition to dynamically size the HTL reactor and upgrading equipment and determine total fuel output.

Table 3-2. Specific energy consumption for selected strains within the algae farm and associated outlet pump pressures. Simulations were developed for scenarios with high (69%) CUE and target growth rates. Minimum and maximum numbers refer to a sampling period of 1 h of algae growth for 1 year (8760 h) of operation.

Row #	Stream	Outlet pump pressure (atm)	Specific power consumption (W/m^3)	Power requirements during summer (kW)	
				Min	Max
1	Algae suspension from ponds to dewatering facility (flow through harvesting channel)	1.45	18.4	0.01	23.32
2	Fresh water to ponds to account for evaporative loss			0.00	6.08
3	Bicarbonate solution from membrane to storage tank	1.8	33.8	5.91	15.15
4	Solution from storage tank to ponds			0.02	40.84
5	Media added to storage tank solution to achieve correct molarity for ponds			0.00	5.86
6	Media from dewatering through membrane module	2.0	42.3	7.38	18.94
7	Culture medium recirculation from dewatering back to ponds [a]	2.5	57.8	0.00	49.77
8	Medium circulation in raceway (paddlewheel)	-	1.18 [kW/acre]	56.70	56.70

[a] Calculated for a mass flow corresponding to the difference between flowrates through the harvesting channel and the membrane modules.

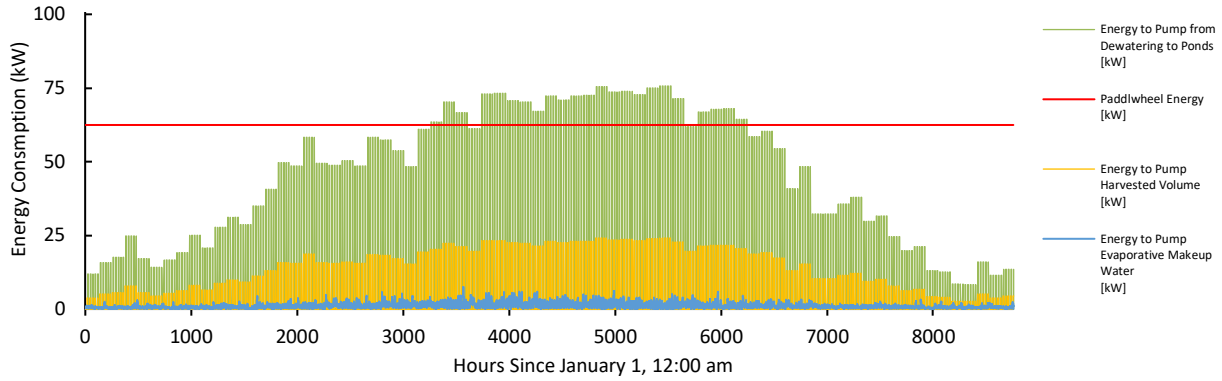

Figure 3-28. Facility wide energy consumption values for a 52 wetted acre facility with baseline scenario assumptions including a 5-day intermittent harvesting sequence, a culture concentration set point of 0.5 g/L and CO_2 delivered via sparging.

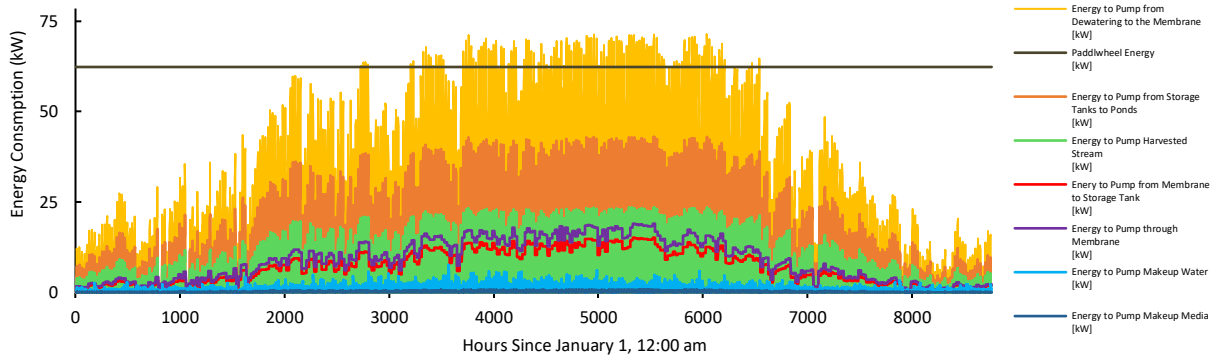

Figure 3-29. Facility wide energy consumption values for a 52 wetted acre facility with continual hourly harvesting, a culture concentration set point of 0.8 g/L and CO_2 delivered via the enzymatic membrane module.

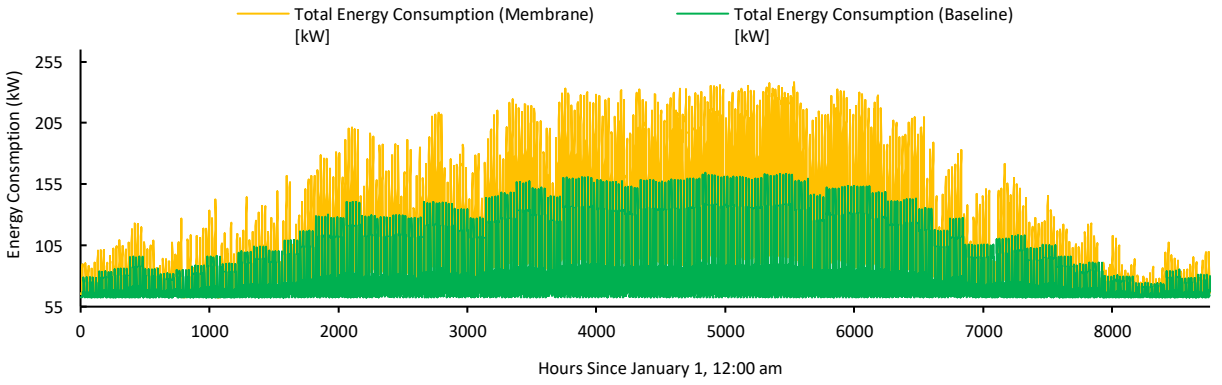

Figure 3-30. Total facility-wide energy consumption values for a 52 wetted acre facility with continual hourly harvesting and a membrane module (yellow lines) and 5-day intermittent harvesting with gas sparging (green lines). On average, the membrane scenario requires 45% more energy for on-site circulation of pond medium.

Subtask 3.5: Concurrent TEA and LCA

Milestone 3.5.1: Establish end-of-project minimum biomass selling price and environmental impact based on final experimentally demonstrated system performance.

Techno-economic analysis and life cycle assessment were established for the enzymatic membrane system for carbon delivery in open raceway ponds. Previous work on this task provided spatio-temporal economic results for the Minimum Biomass Selling Price (MBSP in $/tonne AFDW) and Minimum Fuel Selling Price (MFSP in $/GGE) for the baseline case of gas sparging throughout the United States. These economic metrics were calculated for both a constant cost of CO_2 ($45/tonne CO_2, Davis et al. 2016) and a regionally-varying cost of CO_2 based on stationary point-source emitters throughout the United States (US EPA 2017). Results indicated that a regionally dependent cost of CO_2 (dependent on the source capacity, purity, and proximity to the algae cultivation facility) significantly affected both the MBSP (up to a $520 increase per tonne AFDW) and the MFSP (up to a $5 increase per GGE).

The same economic parameters were evaluated for open raceway pond cultivation using the enzymatic membrane system and operating on a continuous hourly harvesting schedule. Additionally, economic performance of the membrane system was evaluated with a both a constant and varying cost of CO_2. To compare economic performance with the baseline sparging scenario, high impact membrane performance parameters were set to previously established baseline values and general system assumptions regarding CO_2 exchange between open raceway ponds and the atmosphere were harmonized with assumptions in the previous quarterly report. Thus, the results presented are for a system in which 45% of the carbon demand of the ponds is absorbed via the air-pond interface and 55% percent of the stoichiometric carbon demand is supplied by the membrane. While the fraction of the carbon demand is harmonized with the sparging scenario, the overall carbon utilization efficiency was increased to 69% for the membrane system (as opposed to the 25% CUE assumed for the sparging baseline).

In terms of the membrane parameters, the model was configured so that the pond medium exiting the membrane would have a molarity of total iC of 13.31 mM DiC (informed from lab-scale experiments in which membrane effluent achieved molarities upwards of 11 mM DiC). Membrane CAPEX was set to $15/$m^2$, bicarbonate storage tank CAPEX was set to $96/$m^3$ capacity, and biomass composition was unchanged from values used to produce results for the baseline sparging scenario in the previous quarterly report (~15% lipids, ~40% carbs, ~40% proteins, ~5% ash). The purpose of the spatio-temporal analysis performed and presented here is to analyze the impacts of regional variations in productivity and CO_2 cost on the economic performance of the enzymatic membrane system and compare results against the traditional gas sparging system. Results for the MBSP with the membrane system (for both a constant cost and varying cost of CO_2) are presented in Figure 3-31.

From the results in Figure 3-31, the MBSP with the enzymatic membrane systems with the assumptions outlined above ranges between $790 and $3563 per tonne AFDW depending on the location within the US when the CO_2 price is constant. With a varying cost of CO_2, the MBSP for the membrane system ranges between $855 and $3697 per tonne AFDW. Results for the MBSP were compared with the baseline sparging scenario and formulated into additional heatmaps showing the delta between the two carbon delivery systems (Figure 3-32).

The results in Figure 3-32 suggest the use of the membrane system with a constant cost of CO_2 results in an overall higher MBSP (from $80 to $577 increase per tonne AFDW) . This increase is driven by several factors. In the model, when the carbon demands of the pond cannot be met with the membrane (which occurs when the combination of DiC molarity exiting the membrane and available pond volume do not result in enough carbon delivered to the ponds), the system requires the input of sodium bicarbonate to meet the total carbon demand. Additionally, for locations with low productivity, the higher total capital expenses from membrane system and storage tanks as well as the increased energy demand for water pumping are detrimental to system economics. However, when applying a regionally varying cost of CO_2, the membrane shows favorable performance over the sparging system in some locations, lowering the MBSP by as much as $369 per tonne AFDW in areas that are far from CO_2 point sources and have a high CO_2 demand (several locations in Hawaii and the Desert Southwest). With a higher overall DiC concentration exiting the membrane and lower demand from the membrane (due to a higher carbon exchange at the air-pond interface), membrane system economics are significantly more favorable by eliminating the need to add supplemental sodium bicarbonate to the ponds.

In addition to the MBSP, modeling results were carried through the HTL and upgrading model from Chen and Quinn (2021) to produce spatio-temporal results for the MFSP with the membrane system with both a constant and varying cost of CO_2, Figure 3-33. These results suggest the MFSP with the enzymatic membrane system and a constant cost of CO2 (with membrane performance and cost assumptions outlined above) ranges from $8.9 to $35.8 per GGE depending on the location of the facility within the US. With a regionally varying cost of CO_2, the MFSP for the membrane system ranges from $9.5 to $37.3 per GGE. The results in Figure 3-33 were compared with the MFSP for the sparging scenario to show the difference in costs between the two carbon delivery systems (Figure 3-34). This comparison indicates an overall higher MFSP when installing and operating the membrane system with a constant cost of CO_2. Costs increase by $1.6 to $5.9 per GGE depending on location within the US due to higher capital and operational costs for membranes, tanks, and circulation systems as well as the inability of the membrane system to meet the total carbon demand because of insufficient DiC molarity exiting the membrane combined with pond volume limitations. However, when applying a varying cost of CO_2, the membrane system shows favorable economics compared to the sparging system, lowering the MFSP by up to $2.5 per GGE in some locations. This decrease in costs is due to a lower overall CO_2 demand from a higher CUE (69% compared to 25% for the sparging system) which allows the membrane system to cope with increasing regional CO_2 prices.

Modeling infrastructure was developed to evaluate the life-cycle impacts of algae cultivation throughout the US. Regional grid emissions obtained from eGRID (US EPA 2020) and Summers et al. (2021) were used to generate spatio-temporal LCA results for algae cultivation across the US with each of the evaluated carbon delivery systems (Figures 3-35 and 3-36). The results shown in Figures 3-35 suggest higher overall greenhouse gas emissions when using the enzymatic membrane system (from -0.7 to 1.5 kg CO_2-eq/kg AFDW) compared to traditional gas sparging (from -1.3 to 0.9 kg CO_2-eq/kg AFDW). The higher emissions can be attributed to insufficient DiC concentration exiting the membrane and the need for supplemental sodium bicarbonate addition to the ponds. In addition to determining the GWP for algae cultivation, the well-to-wheels GWP was determined for algal cultivation (with both sparging and the membrane) and fuel conversion via HTL (Figure 3-8).

The results in Figure 3-36 suggest a well-to-wheels GWP ranging from 71.7 to 223.7 g CO_2-eq per MJ fuel for when using the membrane system and a GWP ranging from 26.1 to 180.5 g CO_2-eq per MJ fuel when using traditional gas sparging. From the results, there are no locations throughout the US in which the well-to-wheels GWP for the membrane system is below the renewable fuels standard for renewable diesel (~45 g CO_2-eq/MJ fuel); however, however, several locations along the West Coast and in the southern US satisfy the renewable fuels standard when using gas sparging. Regional differences are due to varying productivity as well as varying greenhouse gas intensity for the different grid regions. GWP is higher for the membrane system due to increased facility energy demand and the addition of supplementary bicarbonate when the concentration of DiC in the pond medium is insufficient to meet the total carbon demand given the available pond volume.

The GWP of the membrane system and sparging systems were compared to show the delta between the two systems as a separate heat map (Figure 3-37) [left]. Additionally, the GWP contribution from supplemental bicarbonate addition was plotted throughout the US (Figure 3-37) [right]. These results suggest that well-to-wheels GWP for the enzymatic membrane system is 39.2 to 52.9 g CO_2-eq per MJ higher than cultivation with a traditional gas sparging system. While the renewable fuels standard is not satisfied with the membrane system, this is due to the addition of sodium bicarbonate which contributes between 36 and 48.8 g CO_2-eq per MJ fuel dependent on regional variations in productivity. With a higher DiC concentration exiting the membrane, and higher exchange at the air-pond interface, the need for sodium bicarbonate could be eliminated. Removing the contribution of sodium bicarbonate from the total GWP would result in larger number of locations throughout the us in which the cultivation and conversion of microalgae could provide renewable diesel while satisfying the renewable fuels standard.

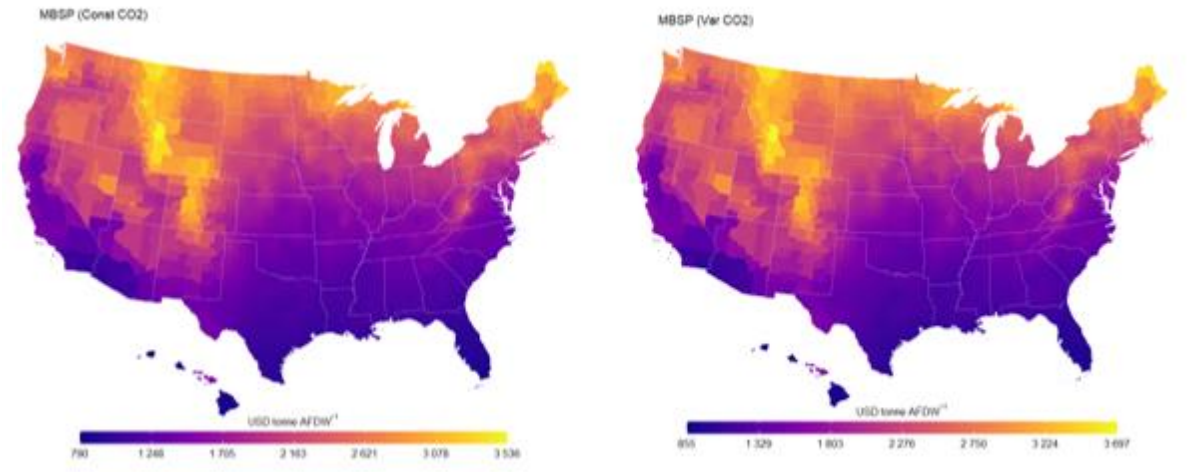

Figure 3-31. Minimum Biomass Selling Price in $/tonne AFDW for algal cultivation in open raceway ponds using the enzymatic membrane system. Costs are presented for both a constant CO_2 price ($45/tonne CO_2) [left] and a regionally-varying cost of CO_2 [right].

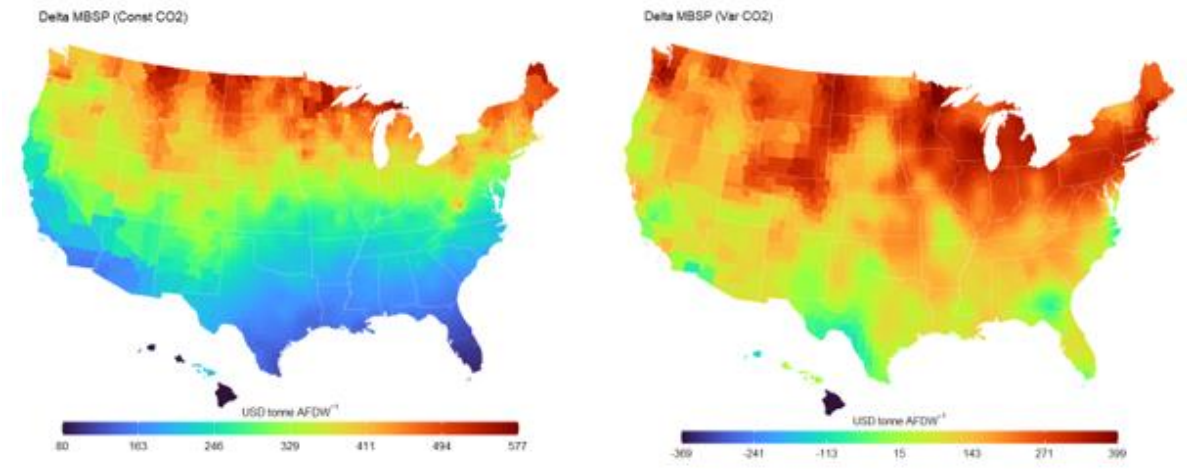

Figure 3-32. Delta in the Minimum Biomass Selling Price in $/tonne AFDW between the membrane and sparging scenarios for both the constant CO_2 price scenario [left] and the varying CO_2 price scenario [right]. The results show the difference between membrane and sparging scenarios, with positive numbers indicating higher MBSP for the membrane system.

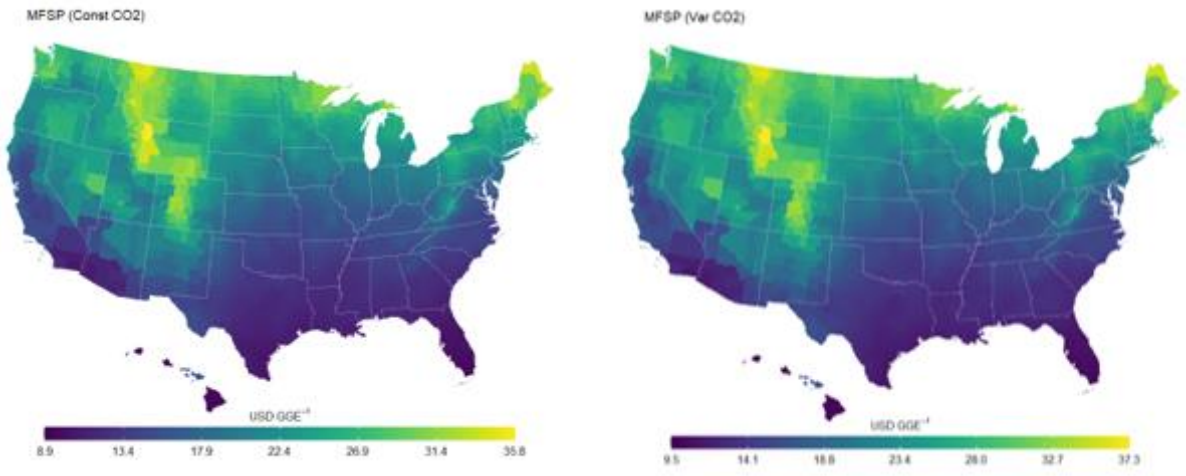

Figure 3-33. Minimum Fuel Selling Price in $/GGE for algal cultivation in open raceway ponds with fuel conversion via hydrothermal liquefaction using the membrane system for carbon delivery. Costs are presented for both a constant CO_2 price ($45/tonne CO_2) [left] and a regionally varying cost of CO_2 [right].

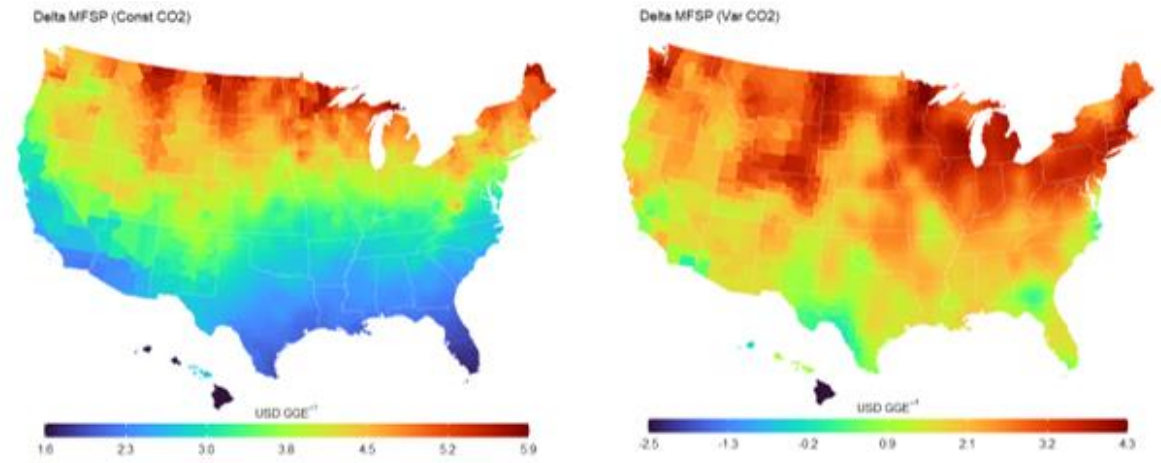

Figure 3-34. Delta in the Minimum Fuel Selling Price in $/GGE between the membrane and sparging scenarios for both the constant CO_2 price scenario [left] and the regionally varying cost of CO_2 [right]. The results show the difference between the membrane and sparging scenarios, with positive numbers indicating high costs for the membrane system.

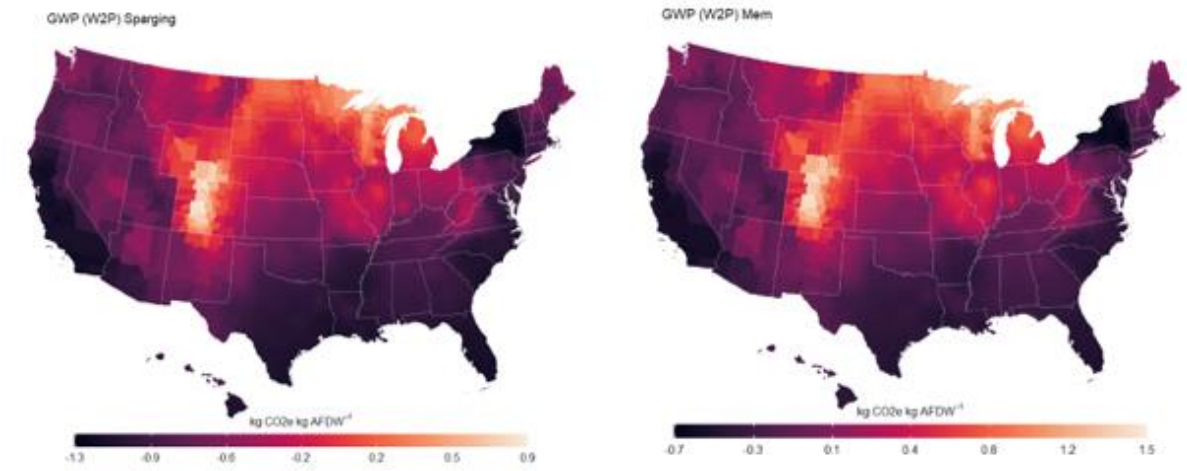

Figure 3-35. Spatio-temporal Global Warming Potential expressed in kg CO_2-eq/kg AFDW for algal cultivation with a traditional gas sparging system [left] and membrane system [right].

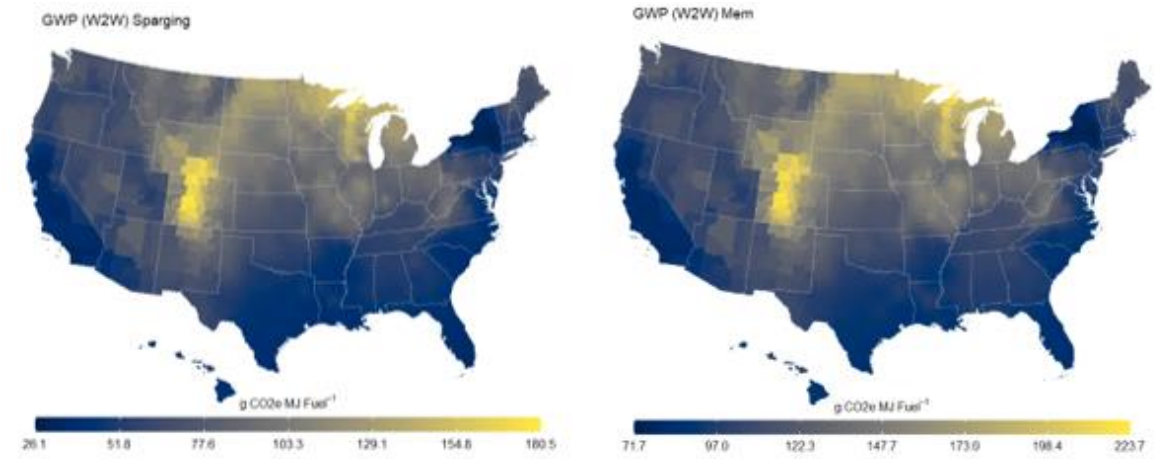

Figure 3-36. Spatio-temporal well-to-wheels Global Warming Potential (GWP) expressed in g CO_2-eq/MJ fuel for algal cultivation with conversion via hydrothermal liquefaction. Results show the GWP for the traditional gas sparging system [left] as well as the system with the membrane for carbon delivery [right].

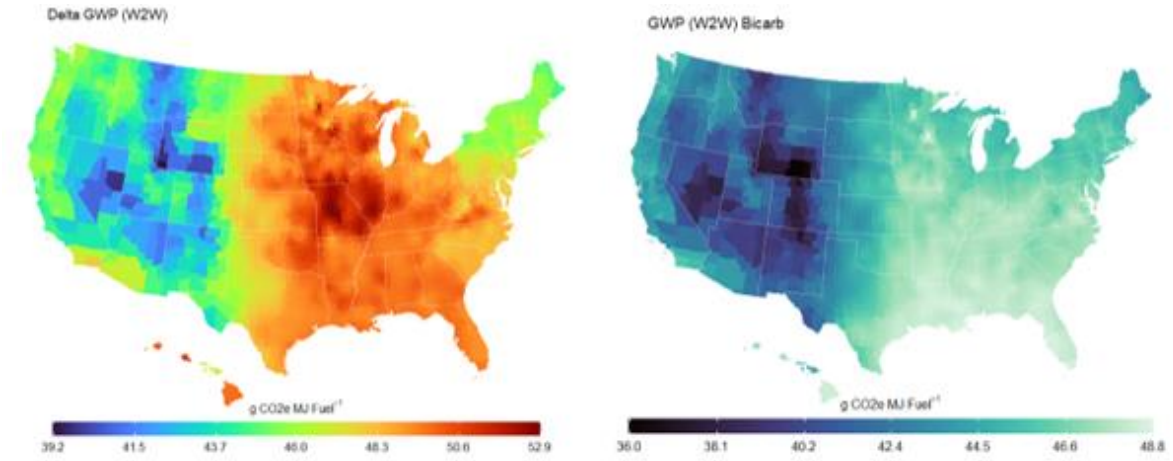

Figure 3-37. Delta in the well-to-wheels Global Warming Potential (GWP) between cultivation systems utilizing the membrane vs. traditional gas sparging [left]. Results shows the difference between the membrane and sparging systems with positive numbers indicating higher GWP for the membrane system. Additionally, the contribution to the GWP from the addition of bicarbonate is shown as a separate map [right].

Go/No-Go 1: Demonstration of enzymatic membrane module for inorganic carbon delivery into an aqueous phase at a minimum flux of 2 x 10^{-4} mol/s·m^2 at pH 7 and 30 °C.

Higher inorganic fluxes are required to lower the membrane surface area (and thus to lower costs). This milestone served as a checkpoint on the development path for the enzymatic membrane technology. By adjusting several design and operational parameters, the team constructed an enzymatic membrane system with performance that exceeded the milestone target.

CA membranes were manufactured using the polystyrene-polyethylene oxide-anthracene block copolymer in a solution of 10 mg/mL bovine CA. The microfluidic prototype module design incorporated a larger and wider flow channel (1 cm^2 to 5 cm^2) (Figure G1-1). Hydrogel encapsulated enzyme was sandwiched between a hydrophobic filter membrane layer and a metal mesh screen layer. By incorporating the hydrophobic PVDF membrane (0.45 µm pores, 75% porosity), water was prevented from entering the gas side of the chamber and excluded from the filter membrane pores. This decreased gas to liquid diffusional distance and increased flux by putting the hydrogel in direct contact with the gas filled pores. Additionally, the mesh screen layer (~1 mm x 1 mm pores, ~75% porosity) on the solution side of the membrane allowed for higher gas pressures to be applied to the membrane.

Initial testing of the updated prototype design and hydrogel membrane manufacturing using the developed module testing setup, resulted in improved transfer of bicarbonate that met the Go/No Go milestone of 2 x 10^{-4} mol/s·m^2. Table G1-1 shows that bicarbonate flux measured from pulled samples for TIC (total

inorganic carbon) content over 24 hours for four different membrane modules tested, two with carbonic anhydrase and two without. Incorporating carbonic anhydrase appears to have significantly improved bicarbonate flux (nearly double). Additionally, increasing the pressure from 3 psi to 7 psi resulted in an increase in dissolved carbon content (nearly double) to meet the Go/No Go milestone. While the module was tested at a slightly lower temperature (RT = 25 °C instead of 30 °C) than the Go/No Go Milestone, the slightly elevated temperature is expected to increase enzyme activity.

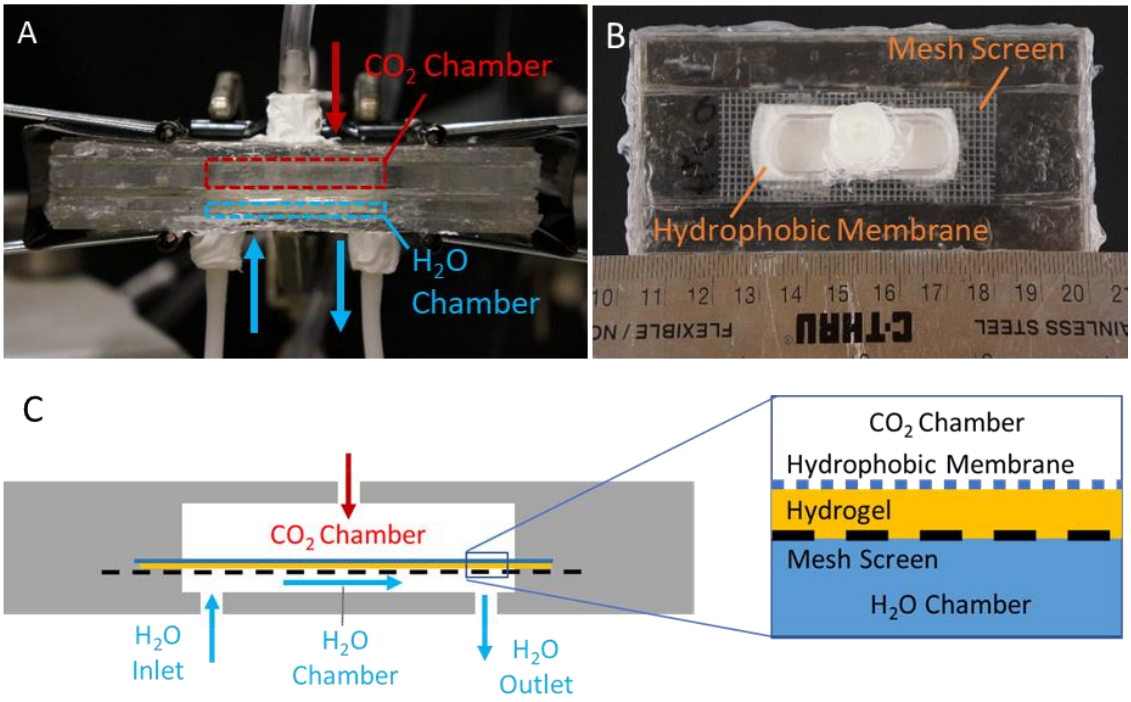

Figure G1-1. Photos of the miniature membrane module used for flux testing with the (A) side view labeled for gas and fluid chambers and the (B) top view labeled with membrane components and (C) side view schematic of gas and solution chambers with flow and membrane components.

Table G1-1. Dissolved inorganic carbon (DIC) flux measurements through four different membrane modules, two with hydrogel only and two with CA-encapsulated hydrogel run continuously over 25 hours at 3 psi and 7 psi.

CO_2 Pressure	**Membrane***	**TIC (mol/m^3)**		**Δ TIC (mol/m^3)**	**Flux ($mol/m^2 \cdot s$)**
		Inlet	**Outlet**		
3 psi	Hydrogel only	0.0956	3.722	3.626	7.2E-05
	CA Hydrogel	0.0985	6.265	6.167	1.2E-04
7 psi	Hydrogel only	0.2526	6.833	6.581	1.3E-04
	CA Hydrogel	0.4308	11.815	11.384	**2.3E-04****

*5 cm^2 membrane area
**pH 7.35, RT=25 °C

Go/No-Go 2: At least one developed variant of N. oceanica *demonstrates at least 20% higher growth in laboratory-based high bicarbonate environments relative to parent strain.*

One of the transformed *N. oceanica* strains (TKK012-20) was found to have higher growth rates when culture media is supplemented with bicarbonate. This was verified by two separate experiments. In the first, WT and TKK012-20 were grown in shake flasks at 300 µmol photons m^{-2} s^{-2} and 25 °C. Triplicate cultures were supplemented with 5 mM $NaHCO_3$, once per day. Growth rates were calculated from daily measurements of OD680. In this experiment the mutant showed <25% increase in daily specific growth rate (d^{-1}) on 4 out of 6 days of cultivation, one day with ~20% increase and one day with slightly lower growth rate compared to the WT strain (Figure G2-1).

A second assessment of growth was performed in similar conditions to those described above, but cultures were grown to an OD 0.2 and then supplemented twice daily with 0.2 mM $NaHCO_3$. Relative changes in biomass were again measured at OD680 and relative growth rates were calculated from 4 subsequent days of growth. TKK012-20 showed a 29% increase in growth over the WT in these conditions, satisfying the Go/NoGo metric (Figure G2-2).

In addition to the BicA strain development in Subtask 2.1, the work of Subtask 2.2 was aimed at creating a strain that is more tolerant to higher bicarbonate concentrations. To achieve this adaptation, an EMS mutant population of *Nannochloropsis* was subjected to continuous adaptation to higher bicarbonate concentration. Three mutagenized populations that outcompeted the growth rate of the WT *Nannochloropsis* by at least 20%. Of these populations, a pair of mutants of *Nannochloropsis* (10-4 and 10-5) were isolated that continue to demonstrate an increased growth rate relative to the wild type under stress-inducing high pH conditions (Figure G2-3).

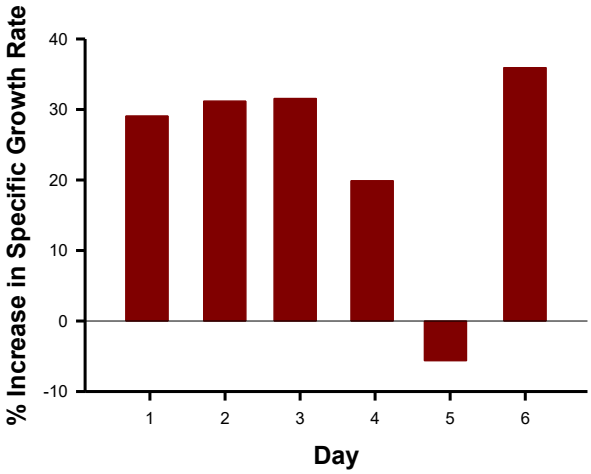

Figure G2-1. Relative increase in growth rate (d-1) of TKK012-20 compared to WT cultures in shake flasks supplemented with 5mM $NaHCO_3$, once per day. Values are averages of biological triplicates.

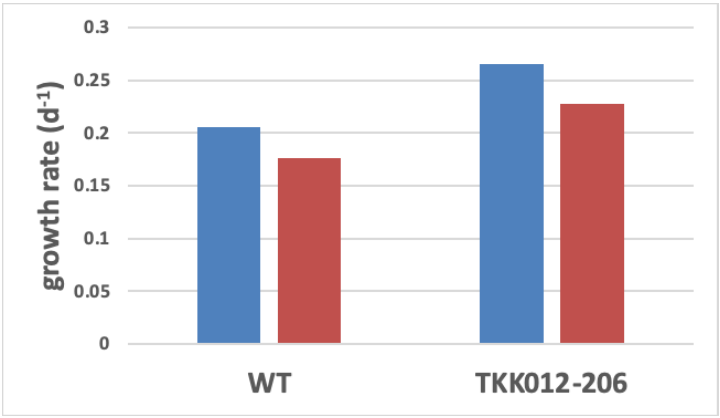

Figure G2-2. Relative growth rates (d^{-1}) of WT vs TKK012-206 (BicA) showing an average of 29% increase of the mutant over the WT. Data for n=2 cultures are shown.

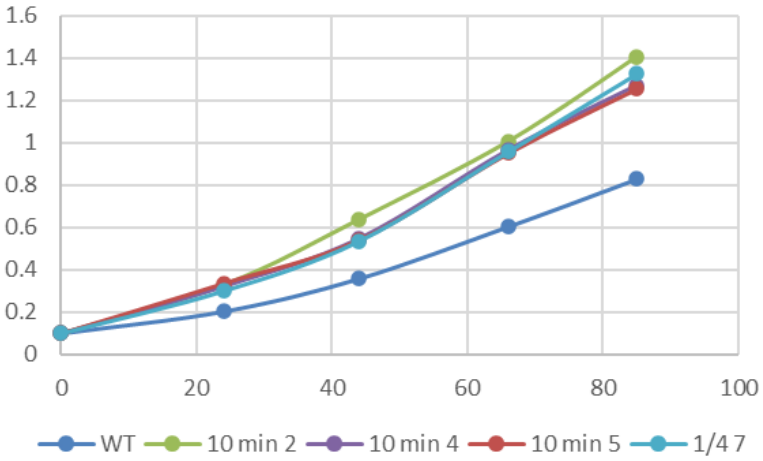

Figure G2-3. Summary of growth rate of mutants relative to the WT *N. oceanica* at pH 9, tracked as OD over time in flask cultures (10 min-4 and 10 min-5 have been selected for further characterization).

Go/No-Go 3 (final): Demonstration of 25% increase in baseline inorganic carbon utilization efficiency over a 6-week continuous cultivation demonstration run at QH test site (mini-ponds plus membrane module plus CO_2 monitoring) and 20% growth rate increase in the integrated systems at CSU and NREL.

<u>CUE increase with use of the membrane module</u>

Milestones 1.2.2 and the Go/No Go 1 milestone were met using bovine carbonic anhydrase (BCA) entrapped in our cross-linked (ω-anthracenylpolystyrene-b-poly(ethylene oxide) diblock copolymer (SO-An). However, due the fabrication limitations that created a thicker hydrogel layer, the UV-crosslinked SO-An hydrogel with entrapped CA resulted in higher gas pressure requirements and decreased

regional pH for the enzyme that likely deactivated the enzyme. Alternative hydrogels with thinner fabrication capabilities were investigated and it was found that covalently attached BCA hydrogel with bovine serum albumin as the matrix using glutaraldehyde as a crosslinker created a thin film with increased carbon flux over membranes that did not contain BCA and maintained good lifetime even after 2 months refrigerated.

Recognizing our limitations in manufacturing large-scale enzyme membranes, we pivoted to the use of commercial hollow fiber membranes for CO_2 transfer. This CO_2 transfer system could be operated in either of two modes: direct feeding (Figure G3-1) and recirculation (Figure G3-2). In both, a membrane contractor (3M™ Liqui-Cel™ EXF-2.5x8) (Figure G3-3A) was connected to a CO_2 gas controller to make dissolved inorganic carbon (DIC) solution, and a dewatering module (Figure G3-3B) was used to produce a clarified solution from the algal cultivation before it was fed to the membrane contactor. The tradeoffs between the two configurations were that the recirculation mode enabled higher DIC levels to be achieved for a given membrane surface area (lower membrane cost) vs. higher pumping and storage tank costs.

The output of the membrane contactor (direct mode) or storage tank (recirculation mode) was pumped into the cultivation pond upon demand to control pH and supply carbon for algal cultivation. The dewatering module (Figure G3-3B) was controlled by an Arduino-based control module and connected with a water level sensor in the algal cultivation pond (Figure G3-3C). When the liquid level was over the set point, the dewatering pump was triggered to remove extra medium into the bicarbonate solution container. The entire DIC solution feeding system was constructed to control the pH and feed carbon in the cultivation pond automatically. All pumps were controlled by a central unit, including the feed to the pond, the storage tank/recirculation loop, the dewatering system and optional freshwater feed using pH and level sensors. pH sensors were used to ensure the membrane module was properly dissolving carbon into the storage tank, to control when the pond needs acidified media fed from the storage tank, and to ensure that the pH in the mixing tank is at an appropriate level. The level sensors for the pond, storage tank, and mixing tank ensured that none of the tanks overflowed and that the pond was fed the appropriate amount of freshwater or acidified medium to make up for evaporative loss as well as nutrient and carbon consumption. Each mode was used in several multi-week experiments.

When the recirculation configuration (Figure G3-2) was used in a 30-d cultivation of WT *N. oceanica* in mini-raceway ponds, the pH controller in the DIC storage tank turned on the pump to make DIC solution by recirculation to the membrane contactor when the pH was above 6.2 and turned off the pump when the pH was below 6.0. The DIC solution in the storage tank was pumped into the cultivation pond to control pH at 8.0 and supply carbon for algal cultivation. Samples were collected daily to analyze the algal cell growth and carbon content during the cultivation. During the 30-day cultivation, the algal biomass was harvested from half of the volume of the ponds at Day 11 and Day 20.

The algal cell growth in both mini-raceway ponds either using CO_2 sparging or the bicarbonate solution feeding system was the same during the 30-d cultivation

(Figure G3-4). Both DIC and non-purgeable organic carbon (NPOC) levels between the CO_2 sparging system and the DIC solution feeding system were the same – except in the first 11 days (Figure G3-5). In that interval, the DIC content in the CO_2 sparging pond was significantly lower than that of the pond with DIC solution feeding. The DIC solution approach was more effective in transferring carbon to the growth medium in this early period, although why this was not the case throughout the cultivation is not known.

The CO2 consumption in the CO_2 gas sparging system and the DIC solution feeding system was monitored daily (Figure G3-6). In the CO_2 gas sparging system, the CO_2 consumption was in the range of 18.4 to 41.0 g/day with average at 29.9 g/d per 75 L cultivation. In contrast, the pond with the DIC solution feeding system consumed on average 15.8 g/d CO_2, ranging from 8.4 to 24.5 g/d, indicating a 90% improvement in the CO_2 utilization efficiency (CUE) on average (Figure G3-7).

Similar results were obtained in a second, 20-day cultivation of WT *N. oceanica* with the CO_2 transfer system in recirculation mode. When the pH in the storage tank was above 6, the pH controller turned on the pump to circulate the solution through the membrane contactor until the pH reached 6. The DIC solution in the storage tank was pumped into the cultivation pond to control pH at 8.0.

During the 20-day cultivation, the algal cell growth as measured by turbidity (OD750) in the mini-raceway ponds, one using CO_2 sparging and the other using the DIC solution feeding system, were statistically the same (Figure G3-8). As before, the DIC concentration in the DIC solution feeding system mini-pond was higher than in the CO_2 sparging system mini-pond in the first 8 days of cultivation (Figure G3-9). However, the DIC concentrations were at similar levels in both ponds in the next 12 days of cultivation.

As shown in Figure G3-10, the CO_2 consumption in the CO_2 sparging system was significantly higher than that of the DIC solution feeding system during the 20 days of cultivation. In the CO_2 sparging system, the daily CO_2 consumption was in the range of 17.9 to 72.8 g/d, averaging 40.9 g/d per 75-L cultivation. In contrast, the pond with the DIC solution feeding system consumed on average about 16.7 g/d CO_2, ranging from 10.7 to 25.2 g/d. The CUE in the DIC solution feeding system pond was 53.6% while the CUE in the CO_2 sparging pond was 28.9% (Figure G3-11). Therefore, the CUE was improved by 85% by using the DIC solution system.

The algal biomass from both mini-ponds was collected at the end of the cultivation and freeze-dried to analyze the algal biomass composition. The DIC solution feeding resulted in higher protein content and lower carbohydrate content than those of the CO_2 sparging system (Figure G3-12). There was no significant difference in ash content and lipid content. The FAME profile analysis showed that the DIC solution feeding resulted in higher C16:0 and C16:1 content than those of the CO_2 sparging system, while the C20:5n3 was significantly lower.

Similar results were also obtained when the direct feeding configuration (Figure G3-1) was used in a 2-week cultivation in mini-raceway ponds. The algal growth was similar whether using CO_2 sparging or the DIC solution feeding system (Figure G3-13). The OD750 and cell dry weight reached the highest at Day 12 in both cases. No

significant difference between the DIC levels resulting from use of the CO_2 sparging system vs. the DIC solution feeding system were found after Day 6 (Figure G3-14).

The CO_2 consumption using CO_2 sparging and the DIC solution feeding system were calculated and compared. In the CO_2 sparging system, the CO_2 consumption was approximately 24 ±1.5 g/d per 75-L raceway cultivation. The pond using the DIC solution feeding system consumed about 10 ± 0.9 g/d CO_2 per 75-L raceway cultivation, indicating a 140% improvement in the CUE on average over sparging.

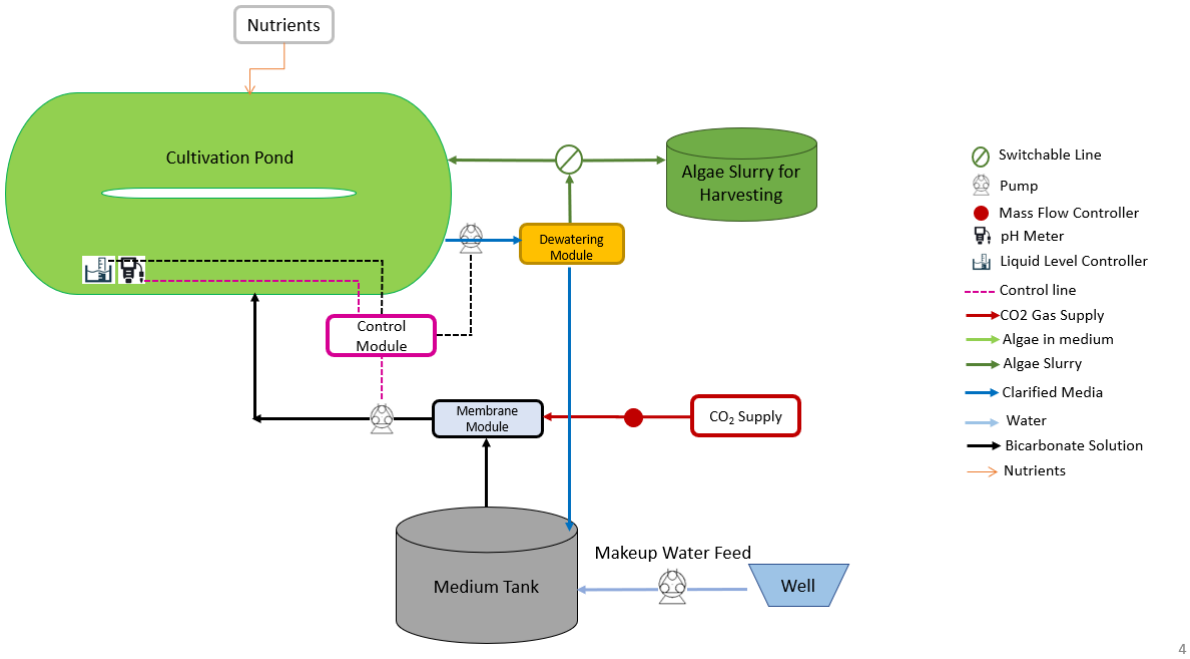

Figure G3-1. Diagram of the direct mode of the DIC solution feeding system .

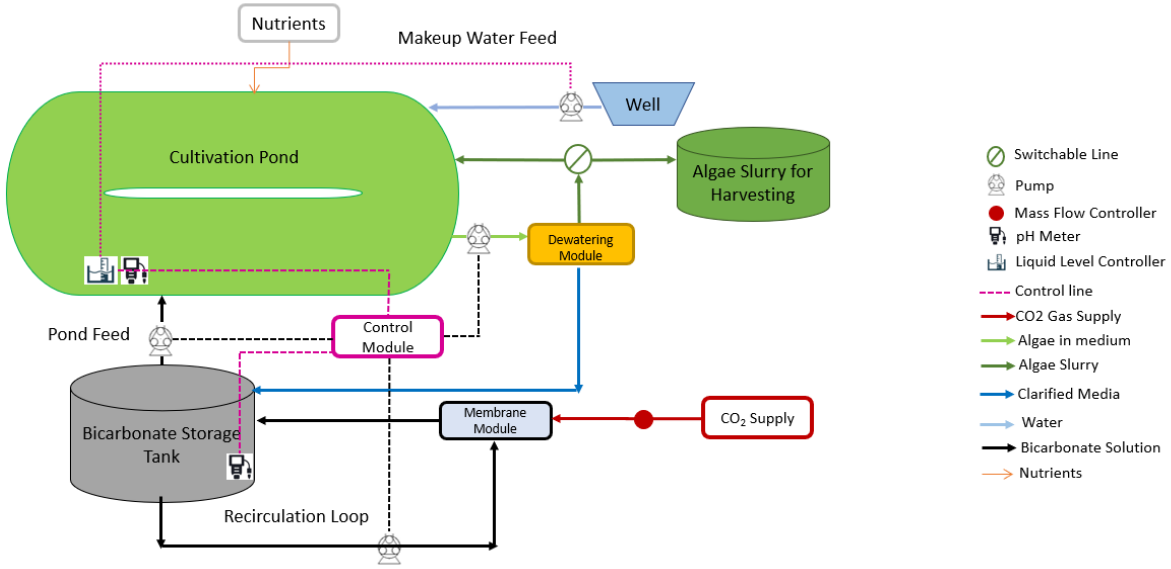

Figure G3-2. Diagram of the recirculation mode of the DIC solution feeding system.

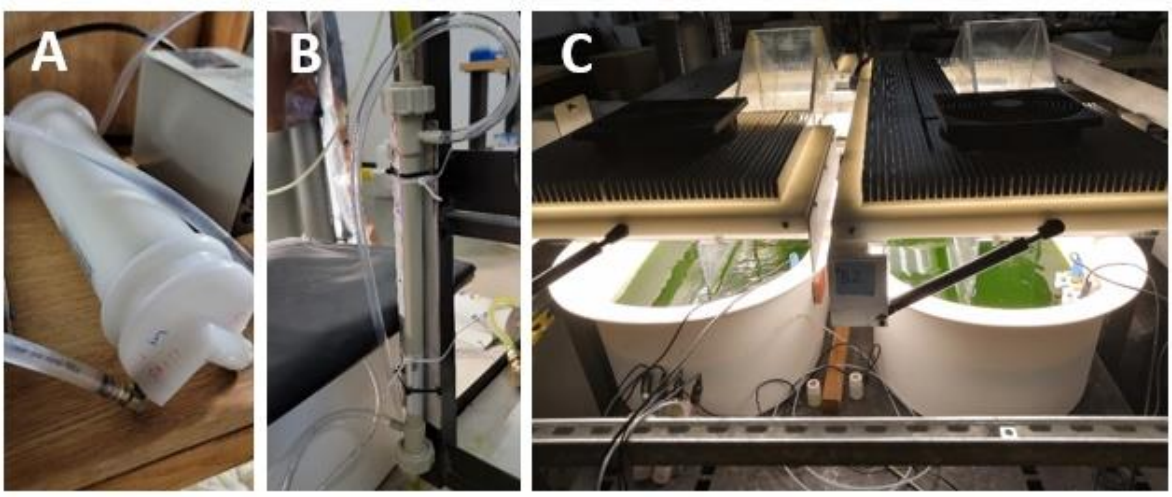

Figure G3-3. A: membrane contractor (3M™ Liqui-Cel™ EXF-2.5x8). B: dewatering module. C: Algal cultivation in mini-raceway ponds.

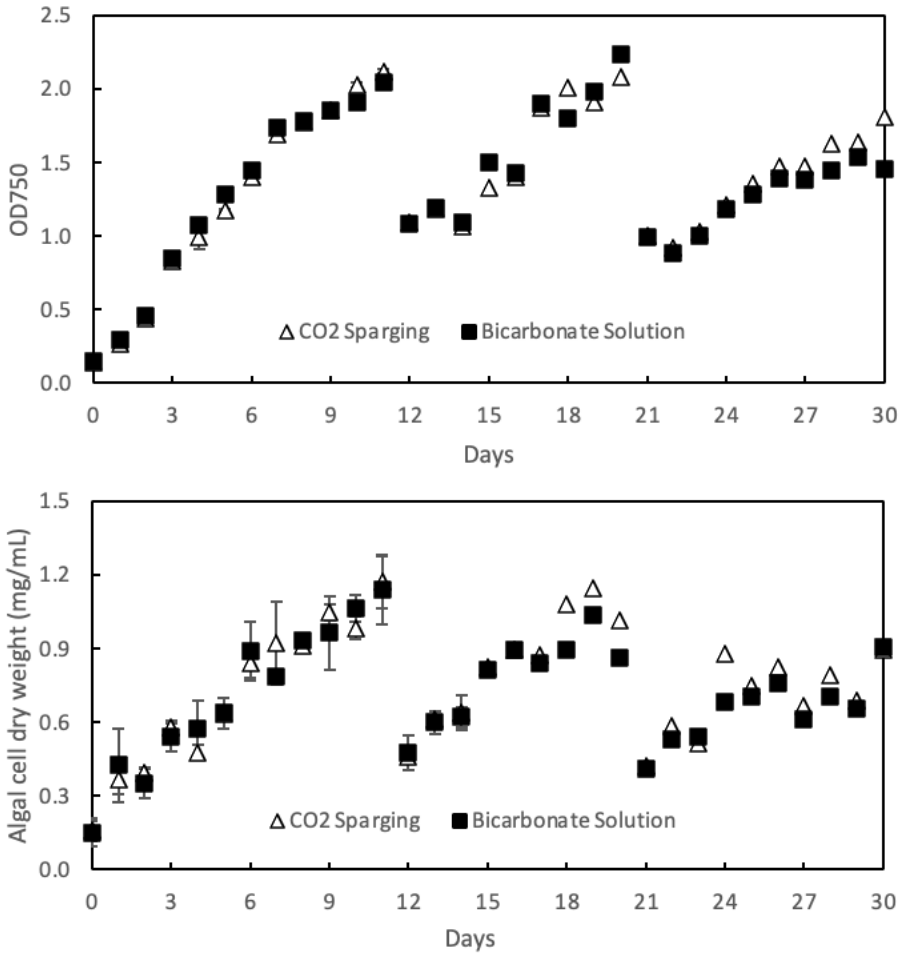

Figure G3-4. Growth of WT *N. oceanica* in the mini-raceway ponds during the 30-day cultivation. CO_2 was supplied either by CO_2 sparging or the DIC solution. Top: OD750; Bottom: algal cell dry weight (mg/mL).

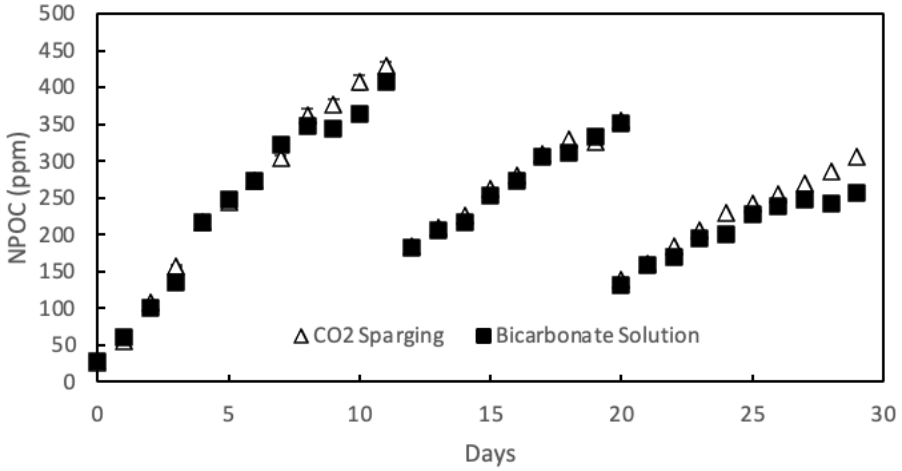

Figure G3-5. DIC and non-purgeable organic carbon (NPOC) concentrations during the 30-day cultivation.

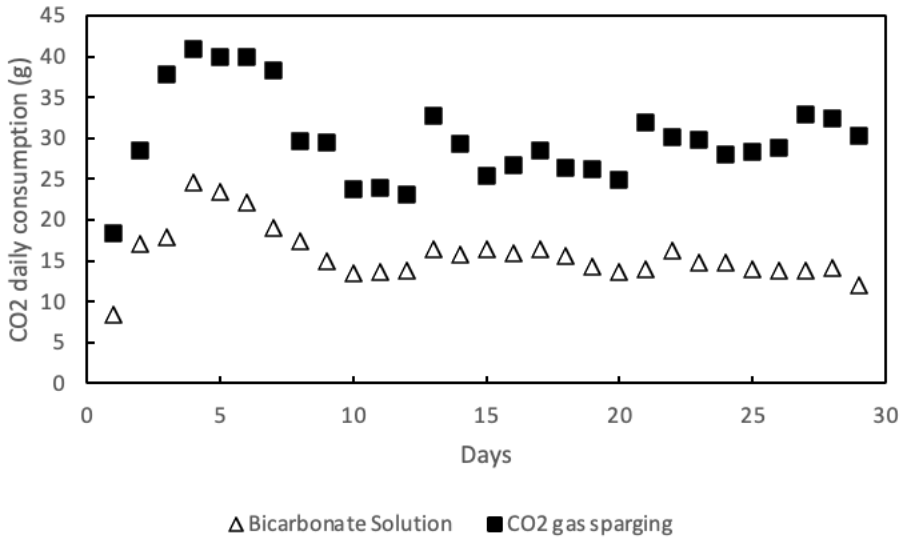

Figure G3-6. CO_2 daily consumption in the mini-raceway ponds. CO_2 was supplied either by sparging or as a DIC solution.

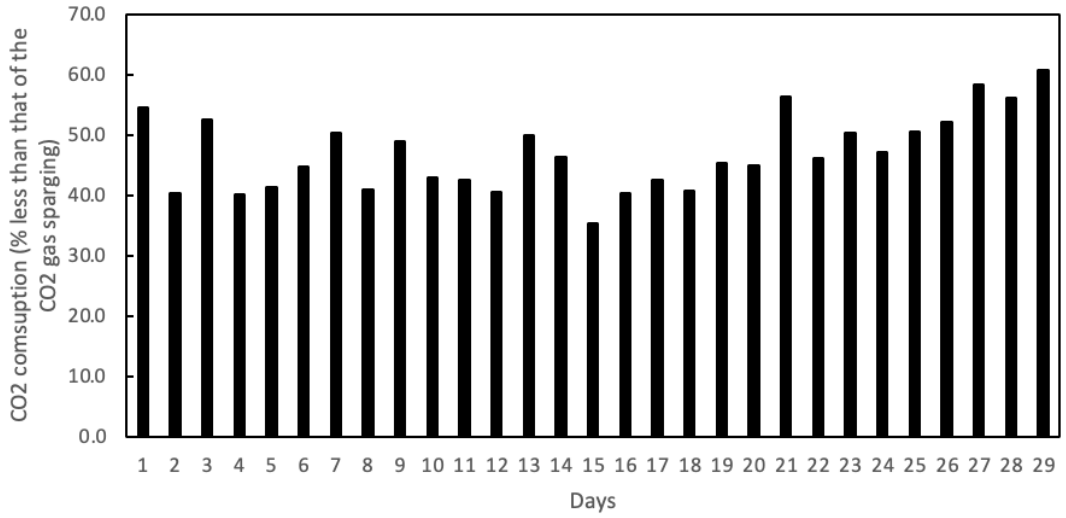

Figure G3-7. Daily CO_2 consumption in the DIC solution feeding system compared to that of the CO_2 sparging.

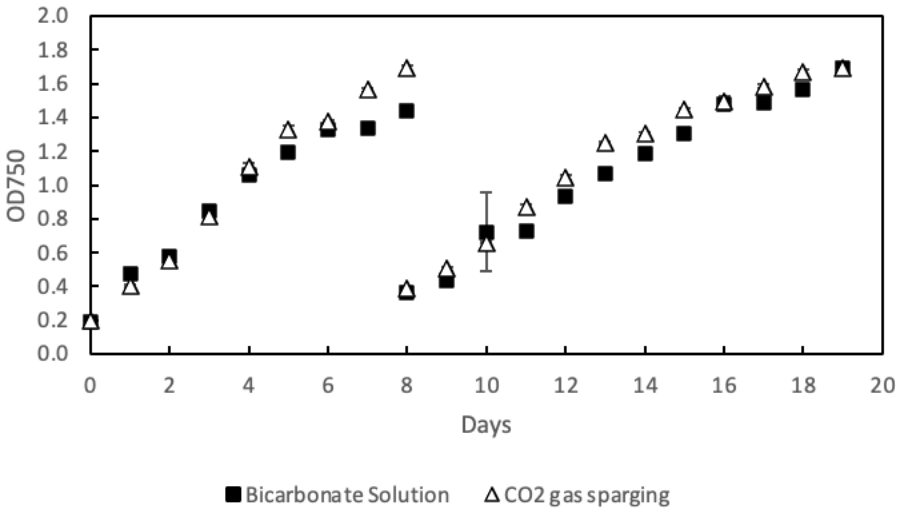

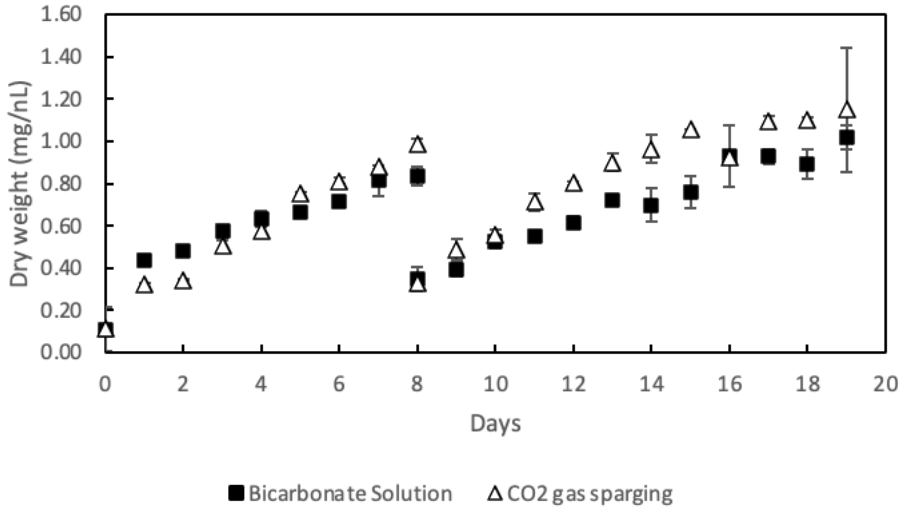

Figure G3-8. Algal cell growth of WT *N. oceanica* in the mini-raceway ponds during a 20-day cultivation. CO_2 was supplied either by CO_2 sparging or the DIC solution (recirculation mode). Top: OD750; Bottom: algal cell dry weight (mg/mL).

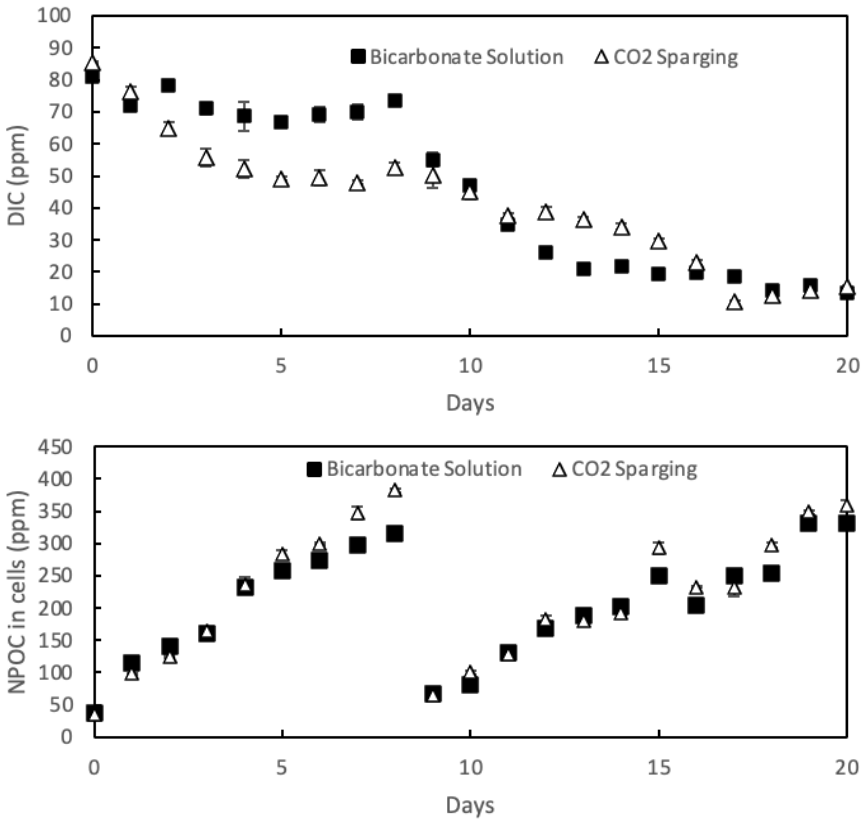

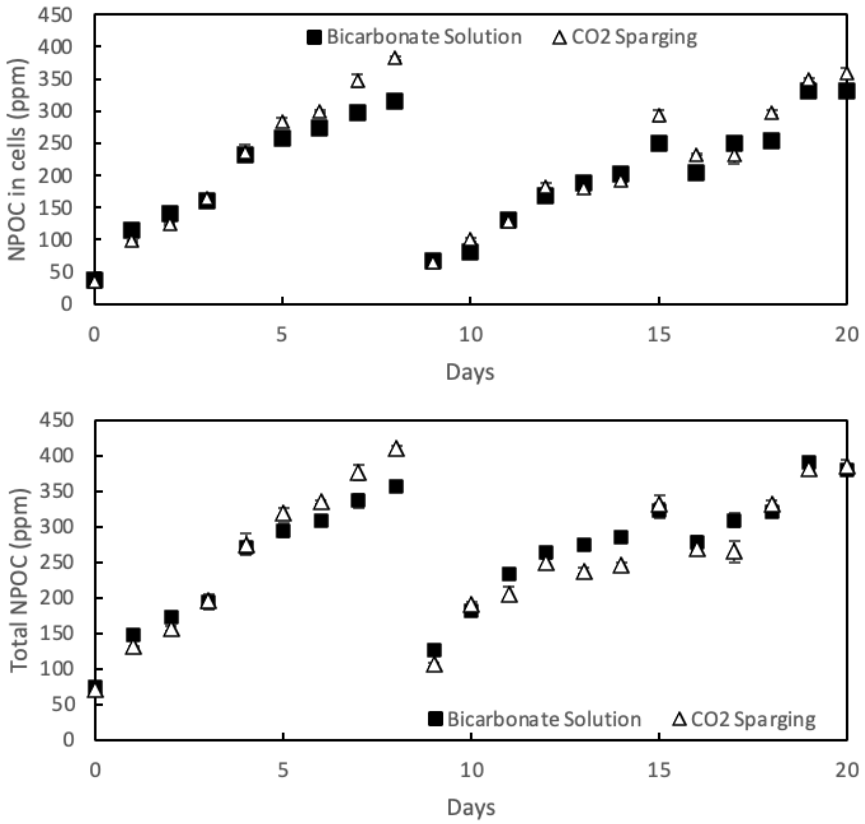

Figure G3-9. DIC, non-purgeable organic carbon (NPOC) in cells, NPOC in medium, and total NPOC content in both ponds during the 20-day cultivation. Carbon transfer system in recirculation mode.

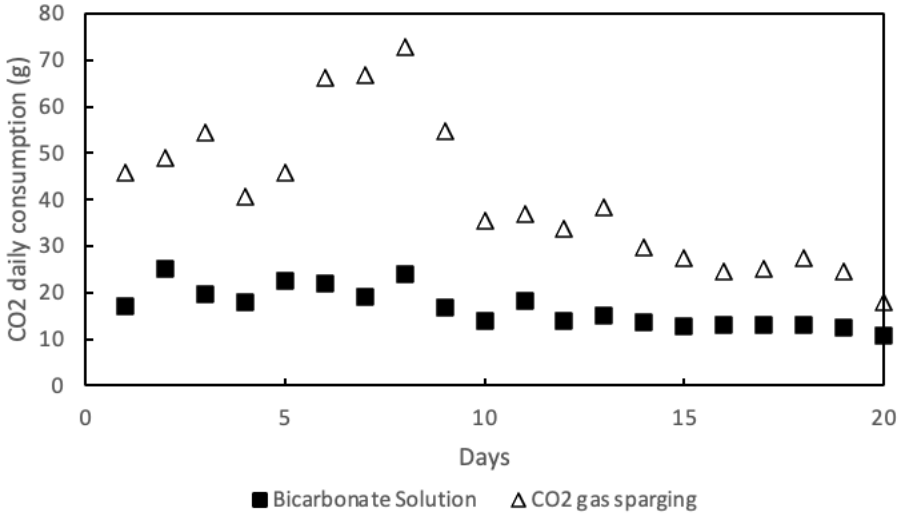

Figure G3-10. CO_2 daily consumption in the mini-raceway ponds in the 20-day cultivation. CO_2 was supplied either by CO_2 sparging or the DIC solution (recirculation mode).

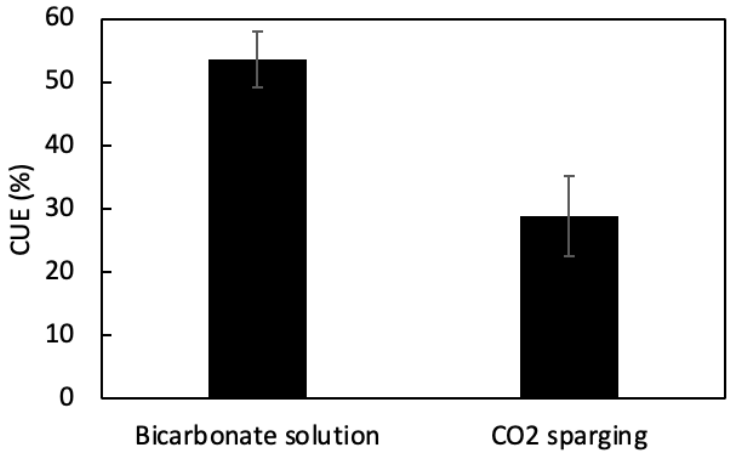

Figure G3-11. CO_2 utilization efficiency (CUE) in the mini-raceway ponds over the 20-day cultivation. Carbon transfer system in recirculation mode.

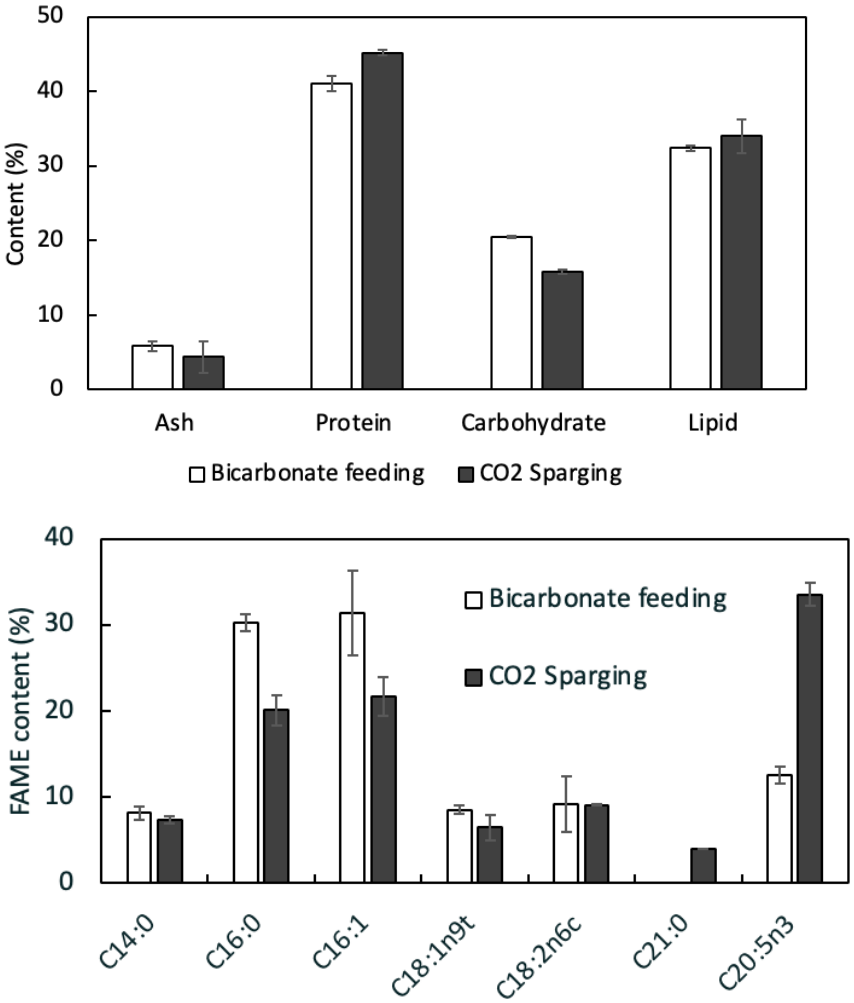

Figure G3-12. The algal biomass composition in the mini-raceway ponds after a 20-day cultivation. CO_2 was supplied either by CO_2 sparging or the DIC solution (recirculation mode). Top: algal biomass composition; Bottom: FAME profile.

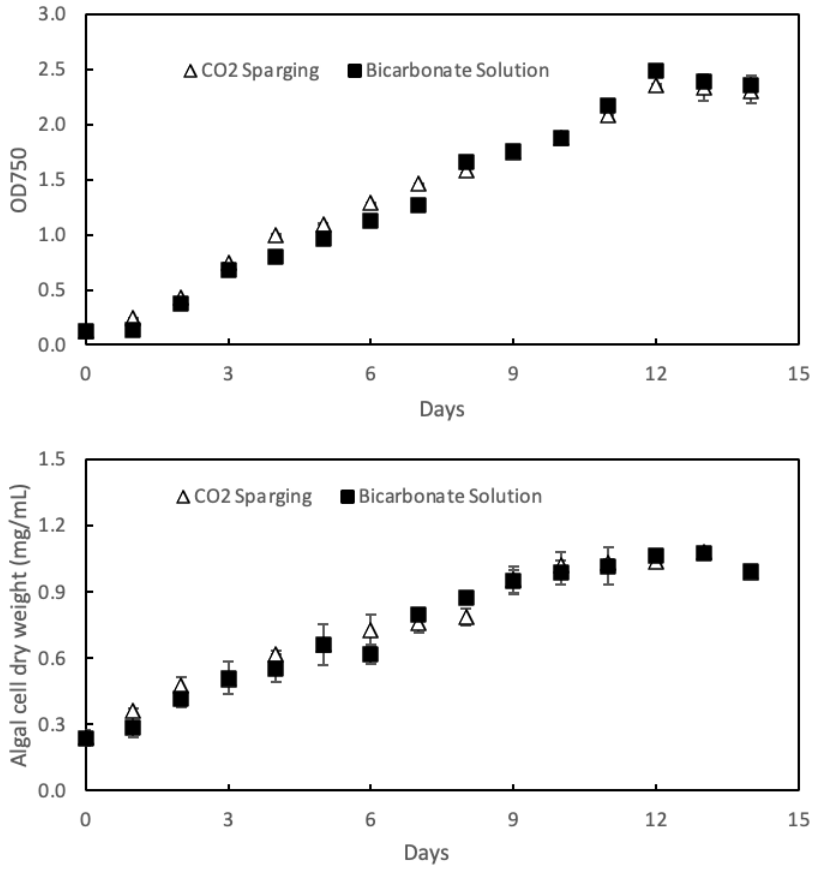

Figure G3-13. Algal cell growth of a 2-week cultivation of WT *N. oceanica* in the mini-raceway ponds. CO_2 was supplied either by CO_2 sparging or the DIC solution (direct mode). Top: OD750; Bottom: algal cell dry weight (mg/mL).

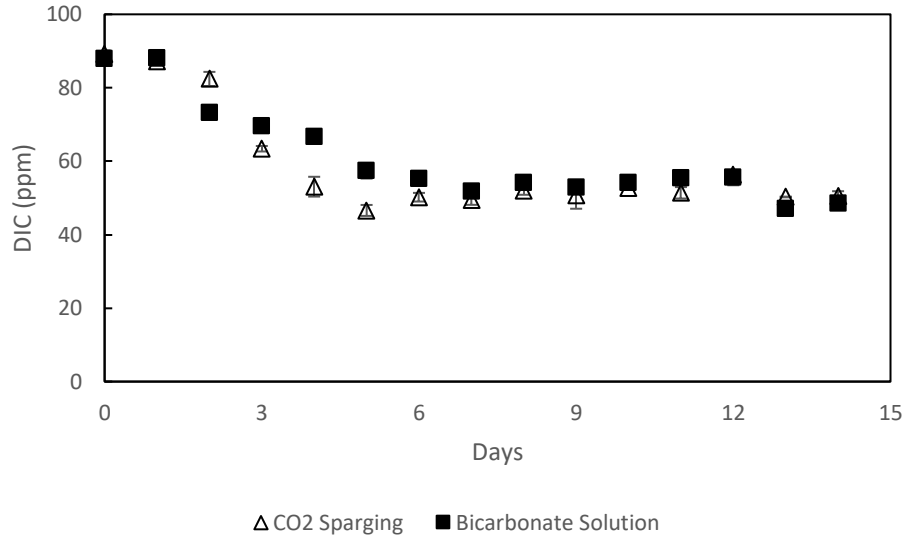

Figure G3-14. Dissolved inorganic carbon (DIC) content in the mini-raceway ponds (direct mode).

Use of the membrane module system in outdoor mini-ponds at Qualitas Health

Qualtias Health deployed the membrane module carbonation unit (recirculation mode) in a 730-L minipond at the Imperial, Texas algae farm from September to November 2023. Overall, the technology of bringing highly carbonated, low pH media to the pond as an alternative to inefficient CO_2 injection is industrially attractive due to the cost of CO_2 and a very low CUE. There are a few key challenges that we identified with the system that need to be addressed as this technology continues to develop, mainly the large amounts of water that must be moved in and out of the ponds to maintain optimal pH setpoints in the ponds.

For the experiment, two 1000-L miniponds (730-L working volume, 9” depth) were cleaned, a small shed moved to the mini-pond area to offer an enclosure for the electronics for the membrane system, a CO_2 gas cylinder purchased, and a 50-gallon plastic drum obtained to serve as the reservoir for the carbonated medium. The CSU carbonation technology was installed and the Qualitas staff trained on its operation and troubleshooting. It was also evident that the system could be connected directly into the CO_2 lines that already existed to supply CO_2 to the miniponds, allowing a consistent flow of CO_2 without needing CO_2 tanks that had limited capacities. By September 21, 2024, the carbonation unit was installed and actively running (Figure G3-15).

However, throughout the roughly two-month run time, the Qualitas staff had limited success with operating the technology. Several challenges arose that proved to be great learnings for the continued development of this technology:

- Software Issues – The CO_2 logging software would take CO_2 flow rate measurements autonomously, but if the computer powered down or went into sleep mode, these recording would stop. Several times throughout runs, the software would stop recording data. The QH staff fixed computer settings to ensure that the machine was always powered on and plugged in, and that solved some of these issues.
- Weather – The Imperial farm experiences extreme weather throughout the fall, from daily temperatures exceeding 100 °F, to dust storms, and violent, unexpected rain events. Even with the small outdoor shed to protect the electronics from the elements, there were still had issues. High temperatures overheated the computer, resulting in the computer turning off and not collecting data. Dust events were proactively planned for by covering the electronics with a plastic tub, but that also led to overheating.
- Debris in the ponds – Operating open raceway systems results in some debris/detritus building up in the ponds. The inlet line that pulls pond medium goes through a diaphragm pump that contains a pre-filter to protect the pump from solids. This filter could clog easily, resulting in no water flowing through the pump, but the pump technology would still have the pump turned on since the carbonation reservoir required water. This resulted in the pump running dry continuously overnight and the motor burning out. We purchased a new pump, and installed meshing over the inlet in the pond that successfully filtered out large solids prior to the pump pre-filter.

- Top-Off Sensor Failure – The mini-pond had a float sensor installed to trigger the pumps for when the pond required medium (“top off”) and shut off pumps once desired depth was achieved. In a few instances, this float sensor did not successfully turn off the pumps during refilling, and the pond overfilled from 9” to 11”. The ponds did not overflow because the reservoir of water for refilling was not large enough to exceed the mini-pond capacity. The sensor failed due to debris adhering to it in one instance, and salt build up contributed to the second instance.
- Inadequate Carbonation Rate – One technological issue with the unit was the rate at which CO_2 was being dissolved into the medium. It seemed that the carbonation unit was either dirty or undersized for the 50-gallon reservoir. The pH in the reservoir did not go below 6.5 without the intervention of a starting volume of water being directly sparged with CO_2. By not achieving low enough pH in the reservoir tank, this meant a large volume of the mini-pond needed to be removed and replaced with a large volume of carbonated medium to maintain the optimal pH range of our system. The carbonation membrane unit was cleaned to restore it to full capacity. The water filters also had to be changed regularly due to the high minerality of the Imperial well water. Some of these issues resulted from the use of the recirculation mode in the QH deployment; the direct feeding mode is likely to have performed better.

Figure G3-15. The installed DIC feeding system in 900-L raceway ponds at the Qualitas Health facility.

<u>BicA mutant cultivation in mini-ponds:</u>

N. oceanica TKK012, the BicA-expressing strain created in Task 2.1, was cultivated in the mini-raceway ponds at CSU. The wild type *N. oceanica* (strain CCAP 849/10) was used as a reference. The cultivation lasted for 47 days. The ponds were harvested every 8 to 10 days. The cell growth was monitored by checking OD750 and dry biomass weight concentration daily.

There was no significant difference in the cell growth of WT *N. oceanica* and the engineered strain TKK-012 under the cultivation conditions used (Figure G3-16). Both OD750 and cell dry biomass weight showed similar patterns in each cycle of the 47-day cultivation. In addition, the growth of the engineered strain TKK-012 was compared using CO_2 sparging or the DIC solution feeding system during the 47 days of cultivation (Figure G3-17). The TKK-012 cultivation had lower OD750 and cell dry biomass weight concentration using the DIC solution feeding in comparison to those of the pond using CO_2 sparging. The reasons for these observations are unclear.

The CO2 consumption in each pond was recorded using CO_2 mass controllers. The WT *N. oceanica* and the engineered *N. oceanica* TKK-012 used similar amounts of CO2 during the 47-day cultivation (Figure G3-18).

As expected from the prior cultivation experiments, the DIC solution system used significantly less CO_2 that the CO_2 sparging system during the cultivation of *N. oceanica* TKK-012 in the mini-raceway ponds. On average, the DIC solution feeding system used about 43% less CO_2 than that of the CO_2 sparging system.

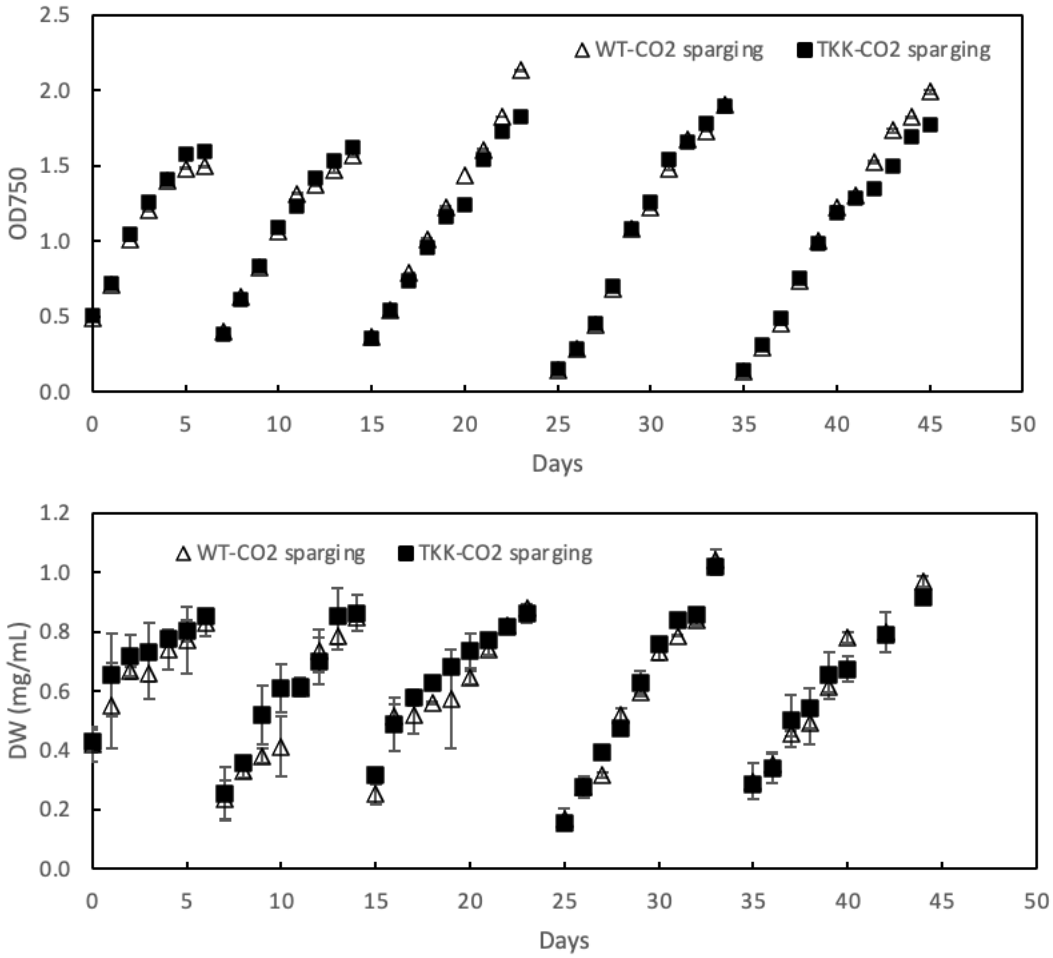

Figure G3-16. Algal cell growth of WT *N. oceanica* and the engineered strain TKK-012 in the mini-raceway ponds during the 47 days of cultivation. CO_2 was supplied by CO_2 sparging to control pH. Top: OD750; Bottom: algal cell dry weight (mg/mL).

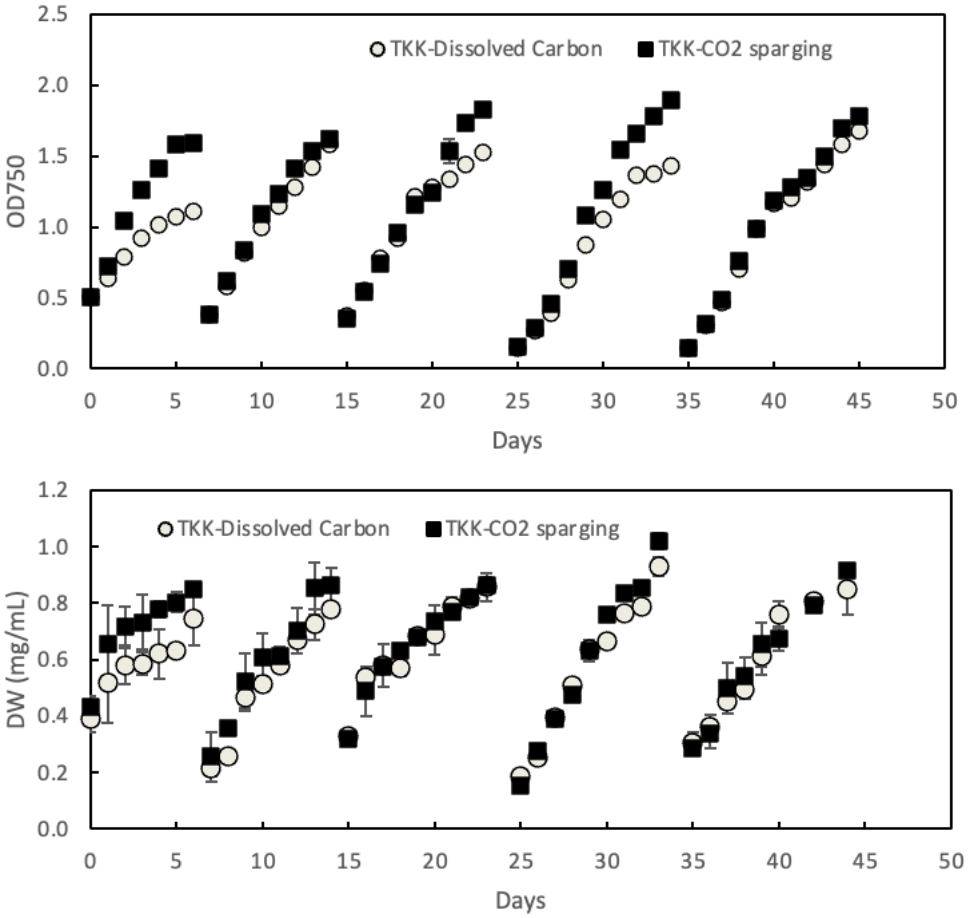

Figure G3-17. Algal cell growth of the engineered *N. oceanica* TKK-012 in the mini-raceway ponds during the 47 days of cultivation. CO_2 was supplied either by CO_2 sparging or dissolved carbon solution. Top: OD750; Bottom: algal cell dry weight (mg/mL).

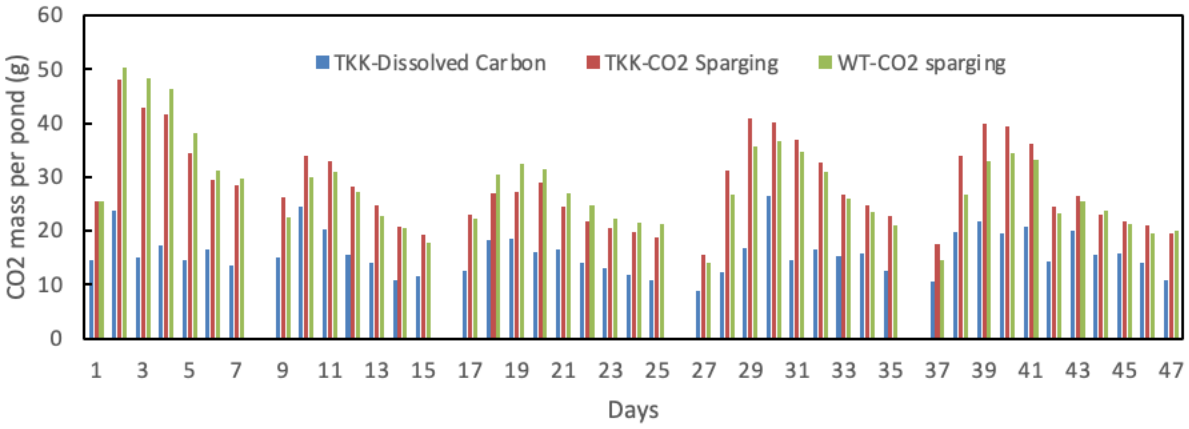

Figure G3-18. CO_2 daily consumption in the mini-raceway ponds.

End of Project Goal: The end-of-project goal is to demonstrate the use of model-directed, optically controlled, dissolved inorganic carbon delivery that achieves a 25% increase over baseline inorganic carbon utilization efficiency in the integrated system measured over a 6-week semi-continuous cultivation demonstration run at the QH test site (mini-ponds plus membrane module plus CO_2 monitoring). enhanced carbon delivery strategy, combined with targeted and/or adapted modification of N. oceanica*, will result in a 20% growth rate increase.*

As described in the results presented for the Go/No-Go 3 goal, the carbon transfer system developed in this project improved the CUE by at least 90% over standard sparging in several multi-week cultivations in indoor mini-ponds, considerably exceeding the target of 25% improvement. While the carbonation system was deployed outdoors at the QH test site, technical difficulties prevented the system from operating long enough to measure CUE improvements.

The strain improvement research resulted in the development of a BicA-expressing strain of *N. oceanica*, which was shown to have growth rates more than 20% faster than the wildtype in indoor flask cultivations. However, those growth differences were not observed in indoor mini-ponds, most likely because those cultivations were performed under light-limited conditions rather than carbon-limited ones. Further testing of the engineered strain at lower cell concentrations is warranted since those conditions are likely to lead to higher growth rates in general.

8. Significant Accomplishments and Conclusions:

This project produced several important accomplishments. The details are presented in the task/milestone section. In summary:

- Carbonic anhydrase variants (Subtask 1.1): A combination of protein engineering and database mining led to the design, expression, and evaluation of many novel CA variants. Many of these have significantly improved properties (pH tolerance, salt tolerance, lifetime) compared to the standard commercial bovine CA. These novel CA variants could be used in a range of approaches to more rapidly transfer CO_2 into algal cultivations and could find application in other carbon capture technologies.
- Development of a BicA-expressing variant of *N. oceanica* (Subtask 2.1): For the first time, the bicarbonate transporter from a cyanobacterium was expressed in *Nannochloropsis*. The variant was found to grow more than 20% faster than the wildtype in flask cultivations under conditions in which light was not limiting. Field trials under similar conditions are warranted because of the large productivity increase that could result.
- Membrane-based CO_2 transfer system (Subtask 1.2, 1.3, and 3.3): A system based on hollow-fiber membrane modules for clarification and bubble-free solution carbonation was developed with automated control of pH and level. This system, in both a direct feeding mode and a recirculation mode, was shown to increase CUE by at least 90% over standard gas sparging. Outdoor tests revealed opportunities for improving the system robustness, but overall,

the approach was successful in improving CUE far more than the target metric of 25%, and should be developed further.

- Computational fluid dynamics modeling of mixing in open raceway ponds (Subtask 3.1): A detailed CFD model revealed new insights into fluid flow and cell movement in ponds, including the long periods spent in the dark by cells and the passive mixing that occurs at the first bend in the raceway flow after the paddlewheel. These insights also led to the idea of using passive vortex generators in ponds. However, there was not sufficient time to evaluation this approach.

The primary pivot that was made was in Subtasks 1.2 and 1.3, focused on development of carbonic anhydrase-containing membranes. It proved difficult to cast the original hydrogel material planned for the project in layers thin enough to have minimal mass transfer resistance. A second enzyme immobilization method was used with better results, but membranes made with this approach also had mass transfer resistances that were high enough to mitigate the benefits of the immobilized CA. We thus pivoted to the use of commercial hollow fiber modules. It would be ideal to work with a hollow fiber manufacturer to be able to immobilize enzymes in the fibers, considering their large surface areas.

The Covid-19 pandemic clearly impacted the timeline of this project in several ways, with lab closures and restricted access. The only effect of the pandemic on the project scope was the elimination of tests at New Belgium Brewery. However, the brewery staff provided access to their fermentation off-gas CO_2 supply so we could evaluate its capability to support the growth of *N. oceanica*.

9. Path Forward:

Concepts and developments from this project, including the membrane module approach, the BicA variant, and CFD model, are being used in a current BETO project, DE-EE0009672, Advancing Algal Productivity through Innovation in Cultivation Operation and Strain Traits.

Furthermore, the membrane module approach is being used in a current FECM project, DE-FE0032229, Algal Biorefinery Conversion of Utility CO_2 to High-Value Products.

Invention disclosures were filed for the carbonic anhydrase variants developed at NREL and for the BicA variant of *N. oceanica* developed at CSU. A PCT patent application was ultimately filed for the BicA variant.

10. Products:

Publications to date

“Mapping swirling motion in a mesoscale raceway pond predicted by three-dimensional computational fluid dynamics simulations using LES and k-ε models,” C. Shen and D.S. Dandy, submitted.

"Investigation of the light environment in a raceway pond using particle tracking," C. Shen and D.S. Dandy, submitted.

"Dimensional analysis of strength and persistence of swirling motion in raceway pond systems coupled with computational fluid dynamics," C. Shen and D.S. Dandy, submitted.

"Application of passive vortex generators to enhance vertical mixing in an open raceway pond," C. Shen and D.S. Dandy, *Algal Res.* **79**, 103434, 2024.

Conference presentations to date

Huang, X.-F., C. Shen, J. Greene, D.S. Dandy, J.C. Quinn, and K.F. Reardon. 2024. Increased Carbon Utilization Efficiency of *Nannochloropsis oceanica* Cultivation by Using a Membrane Module. International Conference on Algal Biomass, Biofuels and Bioproducts, Clearwater Beach, FL. 10-12 June.

Huang, X.-F. and K.F. Reardon. 2023. Increased Carbon Utilization Efficiency of *Nannochloropsis oceanica* Cultivation by Using Bicarbonate Membrane Module. Algae Biomass Summit, Madison, WI. 9-11 October.

JM Greene, D Quiroz, S Compton, JC Quinn. 2022. Modeling algae cultivation at scale: Productivity, pond reliability, and resource consumption across the United States." International Symposium on Sustainable Systems and Technology (ISSST). Pittsburgh, PA; June.

JM Greene, D Quiroz, KF Reardon, J Adkins, JC Quinn. 2022. Life cycle assessment of suspended algal cultures in outdoor open pond systems: investigating carbon utilization efficiency and CO_2 sourcing. Algae Biomass Summit – Algae Biomass Organization (ABO); Virtual Conference; Sept – Oct.

JM Greene, C Hawthorne, K Reardon, D Dandy, JC Quinn. 2021. Evaluating the Economic Impacts of Using Enzymatic Membranes to Optimize Bicarbonate Production and Delivery to Open Raceway Ponds. Algal Biomass Biofuels and Bioproducts (ABBB); Virtual Conference; June.

Reardon, K.F., T.S. Bailey, D.S. Dandy, R. Davis, L. Laurens, J. Nalley, G. Peers, J.C. Quinn, D. Sammond, and R. White. 2019. Integrating an Industrial Source and Commercial Algae Farm with Innovative CO_2 Transfer Membrane and Improved Strain Technologies. Algae Biomass Summit, Orlando, FL. 16-19 September.

C. Shen and D.S. Dandy. 2019. Three-dimensional, multiphase CFD simulation of cyanobacteria light histories in a raceway pond. International Conference on Algal Biomass, Biofuels and Bioproducts 2019, Boulder, Jun 17–19.

Reardon, K.F., T.S. Bailey, D.S. Dandy, R. Davis, L. Laurens, J. Nalley, G. Peers, J.C. Quinn, D. Sammond, and R. White. 2019. Increasing CO_2 utilization efficiency and algal cultivation productivity with innovative CO_2 transfer and improved strain technologies. 9th International Conference on Algal Biomass, Biofuels and Bioproducts, Boulder, CO. 17-19 June.

C. Shen and D.S. Dandy. 2017. Three-dimensional, multiphase CFD simulation of cyanobacteria light histories in a raceway pond. International Conference on Algal Biomass, Biofuels and Bioproducts 2017, Miami, Jun 18–21.

C. Shen and D.S. Dandy. 2016. Three-dimensional, multiphase CFD simulation of cyanobacteria light histories in a bench-scale photobioreactor system. International Conference on Algal Biomass, Biofuels and Bioproducts 2016, San Diego, June 26–29.

Inventions to date

Tech 2021-068 was disclosed 3/22/2021, reported to DOE on 5/20/2021 (iEdison IR#1725201-21-0002). Title was elected 11/4/2021. A PCT patent application (PCT/US2022/079266, "EUKARYOTIC ALGAE COMPOSITIONS AND METHODS THEREOF") was filed 11/4/2022 and then nationalized into the US (Serial No 18/706,453) and Australia (Serial No 2022381194) on 5/1/2024.

11. Project Team and Roles:

The project consortium included together world-class researchers and practitioners from Colorado State University (CSU), the National Renewable Energy Laboratory (NREL), and Qualitas Health (QH) with expertise in polymers, enzyme engineering, algal strain engineering, photophysiology, systems biology, algal cultivation from laboratory to production scales, LCA, and TEA.

Name	Affiliation	Role/Contribution
Kenneth F. Reardon, PhD	CSU	PI. Lead of Tasks 1.3, 2.3, 3.3
Travis Bailey, PhD	CSU	Co-PI. Lead of Task 1.2
David S. Dandy, PhD	CSU	Co-PI. Lead of Task 3.1
Graham Peers, PhD	CSU	Co-PI. Lead of Task 2.1, 2.3
Jason C. Quinn, PhD	CSU	Co-PI. Lead of Task 3.4, 3.5
Jaclyn Adkins, PhD	CSU	Investigator. Tasks 1.2, 1.3
Devon Osbourne, PhD	CSU	Investigator. Task 1.1
Will Morris	CSU	Graduate student. Task 1.2
Jonah Greene	CSU	Investigator. Tasks 3.4, 3.5
Seijin Park	CSU	Investigator. Tasks 2.3
Chen Shen	CSU	Graduate student. Task 3.1
David Quiroz	CSU	Graduate student. Tasks 3.4, 3.5
Bjorn Andersson	CSU	Graduate student. Task 2.1
Michael Cantrell	CSU	Graduate student. Task 2.1
Maxwell Ware	CSU	Investigator. Task 3.3

Lieve Laurens, PhD	NREL	Co-PI. Lead of Tasks 1.1, 2.2, 3.2
Ryan Davis, PhD	NREL	Investigator. Tasks 3.4, 3.5
Bruno Klein, PhD	NREL	Investigator. Tasks 3.4, 3.5
Deanna Sammond, PhD	NREL	Investigator. Task 1.1
Damien Douchi, PhD	NREL	Investigator. Task 2.2, 3.2
Foteini Davrazou, PhD	NREL	Investigator. Task 1.1
Jessica Loob, PhD	NREL	Investigator. Task 2.2
Jacob Nalley, PhD	QH	Collaborator. Task 3.3.

12. References:

Alvizo, O., L.J. Nguyen, C.K. Savile, et al. 2014. Directed evolution of an ultrastable carbonic anhydrase for highly efficient carbon capture from flue gas. PNAS 111 (46) 16436-16441. https://doi.org/10.1073/pnas.1411461111

Bilad, M.R., H.A. Arafat, I.F.J. Vankelecom. 2014. Membrane technology in microalgae cultivation and harvesting: a review. Biotechnol. Advances. 32(7), 1283-1300. doi: 10.1016/j.biotechadv.2014.07.008

Chen, P.H. and J. C. Quinn, “Microalgae to biofuels through hydrothermal liquefaction: Open-source techno-economic analysis and life cycle assessment,” Appl. Energy, vol. 289, p. 116613, May 2021, doi: 10.1016/j.apenergy.2021.116613.

Davis R, Markham J, Kinchin C, Grundl N, Tan ECD, Humbird D. Process Design and Economics for the Production of Algal Biomass: Algal Biomass Production in Open Pond Systems and Processing Through Dewatering for Downstream Conversion. National Renewable Energy Lab. (NREL), Golden, CO (United States); 2016. https://doi.org/10.2172/1239893.

de Oliveira Maciel, A. P. Christakopoulos, U. Rova, and I. Antonopoulou. 2022. Carbonic anhydrase to boost CO_2 sequestration: Improving carbon capture utilization and storage (CCUS). Chemosphere, 299, 134419. https://doi.org/10.1016/j.chemosphere.2022.134419

Giordano, M.; Beardall, J.; Raven, J. A., Annual Review of Plant Biology 2005, 56 (1), 99-131.

Greene JM, Quiroz D, Compton S, Lammers PJ, Quinn JC. A validated thermal and biological model for predicting algal productivity in large scale outdoor cultivation systems. Algal Research 54, 102224, 2021.

Holm, L. and L. M. Laakso, "Dali server update," Nucleic Acids Res, vol. 44, no. W1, pp. W351-5, Jul 8 2016.

Li, F., J. Xie, X. Zhang, and L. Zhao, "Improvement of the optimum pH of *Aspergillus niger* xylanase towards an alkaline pH by site-directed mutagenesis," J Microbiol Biotechnol, vol. 25, no. 1, pp. 11-7, Jan 2015.

Jones SB, Zhu Y, Anderson DB, Hallen RT, Elliott DC, Schmidt AJ, et al. Process Design and Economics for the Conversion of Algal Biomass to Hydrocarbons: Whole Algae Hydrothermal Liquefaction and Upgrading. 2014. https://doi.org/10.2172/1126336.

Ma, F. et al., "Sequence homolog-based molecular engineering for shifting the enzymatic pH optimum," Synth Syst Biotechnol, vol. 1, no. 3, pp. 195-206, Sep 2016.

Mokashi, K.; Shetty, V.; George, S. A.; Sibi, G., Achievements in the Life Sciences 2016, 10 (1), 111-117.

Molina-Fernández, C. and P. Luis. 2021. Immobilization of carbonic anhydrase for CO_2 capture and its industrial implementation: A review. Journal of CO2 Utilization. 47, 101475. https://doi.org/10.1016/j.jcou.2021.101475

Pancha, I.; Chokshi, K.; Ghosh, T.; Paliwal, C.; Maurya, R.; Mishra, S., Bioresource Technology 2015, 193, 315-323

Poliner E, Pulman JA, Zienkiewicz K, Childs K, Benning C, and Farré EM (2018). A toolkit for *Nannochloropsis oceanica* CCMP1779 enables gene stacking and genetic engineering of the eicosapentaenoic acid pathway for enhanced long-chain polyunsaturated fatty acid production. Plant Biotechnology J., pp. 298-309.

Poliner E, Tackeuchi T, Du ZY, Benning C, and Farré EM (2018). Non-transgenic marker-free gene disruption by an episomal CRISPR system in the oleaginous microalga, *Nannochloropsis oceanica* CCMP1779. ACS Synth. Biol., 7 (2018) pp. 962-968.

Qiu, S. and L. Lai, "Tailoring the pH dependence of human non-pancreatic secretory phospholipase A2 by engineering surface charges," Appl Biochem Biotechnol, vol. 171, no. 6, pp. 1454-64, Nov 2013.

Rogers JN, Rosenberg JN, Guzman BJ, Oh VH, Mimbela LE, Ghassemi A, et al. A critical analysis of paddlewheel-driven raceway ponds for algal biofuel production at commercial scales. Algal Research 2014, 4:76–88. https://doi.org/10.1016/j.algal.2013.11.007.

Shao, P., J. Ye, Y. Shen. S. Zhang, and J. Zhao. 2024. Recent advancements in carbonic anhydrase for CO_2 capture: A mini review. Gas Science and Engineering, 123, 205237. https://doi.org/10.1016/j.jgsce.2024.205237

Sheehan JD, Savage PE. Modeling the effects of microalga biochemical content on the kinetics and biocrude yields from hydrothermal liquefaction. Bioresource Technology 2017, 239:144–50. https://doi.org/10.1016/j.biortech.2017.05.013.

Somers MD, Quinn JC. Sustainability of carbon delivery to an algal biorefinery: A techno-economic and life-cycle assessment. Journal of CO2 Utilization 2019, 30:193–204. https://doi.org/10.1016/j.jcou.2019.01.007.

Summers, H. M., E. Sproul, and J. C. Quinn, “The greenhouse gas emissions of indoor cannabis production in the United States,” Nat. Sustain., pp. 1–7, Mar. 2021, doi: 10.1038/s41893-021-00691-w.

Takashi, Y.; Hideya, F., Journal of Basic Microbiology 2009, 49 (1), 42-51.
Hanson, D. T.; Collins, A. M.; Jones, H. D. T.; Roesgen, J.; Lopez-Nieves, S.; Timlin, J. A., Photosynthesis Research 2014, 121 (2), 311-322.

Talekar, S. B.H. Jo, J.S. Dordick, and J. Kim. 2022. Carbonic anhydrase for CO_2 capture, conversion and utilization. Curr. Op. Biotechnol. 74, 230-240. https://doi.org/10.1016/j.copbio.2021.12.003

US EPA, “Inventory of U.S. Greenhouse Gas Emissions and Sinks,” Feb. 08, 2017. https://www.epa.gov/ghgemissions/inventory-us-greenhouse-gas-emissions-and-sinks (accessed Jul. 28, 2021).

US EPA, “Emissions & Generation Resource Integrated Database (eGRID),” Jul. 27, 2020. https://www.epa.gov/egrid (accessed Jun. 27, 2022).

Vieler A., Wu G., Tsai C.-H., Bullard B., Cornish A.J., Harvey C., Reca I.-B. et al (2012) Genome, functional gene annotation, and nuclear transformation of the heterokont oleaginous alga *Nannochloropsis oceanica* CCMP1779. PLoS Genet. 8, e1003064

Yang, Z., H. Pei, F. Han, Y. Wang, Q. Hou, and Y. Chen. 2018. Effects of air bubble size on algal growth rate and lipid accumulation using fine-pore diffuser photobioreactors. Algal Research. 32, 293-299. https://doi.org/10.1016/j.algal.2018.04.016

Zhang, Y., J. Zhu, J. Hou, S. Yi, B. Van der Bruggen, and Y. Zhang. 2022. Carbonic anhydrase membranes for carbon capture and storage. Membrane Sci. Lett. 2(2), 100031. https://doi.org/10.1016/j.memlet.2022.100031